MAL-DISTRIBUTION OF GAS-SOLID FLOW THROUGH IDENTICAL PARALLEL PATHS

by

MOHAMMAD SADEGH MASNADI-SHIRAZI

B.Sc., Iran University of Science & Technology, Iran, 2007

A THESIS SUBMITTED IN PARTIAL FULFILLMENT OF
THE REQUIREMENTS FOR THE DEGREE OF
MASTER OF APPLIED SCIENCE

in

THE FACULTY OF GRADUATE STUDIES

(Chemical & Biological Engineering)

The University of British Columbia

(Vancouver)

June 2009

ABSTRACT

Two-phase flow in identical parallel paths is associated with various industrial applications in which the two phases are distributed among parallel branches, with common inlet and outlet manifolds. Evidence in the literature shows that the distribution of multi-phase flow travelling through identical parallel paths can be significantly non-uniform. This may have many harmful operating consequences in practice.

In order to provide a better understanding of this fluid mechanics phenomenon, a fundamental analytical and numerical study is performed on the distribution of gas-solid pneumatic flow passing across a 'Y branch'. While many steady-state gas-solid distribution solutions, including a uniform distribution, are the outputs of the governing equations, instability analysis is performed to examine the stability of the solutions. In addition, the behaviour of the system is analysed using computational fluid dynamics. The results indicate that the uniform distribution is the stable output in this case.

Next the distribution of gas-solid flow through identical parallel cyclones is investigated based on an analytical model which includes a semi-empirical equation from the literature for cyclone pressure drop. Using the proposed model, many steady-state distribution solutions are obtained. The solution with maximum energy consumption is considered as the unlikely solution of the system. The results indicate that the non-linearity of the system can cause the distribution to be non-uniform for high solids loadings, whereas lower loadings will result in distributions that are uniform, or so close to being uniform that experimental results will not be able to distinguish difference between the flows. Moreover a number of experimental studies were carried out for a pair of identical standard cyclones of diameter 101.6 mm on the distribution of dilute gas-solid flow. The results are compared with the proposed cyclone model. The model can be used for multi-paths (>2) as well. Finally, available techniques, to make the distribution of gas-solid flow through parallel paths uniform, are presented.

TABLE OF CONTENTS

LIST OF TABLES

LIST OF FIGURES

NOMENCLATURE

A	cross-section area of pipe, m^2
$\tilde{b}$	dimensionless cyclone inlet width, b/D, -
C	constant coefficient of gas flow term in cyclone pressure drop relationship, $kg^{-1}m^{-1}$
$C_{D\infty}$	drag coefficient for single particle at infinite dilution, -
$C_{D\varepsilon}$	drag coefficient for single particle when the voidage is ε, -
C_i	Inlet dust loading in path i, kg/m^3
$\tilde{d}_r$	dimensionless cyclone outlet diameter, d/D_e, -
D	pipe diameter, m or cyclone diameter, m
D_s	particle diameter, m
E	electrical field, N/C
f	Solid Fanning friction factor, -
$f\,(Q_s, \varepsilon, k)$	steady-state pressure drop across parallel paths dividing by ΔL, $kg/(m^2.s^2)$
$f\,(m_s)$	function giving dependence of cyclone pressure drop on solids mass flow rate, -
f_L	Gas Fanning friction factor, -
F	Force, N
$\tilde{F}_s$	dimensionless area of the contact surface, $4F_s/(\pi D^2)$, -
Fr	Froude number related to air velocity, $u'_{gi} / (D.g)^{0.5}$
Fr^*	Froude number related to solid velocity, $u_s / (D.g)^{0.5}$
g	gravitational acceleration, m/s^2
k	flow coefficient in equation (2-38), -
k_i	correction coefficient of expansion loss, -

K	constant in cyclone pressure drop relationship, Pa
K_A	inlet area ratio, -
$K_{sg}(=K_{gs})$	interphase momentum exchange coefficient, kg/(m^2.s)
m_g	mass of displaced fluid, kg
m_{gi}	mass flow rate of gas passing path i, kg/s
m_{gt}	total mass flow rate of gas to complete array of N paths, kg/s
m_s	mass of particle of diameter D_s, kg
m_{si}	mass flow rate of solids passing through path i, kg/s
m_{st}	total solids mass flow rate to complete array of N paths, kg/s
n	swirl exponent, -
N	number of identical parallel paths, -
q	charge on particle, C
q_s	perturbed volumetric flow rate, m^3/s
Q_{gi}	gas flow rate passing path i, m^3/s
Q_{gt}	total inlet gas flow rate, m^3/s
Q_{si}	solids flow rate passing path i, m^3/s
Q_{st}	total inlet solids flow rate, m^3/s
$\tilde{r}_c$	dimensionless radius of the core flow, r_c/R, -
Re	Reynolds number related to pipe diameter, $u_g D/\upsilon$
$\mathrm{Re_s}$	solids Reynolds number, $u_s D_s/\upsilon$
t	time, s
u_g	actual gas velocity in the voids or velocity of porosity wave, m/s
u'_{gi}	superficial gas velocity passing path i, m/s
u_s	solid velocity, m/s
u_{t0}	single particle settling (or terminal) velocity in an undisturbed fluid, m/s

u'_{si} superficial solid velocity passing path i, m/s

$\tilde{V}_{\theta w}$ dimensionless tangential velocity at radius R, $V_{\theta w}/u'_{gi}$, -

Greek Symbols

α dimensionless deviation from uniform gas flow, -

α_s solid volume fraction, (1- ε), -

α_g gas volume fraction, -

Δm_s deviation from uniform solids distribution – solids mass in the control volume, kg

Δm_g gas mass in the control volume, kg

ΔP_i pressure drop through path i, Pa

ΔL length of pipe, m

ΔV control volume, m^3

ρ_g gas density, kg/m^3

ρ_s solid density, kg/m^3

ε voidage (volumetric void fraction)

μ gas viscosity, kg/(m.s)

γ fraction of gas flowing through channel 1, -

σ fractions of solids flowing through channel 1, -

δ_s perturbation amplitude, m^3/s

λ eigenvalue (or growth factor), 1/s

$\overline{\overline{\tau_g}}$ gas phase stress-strain tensor, Pa

$\overline{\overline{\tau_s}}$ solid phase stress-strain tensor, Pa

ξ drag coefficient of cyclone for gas flowing without particles, -

ξ_c drag coefficient of cyclone for gas-solid flows, -

ACKNOWLEDGEMENTS

I would not have completed this thesis without the significant help of many great people who have made my life at UBC a pleasant and productive experience. First and foremost, I would like to express my sincere gratitude to my outstanding supervisors, Dr. John R. Grace and Dr. Xiaotao Bi, for their continuous support and patience during my stay at UBC. I consider myself very fortunate for having the opportunity to work with them.

I gratefully acknowledge Dr. Siamak Elyasi for demonstrating the wit and senses required to keep up my courage. He always had time for discussion no matter how busy he was and without him, I could not accomplish this work. I appreciatively thank Syncrude Canada Ltd. for the financial supports. I send a special appreciation to Larry Hackman and Craig McKight for their valuable advices during the project. I would also like to thank the faculty and staff of Chemical & Biological Engineering Department for making up such a great environment for me to learn and grow, and for being my mentors.

Finally, this work is dedicated to my wonderful parents for all their love and support. I always felt them near me, even though they were living far away during my period of study in Canada. They have been my main motivation throughout my studies. Also I would like to thank my dear brothers, specially my older brother, Mostafa, for paving the way for me.

To my Parents

Chapter 1. INTRODUCTION

When a single-phase fluid passes continuously at steady-state through *N* identical parallel paths, the flow distributes itself uniformly among the multiple pathways, as illustrated schematically in Figure 1-1. The criterion that the pressure drop be identical through each of the paths results in a uniform distribution of the fluid (1/*N* fraction in each pass). This outcome is required in single-phase flows by fluid mechanics principles, and there is no known disagreement in the scientific literature. However, when multi-phase suspensions travel through identical paths in parallel, although a uniform distribution is commonly expected, there is evidence that the flow distribution can be significantly non-uniform[1]. Although an even distribution solution is a solution of governing fluid mechanics equations, it may be an unstable steady-state solution.

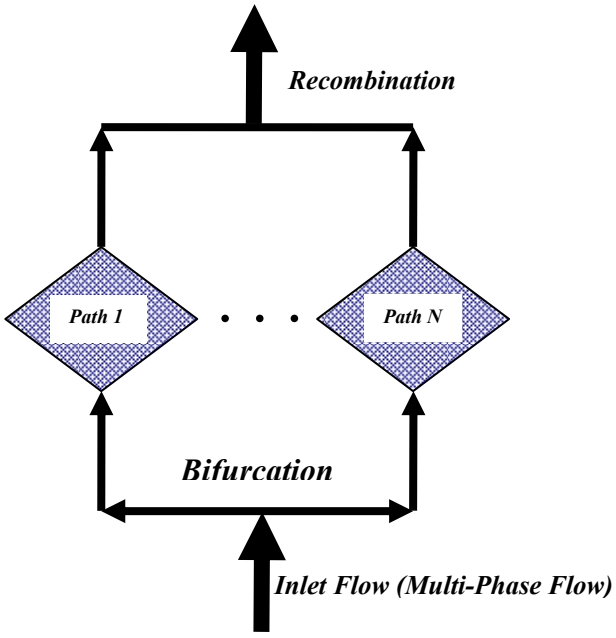

Figure 1-1. Schematic of flow through *N* parallel paths.

[1] References for the statements in this initial introductory section are given beginning in Section 1.1 below.

Two- and three-phase flows are common in engineering applications. Equipment for these operations can take many physical forms. In some cases where steady-state continuous operations are carried out, there are multiple matching branches in the flow path, with the flow expected to pass in a uniform manner through the different equal parallel branches. But unexpectedly, the multi-phase flow may pass non-uniformly through the identical parallel branches. Some examples of this mal-distribution in different systems are as follows:

Gas-Solid System:

- Internal identical parallel cyclones at the exit of fluidized bed reactors or circulating fluidized beds (CFB).
- Flow splitting: Pneumatic/Hydraulic conveying and distribution of particles to multiple feed points in a reactor, rotary kilns, particle dryers and coal power stations.
- Parallel channels inside fluidized beds.

Gas-Liquid System:

- Application of multiple paths in fuel cells.
- Multi-channel boiling in nuclear reactors.
- Application of identical parallel pipes for direct steam generation (DSG) by solar energy.
- Multi-channels of heat exchangers.

Liquid-Liquid System:

- Blood flow through arteries.

Liquid- Solid System:

- Liquid splitting through identical parallel liquid-solid fluidized and packed beds.

The behaviour of two-phase flow, as an example of multiphase flow, in parallel pipes (Figure 1-1) with a common feed is quite complex and difficult to predict. One of the problems that is not well understood is how the two phases distribute among the paths. For example in gas-liquid systems, one may assume that when flow in a single pipe splits into several pipes, the liquid and gas ratio in each of the pipes will be the same in each of the branches. This is not always the case. Instead the distribution may depend on many parameters (gas flow rate, liquid flow rate, fluid properties inclination of parallel pipes, geometry, etc.). There are cases where the flow is strongly preferential. For example most of the gas may enter one pipe (path 1), while the liquid favours the other pipe (path 2). Evidence suggests that not only can non-uniformity occur, but that in practice there are many instances where it does occur and where the non-uniform distribution is in fact a stable outcome. This type of behaviour has recently become the subject of considerable attention, and this non-uniformity may be of considerable practical importance in such cases.

This chapter starts with a brief literature review of gas-liquid two-phase flow through identical parallel paths; next the situation with operation of gas-solid flow through parallel channels is discussed extensively. Also the operating consequences of mal-distribution are discussed. At the end, the motivation and objectives of this work are presented.

1.1. GAS-LIQUID SYSTEMS

1.1.1. Evidence for Mal-Distribution of Parallel Flows

The flow distribution of gas and liquid in parallel channels has received attention due to its importance in such engineering applications as PEM fuel cells, heat exchangers, cooling systems, nuclear reactors, and direct steam generation (DSG) by solar heating.

In fuel cells, flow fields typically consist of multiple parallel mini-channels with sub-millimetre dimensions. Under typical operating conditions, especially for automotive

applications, the reactant gas on the cathode becomes saturated, leading to the presence of liquid water in the flow channels [1]. Therefore, it is important to develop a better understanding of two-phase flow in mini-channels to ensure uniform homogeneous reactant distribution for all operating conditions. Under two-phase flow conditions, equal pressure drop does not ensure even distribution of gas and liquid in multiple channels, because different combinations of gas and liquid flow rates can yield the same pressure drop. The resulting mal-distribution of gas and liquid can lead to flooding or drying in different regions of the active cell area. The presence of flooding and drying regions leads to current re-distribution which can cause the fuel cell performance to deteriorate and can also lead to instabilities characterized by erratic changes in pressure drop and cell performance [2]. Improved fundamental understanding of gas and liquid flow in parallel mini-channels is required in order to design reliable flow fields for stable fuel cell operation.

In the literature, much effort has been devoted to gas and liquid distribution in engineering applications such as heat exchangers, condensers, cooling systems in nuclear reactors and DSG systems [3-4]. Considerable work has been performed on flow in parallel pipes for a boiling system where stability and flow-distribution are important objectives [3, 5, 6, 7].

Taitel et al. [8] investigated experimentally the distribution of gas and liquid in four parallel pipes with a common manifold. They found that under certain conditions the two phases “chose” to flow only in one, two or three of the pipes, while stagnant liquid columns were observed in the other pipes. Their analysis shows that multiple steady-state solutions may satisfy the conditions of equal pressure drop in the four pipes.

Pederson and May [9] and Murphy and May [10] studied two-phase flow instabilities which may arise during the operation of parallel pipes that absorb focused solar energy, producing steam directly in the collectors. They investigated the hydrodynamic transient behaviour of a two-phase boiling system. Five flow instabilities were identified as

potentially harmful to the operation of a DSG system, and generalized maps were drawn to estimate the stability of a parallel-channel solar system.

Jovic et al. [6] investigated experimentally the onset of pressure drop oscillations in three parallel channel flows. It was shown that inter-channel interaction can lead to unstable two phase flow.

Experimental work has been done by Ozawa et al. [3, 11, 12] on two- phase flow systems in capillary parallel pipes of 3.1 mm diameter. They attempted to simulate flow in boiling channels by injecting air and water along the pipes. Injection of air had a destabilizing effect on the pressure drop oscillations. On the other hand, liquid injection had a stabilizing effect, but induced small amplitude oscillations in the liquid flow rates.

Reinecke et al. [13] investigated flow reversal in vertical two-phase flow in parallel channels. Their experimental set-up consisted of six tubes of inner diameter 19.05 mm and length 1.3 m connected to a top and a bottom plenum. A model, based on pressure drop calculations was presented for the prediction of the reversal boundaries.

Tshuva et al. [14] investigated the distribution possibilities of air and water in two parallel pipes, 24 mm in diameter and 3 m long for inclination angles from horizontal to vertical. Their theoretical calculations showed that there is an infinite number of steady-state solutions with different splitting ratios, but the one seen in practice is the one that results in a minimum pressure drop.

1.1.2. Analytical Results

There are more journal papers on the distribution of gas-liquid flow through parallel paths compared to those locating similar problems for gas-solid flow. Mal-distribution of gas-liquid problems can be divided into two main groups:

1. Parallel pipes with diameter greater than 10 mm (application in heat exchangers and etc.)

2. Mini-channels: parallel pipes of diameter less than 5 mm (applied in fuel cells).

For horizontal parallel pipes of diameter 20-50 mm, the distribution of multiphase has been found to be almost uniform [15], whereas mal-distribution was observed in inclined parallel paths. On the other hand, a non-uniform distribution was reported recently by Zhang et al. [2] for fuel cell horizontal mini-pipes (1.59 mm diameter). They believe that the flow pattern is affected by the pipe dimension. In addition, they showed that instability is highly dependant on the geometry of the pipes (e.g. inlet and outlet). Therefore, this type of fluid appears to be highly sensitive to geometry and the dimensions of the system.

Extensive studies have been done since 1985 by Barnea et al. on DSG by solar heating pipes (20-50 mm in diameter). It has been observed that two possible flow configurations can take place: (1) symmetric distribution of liquid and gas in the two pipes, and (2) asymmetric flow in which the two phases flow in one pipe and stagnant liquid is present in the other (Figure 1-2). The asymmetric configuration is observed in upward inclined parallel pipes at low gas and liquid flow rates. The region of asymmetric flow increases with the angle of inclination. For the horizontal case, the flow was symmetric for all flow conditions.

Detailed flow regime maps for gas-liquid two-phase flow in single mini-channels have been studied by Triplett et al. [16] and Kawahara et al. [17], among others. Based on these studies, four distribution flow patterns in identical parallel paths are shown in Figure 1-3. These patterns were used to facilitate the characterization of the flow distribution and to construct the flow distribution map. It is important to note that the flow pattern in the two channels varied during repeated runs, confirming that the mal-distribution across the two channels is not induced by a difference or defect in the two parallel channels.

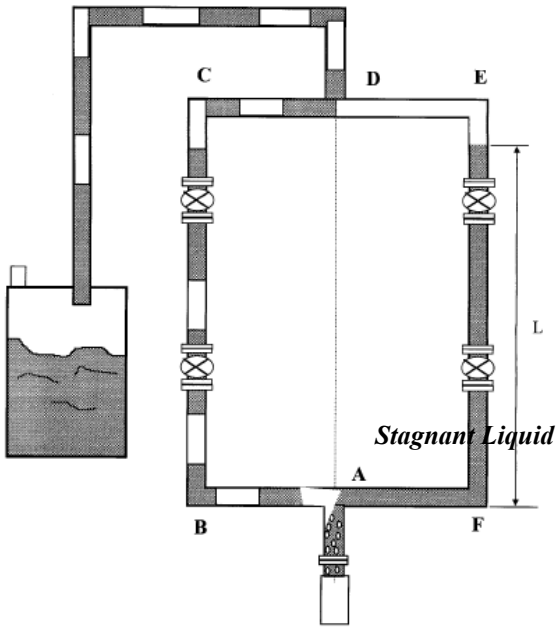

Figure 1-2. Schematic presentation of asymmetric case [14].

Zhang et al. [2] reported nearly identical distribution between two paths for low and high flow rates of gas and non-uniform patterns occurs at intermediate flow rates. They reported an interesting phenomenon in the transition regime when they performed experiments in two ways. In one case, they started with zero gas flow rate, increased it and measured a pressure drop, whereas in the second approach, they started with a high gas flow rate and decreased it gradually (with constant liquid flow in both cases). Although they found the same pressure drop for both cases at low and high gas flow rates, large differences in pressure drop occurred in the transition regime (Figure 1-4, top curves). In addition, they examined two types of outlet for parallel pipes (vertical & straight exits) and found that a straight exit was much better for achieving a uniform distribution, and also the same pressure drop for both the ascending and descending gas flow rate cases (Figure 1-4, bottom curves).

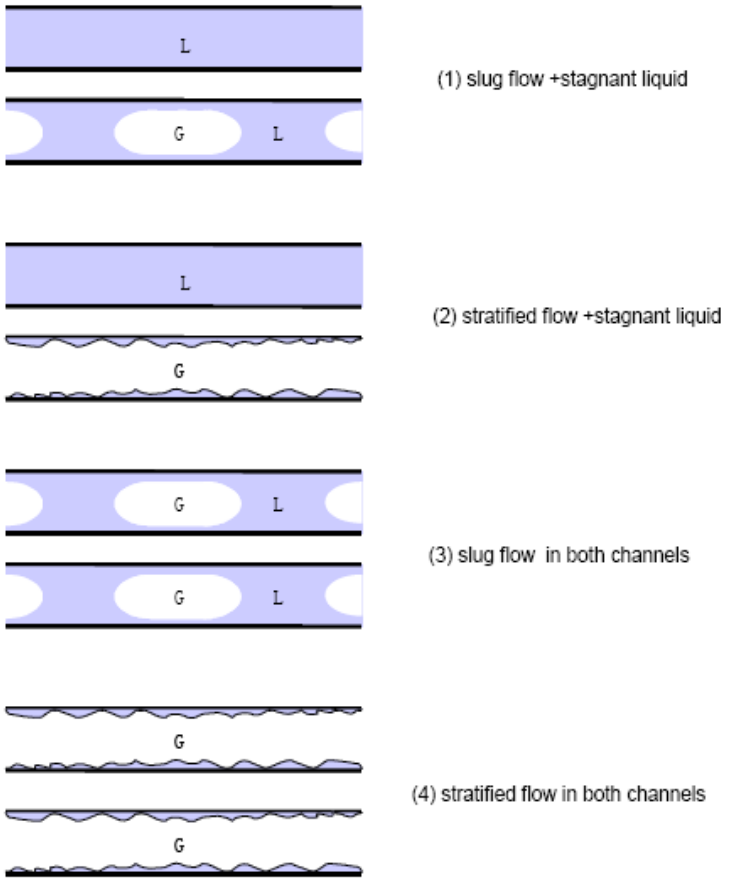

Figure 1-3. Four distribution flow patterns in identical parallel paths [2].

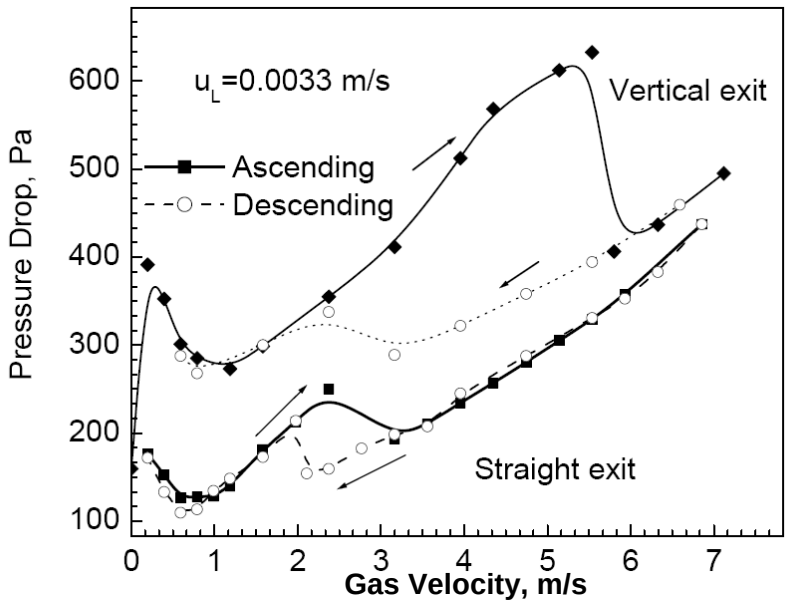

Figure 1-4. Pressure drop in parallel fuel cell channels for vertical and straight exits [2].

1.2. GAS-SOLID SYSTEMS

1.2.1. Experimental Evidence

Notwithstanding the assumption of flow uniformity in the design of parallel pathways, there is mounting evidence in the literature that gas-solid flow through parallel paths can result in significant mal-distribution, even when the flow paths are identical.

1.2.1.1. Identical Parallel Cyclones

In industrial-scale gas-solid reactors, dryers and other process equipment involving solid particles, it is common to require downstream separators to remove entrained particles from the gas. Cyclones are often the separators of choice because of their low capital and operating costs and the lack of moving parts. For large units with high exit flow rates, instead of building a single cyclone, two or more cyclones are often used in parallel. In designing the arrays of cyclones, it is generally assumed (implicitly or explicitly) that the approaching particle-bearing fluid stream will split itself evenly among the individual cyclones in parallel, so that each will operate under the design conditions. This is of importance, both for operational reasons and because both gas cyclones show a maximum efficiency with increasing fluid volumetric flow rate, and the cyclone design is intended to ensure that each cyclone operates at or near this optimum operating condition [18].

In practice, however, Stern et al. [19] reported that parallel operation of cyclones results in problems not encountered when each cyclone is operated independently. Equalizing gas and dust-load distribution among the cyclones presents a major problem. When efficiencies of cyclones in parallel were compared with those of individual cyclones at the same average dust loading and gas flow per unit, those in parallel gave lower collection efficiencies, with the decrease in efficiency tending to increase as the number of cyclones in parallel increased. The likely cause of the decrease is that when linked

together, the parallel cyclones experienced different flow conditions, one or more operating below the condition corresponding to the optimum efficiency, and the others above [18].

Koffman [20] tested various cyclones for engine air cleaning. The test results again showed a reduction in overall efficiency when the individual units were combined into a set, with the efficiency dropping from 96% for an individual cyclone to 92.2% when 14 small cyclones were operated in parallel. Broodryk and Shingles [21] simulated industrial two-cyclone and three-cyclone geometries in cold model experimental rig. The mal-distribution did not disappear at higher gas velocities and hence at higher pressure drops. Smellie [22] tested three identical cyclones in parallel and found that the amount collected was in the ratio of 2:1.5:1 as a result of non-uniform distribution for the individual units. Moreover, there are anecdotal industrial reports on differential erosion and fouling related to AcryloNitrile (AN) and Fluid Coker fluidized bed reactor parallel cyclones. Some related evidence is presented in Chapter 3.

1.2.1.2. Parallel Cyclones inside CFB

Cyclone performance deteriorates with increasing cyclone diameter, in particular once the cyclone diameter exceeds ~8 m [23]. As a result, as CFB combustors, gasifiers and other processes are scaled up, they reach a point where, instead of a single cyclone or cyclone train, cyclones are placed in parallel. For example, there are two cyclones in parallel in the 235 MW_e Turow No. 3 CFB boiler in Poland [24], four in a 200 MW_e anthracite-burning unit in Ukraine [25], and six in the conceptual design of an 800 MW_e supercritical pressure CFB boiler planned for China [26]. A schematic showing two cyclones in parallel is provided in Figure 1-5.

Measurements with water-cooled probes in a 235 MW_e circulating fluidized bed boiler in Poland where there are two cyclones in parallel suggest some asymmetry of the flow at the top of the unit near the cyclone outlets [18]. Kim et al. [27, 28] found markedly different wear patterns in the exit region of a large CFB combustor of 5 m x 10 m cross-

section and 29 m height (Figure 1-6) after extended periods of operation, despite the fact that the two exits were located symmetrically at opposite ends of the combustor. The wear patterns suggested that the solids flow had been significantly greater through one exit than the other. The relevant data, obtained after an extended period of operation, 11.5 years, are plotted in Figure 1-7. They demonstrate a clear difference between the two sides. The reduced thicknesses of the tubes on the west side imply greater solids flow to the west cyclone exit than to the east exit, i.e. asymmetry and mal-distribution of the flow to the cyclones [29].

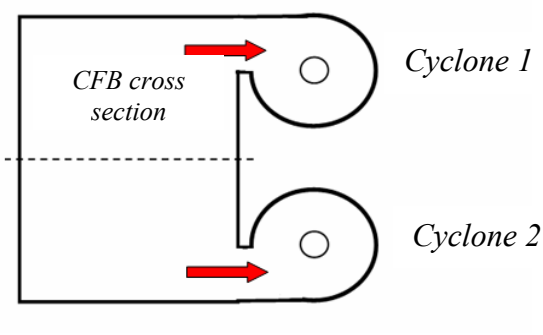

Figure 1-5. Schematic of CFB chamber with identical parallel cyclones.

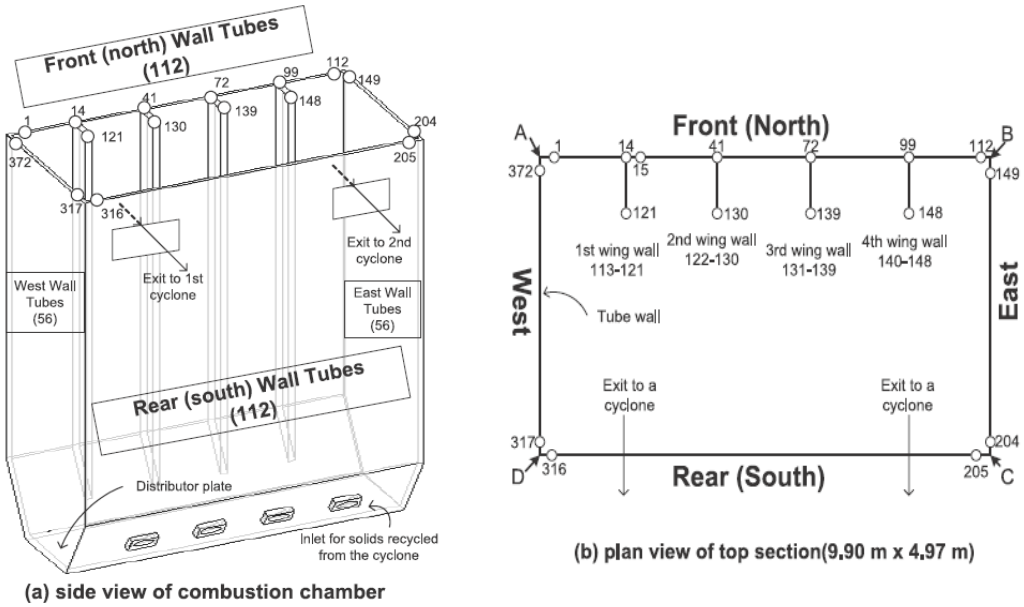

Figure 1-6. Layout of water wall tubes in the combustor and tube numbering scheme: (a) side view of combustion chamber; (b) plan view of top section [27].

It is also notable that as shown in Figure 1-8, numerical simulation of a large CFB furnace equipped with 3 cyclones (Flour and Boucker [30]) predicted marked differences in volumetric solids fractions in the entrance pipes to the individual cyclones.

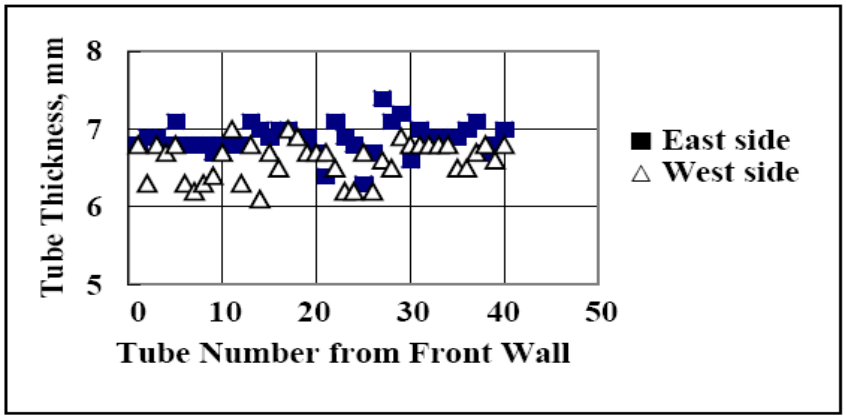

Figure 1-7. Lateral profiles of tube thickness at top of 10 m x 5 m x 29 m tall CFB boiler along east and west walls, 25 m above the bottom, showing difference in the extent of wastage over a period of 138 months of operation. Tube pitch is 88 mm along both walls [29].

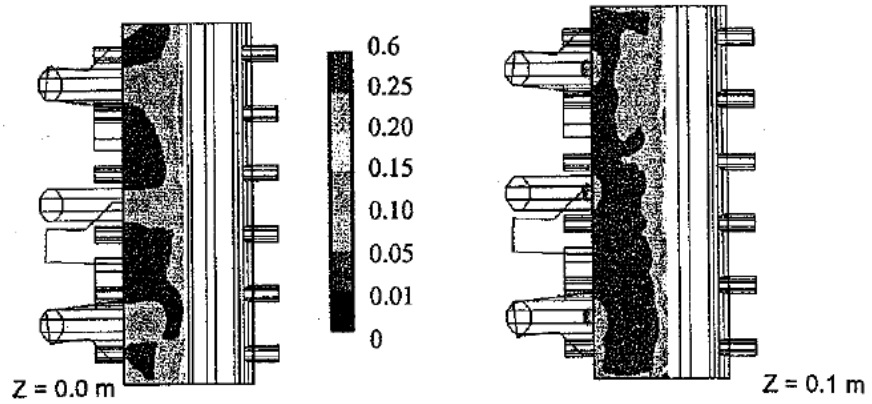

Figure 1-8. Mean volumetric solid fraction in horizontal planes for two different heights [30].

Yue et al. [31] experimentally and numerically studied the hydrodynamics of 300 and 600 MW_e CFB boilers with identical multi-cyclones at the top exit. The layout of the 600 MW_e boiler is sketched in Figure 1-9. It should be pointed out that they controlled the solid circulating rate and solid suspension density in each circulating loop by adjusting the aeration rate (to avoid mal-distribution through the parallel cyclones). Table 1-1 shows the experimental results for 300 MW_e boiler (the experimental data for a 600 MW_e

unit are also presented in the paper). They concluded that the gas flow field was quite uniform at each measurement level in the riser, except in the outlet zone of the cyclone standpipes. Also, the pressure drops and the inlet solid flow rate of the three cyclones were nearly the same, indicating that gas and solid flow rates through each cyclone were approximately the same. They believe that differences in solid fluxes in each circulating loop cause mal-distribution of flow through parallel cyclones and that the inlet solid flow to the cyclones can be regulated by tuning the gas flow rate.

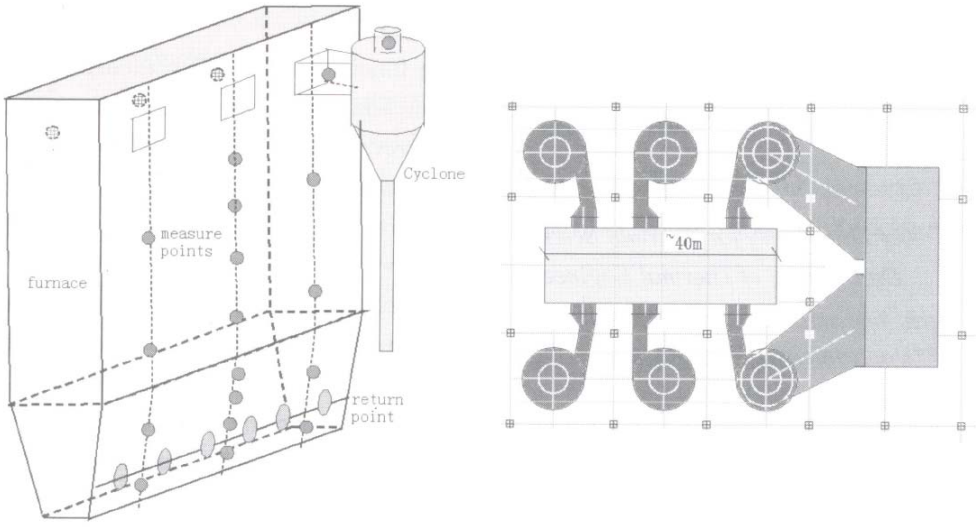

Figure 1-9. Layout of 600 MW_e CFB boiler [31].

Table 1-1. Operational conditions for 300 MW_e CFB boiler [31].

	u_g	m_s	Cyclone Pressure drop, Pa			g_s, kg/s		
Case	**m/s**	**kg**	**left**	**centre**	**right**	**left**	**centre**	**right**
1	0.67	30	333	345	335	0.19	0.21	0.2
2	0.97	30	1012	945	914	1.11	1.1	1.06
3	0.67	50	398	422	416	0.22	0.23	0.22
4	1.01	50	908	959	939	1.19	1.32	1.28
5	0.67	45	381	404	382	0.2	0.22	0.2
6	0.97	45	833	889	858	0.9	1	0.94

1.2.1.3. Bend Flow (Rope) and Flow Splitting

In power plants using large utility pulverized fuel (PF) coal-fired boilers for generation of electricity, the coal is pulverized in coal mills and then pneumatically transported and

distributed to a large number of burners (e.g. 30-40) circumferentially arranged in several rows around the burning chamber of the boiler [32]. In order to avoid the formation of NO_x, as well as lower the level of unburned carbon, it is essential to maintain homogeneous injection of the coal-air mixture into the furnace. This requires good control over the supply of the pulverized fuel (PF) to individual burners [33]. If the amount of fuel being supplied to each burner differs, some burners will exhibit incomplete combustion and produce harmful emissions such as carbon monoxide gases, while others will operate at optimum combustion conditions and some will burn inefficiently with excess air [34].

In reality, uniform distribution of PF through parallel burners rarely exists. The pneumatic pipelines that deliver PF from the mills to the burners from a complex pipe network include numerous bends and junctions. As the PF passes through a bend, the coal particles experience centrifuging actions due to its inertia forming a coal-dense mixture known as a rope downstream from the bend, as shown in Figure 1-10. Thus, the PF concentration becomes non-uniform over the pipe cross-section after the bends. This, subsequently, causes an uneven split of the PF flow at the bifurcation which acts to distribute the coal-air mixture to downstream burners [33].

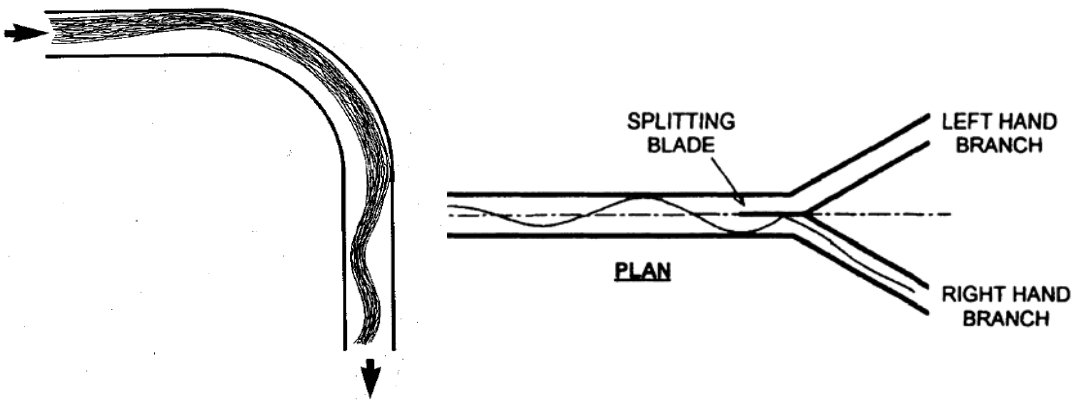

Figure 1-10. Rope like suspension and its effect on flow splitting [34, 35].

Giddings et al. [35] experimentally and numerically studied the splitting of gas-solids flow in connection with the uniformity of pneumatic injection of coal-air mixtures into power stations. For bifurcations the mass flow split varied from 42:58% to 49:51%, whereas at a trifurcation the split ranged from 16:26:58% to 17:38:45%.

Schneider et al. [32] studied a similar geometry, but with a riffle box added at the root of the split to make the downstream input more uniform. In Lagrangian tracking framework, they were unable to obtain a uniform split of particles among the branches. However, their results indicate that in the absence of particle roping, i.e. for a uniform suspension in the main pipe before the bifurcation, the distribution of flow through the parallel paths is uniform.

As presented in Figure 1-11, Kuan and Yang [33] found non-uniformities in computational fluid dynamic[1] predictions and particle image velocimetry[2] studies of gas-solid flow of conveyed gas-solid suspensions into a bifurcation. Although the gas flows were predicted to be almost equal for the two branches, they predicted 5.7 and 9.2% more solids flow to one leg than the other for 66 and 77 μm particles, respectively.

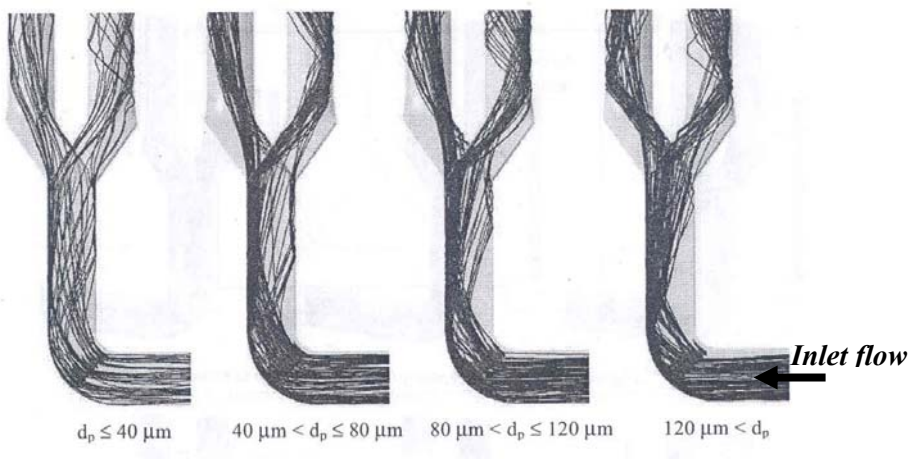

Figure 1-11. Location of different particles in parallel paths using PIV [33].

[1] CFD
[2] PIV

Some techniques have been proposed to make the distribution uniform. These methods are presented briefly in Chapter 4.

1.2.1.4. Parallel Channels inside Fluidized Beds

Bolthrunis et al. [36] describe difficulties which plagued early fluidized bed reactors designed and operated for the production of ethylene oxide by direct oxidation of ethylene, hydrocarbon synthesis via the Fischer-Tropsch process, and phthalic anhydride manufacture. In each of these cases, early reactors featured multiple open vertical heat transfer tubes of equal length and diameter, suspended within fluidized beds. It was intended that the fluidized suspension would pass uniformly through each of the parallel passages. However, in practice there was substantial and recurring mal-distribution. The description provided by the authors is instructive: "In some alternate paths the flow may be almost free of solids and friction losses may predominate; in others there may be almost no gas flow and static head losses prevail. The system is inherently unstable. In extreme cases, some tubes will plug with solids and others will operate with high velocity and low catalyst loading. In a situation where the tubes also act as a heat exchanger, the rate of heat removed will be neither stable nor predictable." Evidently, early operators experienced serious problems associated with parallel chambers and learned empirically to avoid such configurations. No amount of correcting what could have been small differences between the various flow paths was able to avoid the non-uniformity. Only by adopting tubes with the coolant inside, so that the fluidized particles circulated outside, rather than the inside, the tubes, were the operators able to solve the serious non-uniformity problem that existed with the parallel paths in these processes [18].

Boyd et al. [38] encountered similar problems when operating an internally circulating fluidized bed, where parallel vertical membrane panels were suspended within a draft box to create a series of parallel equal vertical slots through which gas and particles were intended to circulate equally, producing hydrogen by catalytic steam methane reforming (Figure 1-12). In practice, some slots experienced much more flow than others, with the result that the overall performance suffered and operation was difficult. Boyd et al. [38]

proposed a method and examined it experimentally to achieve a uniform distribution through the parallel channels. This method is presented in Chapter 4.

Consequences of Non-Uniformity: The major effects of non-even distribution of flow though identical parallel paths can be summarized as follows:

- Decreased overall cyclone efficiency
- Non-uniform return flow to the base can cause sub-optimal reactor performance
- Differential erosion
- Differential fouling
- More frequent shutdowns
- Sub-optimal and unbalanced heat transfer
- Need for mechanical valve in return lines (in order to control the process)

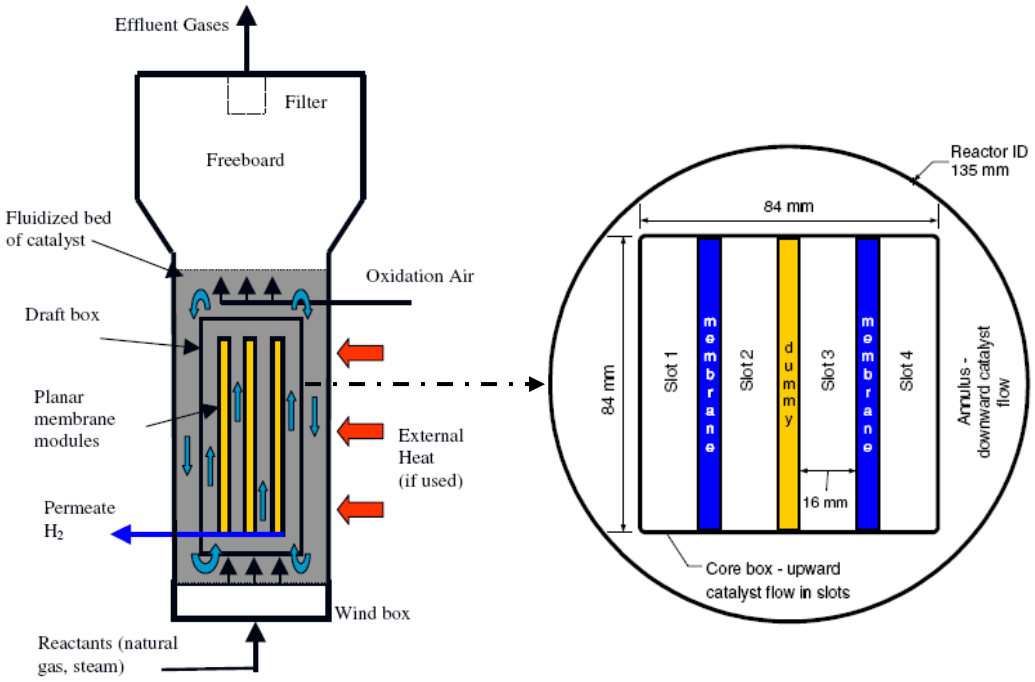

Figure 1-12. Internal circulating fluidized bed membrane reactor with internal parallel channels [37].

1.2.2. Analytical Results

No major focused analysis has been done on mal-distribution of gas-solid flow through identical parallel pipes and from the analytical point of view, only two papers of Grace et al. [18, 29] are available.

1.2.2.1. Degrees of Freedom

Based on the simple analysis performed by Grace [29], in order to understand the above fluid mechanics phenomenon, consider N identical parallel paths (e.g. cyclones or pipes) where each is constructed so that it should have an equal probability of gas and particle entry. Let the total mass flow rate of solids to the complete array of N paths be m_{st} and the total mass flow rate of gas be m_{gt}. It is then evident that mass balances on the solids and gas yield:

$$m_{st} = \sum_{i=1}^{N} m_{si} \tag{1-1}$$

$$m_{gt} = \sum_{i=1}^{N} m_{gi} \tag{1-2}$$

In addition to satisfying overall mass balances, the flows through the different parallel paths are subject to the constraint that the pressure drop from the top of the riser to the exit should be identical for all N paths. Hence we may write

$$\Delta P_1 = \Delta P_2 = \ldots = \Delta P_i = \ldots = \Delta P_N \tag{1-3}$$

Equations (1-1), (1-2) and (1-3) are the constraints that must be satisfied by the flows through the N cyclones in parallel. Clearly the equal pressure drop condition, equation (1-3), is satisfied if each of the cyclones is subject to identical gas and solids flows. However, this condition is not unique, and it may not be a stable solution.

Elsewhere [18], it is shown that for two cyclones in parallel (N = 2) with a two-phase (gas-solids) flow, the number of unknowns exceeds the number of equations by 1, meaning that there can be an infinite number of solutions that satisfy the mass balance and pressure drop constraints. For the more general case of N paths (or cyclones) in parallel, there are N values of m_{si} and N values of m_{gi}, i.e. $2N$ unknowns. On the other hand, there is one overall solids mass-flow balance, one overall gas mass-flow balance, and (N – 1) independent pressure drop equality equations, for a total of (N + 1) constraints. Hence, with $2N$ unknowns and (N +1) constraints, there are (N – 1) degrees of freedom. This means that for a single path (cyclone) there are no degrees of freedom, as is obvious. For two cyclones in parallel and two phases, as noted earlier [18], there is one degree of freedom (one more variable than equation to be satisfied). As indicated in Table 1-2, the number of degrees of freedom grows as the number of parallel paths increases.

Table 1-2. Degree of freedom for two phase flow through identical parallel paths [29].

***N*= number of paths**	***2N*= number of unknowns**	***N+1*= number of constraints**	**N-1= number of degree of freedom**
1	2	2	0
2	4	3	1
3	6	4	2
4	8	5	3
6	12	7	5
8	16	9	7
12	24	13	11

Now consider the question of whether the (commonly assumed) uniform distribution should be expected to be the actual flow distribution. One can approach this matter in at least two ways: ‘Energy Minimization’ and ‘Stability’.

1.2.2.2. Energy Minimization [18]

To simplify the problem, consider first two cyclones in parallel, paths 1 and 2. We can write:

$$m_{g1} + m_{g2} = m_{gt} \tag{1-4}$$

$$m_{s1} + m_{s2} = m_{st} \tag{1-5}$$

Let

$$m_{g1} = (0.5 + \alpha) m_{gt} \tag{1-6}$$

so that

$$m_{g2} = (0.5 - \alpha) m_{gt} \tag{1-7}$$

When α>0, there is more gas flow to branch 1, whereas for α<0, there is a disproportionate flow of gas to branch 2.

Let

$$m_{s1} = (m_{st} / 2) + \Delta m_s \tag{1-8}$$

so that

$$m_{s2} = (m_{st} / 2) - \Delta m_s \tag{1-9}$$

Positive Δm_s means that more solids go to branch 1, whereas negative Δm_s corresponds to a greater proportion of the particles passing through branch 2.

We require that the pressure drops through the two cyclones be equal, i.e.

$$\Delta P_1 = \Delta P_2 \tag{1-10}$$

The expression similar to the one proposed by Chen and Shi [39] applied in Chapter 3, can be chosen at this stage to model the pressure drop through the cyclones:

$$\Delta P_i = C m_{gi}^{\ 2} + K f(m_{si}) \tag{1-11}$$

where C and K are constants and $f(m_{si})$ is a function giving dependence of cyclone pressure drop on solid mass flow rate. Utilizing the above expression, substituting equations (1-6) to (1-9) and rearranging, one obtains

$$\alpha = \frac{K}{2C m_{gt}^{\ 2}} \left\{ f(\frac{m_{st}}{2} - \Delta m_s) - f(\frac{m_{st}}{2} + \Delta m_s) \right\} \tag{1-12}$$

It is of interest to see how the total pressure drop varies as α and Δm_s vary from 0. If we let $m_{gi} = m_{g1}$ and $m_{si} = m_{s1}$, then substitute for m_{g1} and m_{s1} from Equations (1-6) and (1-7), and take the first term of the Taylor series expansion of $f(m_{st} + \Delta m_s)$, one finds

$$\Delta P = C(0.25 + \alpha + \alpha^2) m_{gt}^{\ 2} + K f(\frac{m_{st}}{2}) + K \Delta m_s \left. \frac{df}{dm_s} \right|_{m_{st}/2} \tag{1-13}$$

If one now replaces the derivative in the last term with the aid of equation (1-12), it can be shown that

$$\Delta P = C(0.5 m_{gt})^2 + K f(\frac{m_{st}}{2}) + C\alpha^2 m_{gt}^{\ 2} \tag{1-14}$$

But the first two terms are simply the pressure drop, which we can call ΔP_0, that we would have for the equal distribution case, i.e., for $m_{g1} = m_{g2} = 0.5 m_{gt}$ and $m_{s1} = m_{s2} = 0.5 m_{st}$. That is

$$\Delta P = \Delta P_0 + C\alpha^2 m_{gt}^{\ 2} \tag{1-15}$$

Since C, α^2 and $m_{gt}^{\ 2}$ must all be positive, then the final term must also be positive. As a result, the pressure drop for the uniform distribution case is a minimum, and each of the other solutions of the governing equations results in a total pressure drop through the pair of cyclones greater than for the base (uniform distribution) case.

Li and Kwauk [40] argue that flowing physical systems are likely to approach an extremum in practice, where they, for example, minimize or maximize the rate of dissipation of potential energy. For the $N = 2$ case, it has been shown that the uniform distribution results in a minimum pressure drop. One would expect that the pressure drop would again be minimized for $N > 2$ by having equal flow through each parallel path. Since, as shown above, the two flows in practice end up, at least in some cases, being non-uniform, one must assume that minimization of the rate of energy dissipation is not always applicable for flow through multiple cyclones.

1.2.2.3. Stability and Symmetry Breaking

There are many non-linear problems in engineering where there are multiple steady states and associated complexity and bifurcation phenomena (e.g. see Elnashaie and Grace [27]). These problems typically give rise to multiple solutions of the governing equations, some of which are stable and others unstable. Instability in this case means that if one introduces a small perturbation to a solution, the system will move away from that solution; stability means that a perturbation will set up dynamics that will return the system to the solution from which it has been perturbed.

For flow through parallel cyclones, uniformity of flow is clearly a solution as noted above, but is it a stable solution? Given the geometric symmetry, for every solution on one side of the uniform-flow solution there is a corresponding solution on the other side. This suggests that the (central) uniform-flow solution is an even one.

Based on above approach, Grace [29] suggested that it is likely that the uniform solution is an unstable steady state solution. If this it true, then no matter how perfectly symmetric the geometry and however uniform the distribution of incoming solids feed and incoming gas, the resulting flow in practice will end up being non-uniformly distributed, since any gas-solid system will always be subject to appreciable perturbations, e.g. originating from compressor pulsations and random variations in solids feed. These perturbations will cause the system to migrate to a stable steady state, on one side or the other of the

(unstable) uniform flow solution. Figure 1-13 shows a very simple analogue in which perturbations readily convert an unstable steady state solution into one of two stable steady states.

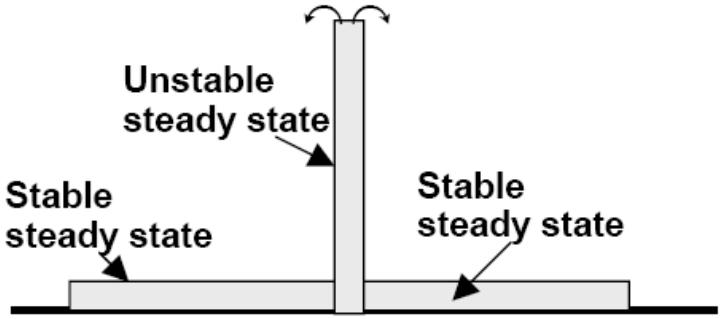

Figure 1-13. Stability representation [29].

Correspondingly, a fundamental Physics phenomenon related to the stability of our case study is 'Symmetry Breaking'. Symmetry Breaking describes a phenomenon where (infinitesimally) small fluctuations acting on a chaotic system crossing a critical point decide a system's fate, by determining which branch of a bifurcation is taken (Figure 1-14). For an outside observer unaware of the fluctuations (the "noise"), the choice appears arbitrary. This process is called symmetry breaking, because such transitions usually bring the system from a disorderly state into one of two more ordered, less probable states. Since disorder is more stable in the sense that small variations to it do not change its overall appearance, the symmetry is broken [42]. Based on this phenomenon and the elements of the system being considered (turbulent flow, non-linear system/multiphase flow and bifurcation), it appears that there are some similarities between the components of our case study and this fundamental concept. In other words, based on the Grace [29] interpretation, the system would have a stable non-uniform distribution solution as the system's fate.

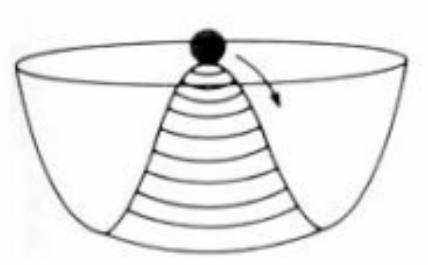

Figure 1-14. Unstable symmetry.

Therefore, instability analysis is needed in order to determine whether or not the uniform distribution solution is a stable one and the stability of other solutions. Instability analysis is performed with the approach and results are presented in Chapter 2.

1.3. MOTIVATION

As mentioned above, although several studies (mathematical and experimental) have been undertaken on the distribution of gas-liquid flow through identical parallel paths, very little focused and fundamental analysis has been reported for gas-solid systems. Given the problems encountered in several gas-solid industrial units, it is necessary to perform a fundamental mathematical/experimental study on the distribution of gas-solid flow through identical parallel paths.

It should also be pointed out that almost no numerical analysis has been done on multi-phase flow through identical parallel paths (even in gas-liquid systems). Therefore it would be interesting to discover whether CFD is a good tool for prediction or representation of stability of such flows.

1.4. OBJECTIVES

The objectives of the current research can be summarized as:

- Chapter 2: To obtain a fundamental understanding of distribution of gas-solid flow through identical parallel paths (Analytical and CFD);
- Chapter 3: To investigate the distribution of gas-solid flow through identical parallel cyclones (Modeling and Experimental);
- Chapter 4: To investigate different possible methods of improving the uniformity of the flow distribution.

Chapter 2. FLOW THROUGH IDENTICAL PARALLEL PIPES

To begin the understanding of mal-distribution of gas-solid flow through identical parallel paths, a simple 'Y branch' geometry is chosen. From this fundamental understanding, more complex systems can be developed involving multiple parallel paths. The chapter begins with analytical modeling and stability analysis of gas-solid distribution through identical vertical parallel paths. It is then continued with numerical modeling of a similar system and comparison between the two approaches.

2.1. MODELING – ANALYTICAL APPROACH

2.1.1. Force Acting on a Single Particle in a Gas Stream

The basic particle dynamic equations contain a number of different terms: drag force, pressure gradient interaction, acceleration of the apparent mass of the particle relative to the fluid, Basset history term accounting for the deviation of the flow from steady flow, and external forces such as those due to gravity, electrical and magnetic fields. A number of researchers [55 to 58] have addressed this dynamic equation.

For pneumatic transport, a practical approach to the dynamic equation is to employ an all-encompassing frictional term. For single particle analysis consider the drag and external force as the dominant forces counterbalancing the mass times acceleration, as presented in Figure 2-1. One can then write:

$$m_s \frac{du_s}{dt} = F_{drag} - F_{external} \qquad (2\text{-}1)$$

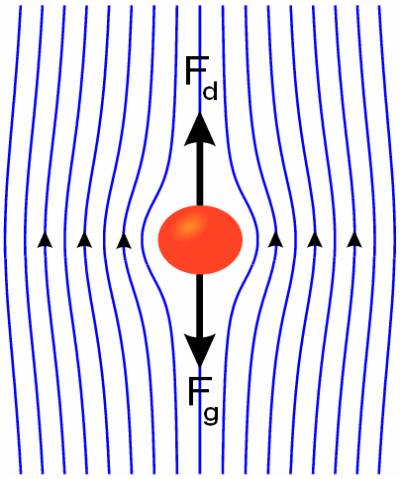

Figure 2-1. Motion of single particle in a gas stream.

The drag force for a single spherical particle can be written:

$$F_{drag} = \frac{3\rho_g m_s C_{D\infty}}{4\rho_s D_s}(u_g - u_s)\left|u_g - u_s\right| \tag{2-2}$$

Magnetic field effects are neglected here. The external forces due to gravity and electrical fields are

$$F_{gravity} = (m_s - m_g)g \tag{2-3}$$

$$F_{electrostatics} = E(\frac{q}{m_s})m_s \tag{2-4}$$

In the above expressions

u_s: particle velocity, m/s

u_g: gas velocity in the voids or velocity of porosity wave, m/s

ρ_g: gas density, kg/m^3

ρ_s: solid density, kg/m^3

$C_{D\infty}$: drag coefficient of single particle at infinite dilution, -

m_s: mass of particle of diameter D_s, kg

m_g: mass of displaced fluid, kg

g: gravitational acceleration, m/s^2

E: electrical field, N/C

q: charge on particle, C

2.1.2. Multiple Particle Systems – Governing Equations for 1-D Two-Phase Flow in a Single Pipe

Systems with multiple particles can be very complex. One could treat each particle-particle interaction together with all particle-wall interactions and arrive at a model that could predict the behaviour of pneumatic transport of many particles under a variety of conditions. In this work, a more pragmatic approach is utilized to develop the multi-particle system along the lines of a single particle system. The equations for the particles and for the transporting fluid are considered separately and together.

Consider an element of length dL containing a number of solid particles as shown in Figure 2-2. For most cases in vertical pneumatic conveying, the radial particle concentration distribution is nearly uniform and gas and solids can be reasonably treated as a first approximation, as being in one-dimensional flow [99]. Consider the simplest Lagrangian trajectory momentum transfer equation for one-dimensional pneumatic conveying of a stream of solids:

$$\Delta m_s \frac{du_s}{dt} = F_{drag} + F_{pressure,s} + F_{gravity,s} + F_{frictioon,s} + F_{electrostatic} \tag{2-5}$$

Comparing this with equation (2-1) for a single particle, we find a term for friction. This frictional term represents the total effects of particle-boundary bombardments.

The gas phase is considered to be incompressible. Application of the linear momentum equation to the gas then yields

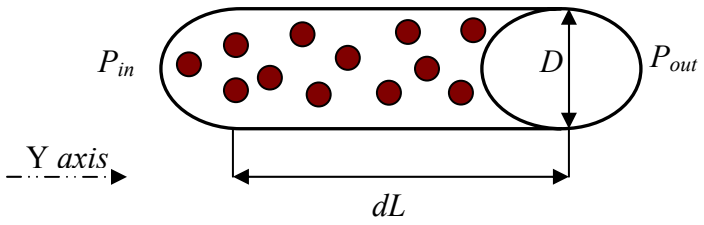

Figure 2-2. Volume element with a number of solid particles.

$$\Delta m_g \frac{du_g}{dt} = F_{drag} + F_{pressure,g} + F_{gravity,g} + F_{frictioon,g} \tag{2-6}$$

Note that Δm_s and Δm_g are the masses of particles and fluid, respectively, within the small control volume.

For this study, the effects of electrostatic force on the particle motion are ignored. Since the solid density is much greater than that of the gas, the added mass effect and Basset force can be neglected [76]. Also the Saffman shear lift force is neglected. The expressions for each of the differential forces must be supplied in order to complete the picture:

$$F_{drag} = \frac{-3\rho_g \Delta m_s C_{D\varepsilon}}{4\rho_s D_s}(u_g - u_s)\left|u_g - u_s\right| \tag{2-7}$$

where $C_{D\varepsilon}$ is a drag coefficient on a single particle corresponding to a voidage of ε, D_s is the average particle diameter (with all particles assumed to be spherical), ρ_g and ρ_s are the gas and solid densities, and u_g and u_s are the gas and solid velocities in the control volume. It should be noted that this drag force acts in the opposite direction on the fluid phase. Therefore there is always equilibrium between the solids and gas drag forces.

Our case study is carried out in an intermediate Reynolds number region ($0.2<Re_s<750$). The drag coefficient empirical expression proposed by Wang et al. [59], a widely-applied

mathematical expression in pneumatic conveying of particles, can be used to approximate $C_{D\infty}$ of single particles at infinite dilution (i.e. ε=1):

$$C_{D\infty} = \frac{24}{\mathrm{Re}_s}(1 + 0.15\,\mathrm{Re}_s^{\,0.687}) \tag{2-8}$$

For mobile particles, Wen and Yu [60] assumed that ($C_{D\varepsilon}/C_{D\infty}$) is dependent only on voidage. By correlating the results in fluidization and sedimentation empirically, they proposed the following relationship for estimating the effect of voidage on drag coefficient for mobile particles:

$$C_{D\varepsilon} = \varepsilon^{-4.7} C_{D\infty} \tag{2-9}$$

where ε is the volumetric void fraction. By using the Wang et al. expression for the drag of a single particle, equation (2-9) is applicable for Reynolds numbers up to 1000, the limit of applicability of equation (2-8). In pneumatic conveying, drag on a mobile particle is more relevant than drag on a fixed particle. Equation (2-9) is useful in estimating particle drag coefficients in pneumatic conveying [60]. It should be pointed out that in equation (2-9), the effect of fluid turbulence is ignored.

For vertical motion[1], the gravity term is given by:

$$F_{gravity,s} = -\Delta m_s g \tag{2-10}$$

For the solid friction and pressure forces

[1] For horizontal flow, other practitioners have used a lift term for the particles which can be expressed as $\rho_s(1-\varepsilon)gu_t/u_g$ where u_t is the particle settling velocity in a cloud [61].

$$F_{friction,s} = -\frac{2 f u_s^{\,2} \Delta m_s}{D} \tag{2-11}$$

$$F_{pressure,s} = (-\frac{\partial P}{\partial L})\frac{\Delta m_s}{\rho_s} \tag{2-12}$$

where *f is* the solid Fanning friction factor and *D* is the pipe inner diameter. The form of the solid frictional term follows the general frictional force in fluid mechanics. Various expressions for frictional factor in equation (2-11) from the literature can be found in Table 2-1. The widely-applied correlation proposed by Konno and Saito [66] is used in this study.

Table 2-1. Friction factor correlations.

Investigator	**Solids friction factor, *f***
Stemerding [62]	0.003
Reddy and Pei [63]	$0.046u_s^{-1}$
Van Swaaij et al. [64]	$0.08u_s^{-1}$
Capes and Nakamura [65]	$0.048u_s^{-1.22}$
Konno and Saito [66]	$0.0285\sqrt{gD}u_s^{-1}$
Yang (vertical) [67]	$0.00315\frac{1-\varepsilon}{\varepsilon^3}\left(\frac{(1-\varepsilon)u_{t0}}{\frac{u_g}{\varepsilon}-u_s}\right)^{-0.979}$
Yang (horizontal) [68]	$0.0293\frac{1-\varepsilon}{\varepsilon^3}\left(\frac{(1-\varepsilon)\frac{u_g}{\varepsilon}}{\sqrt{gD}}\right)^{-1.15}$
Stegmaier [69]	$0.52\mu^{-0.3}Fr^{-1}Fr^{*0.25}(D_s/D)^{-0.1}$
Mathur and Klinzing [70]	$0.395(\frac{u_g}{\varepsilon}-u_s)^{-1.65}$

For the fluid phase the differential terms are:

$$F_{gravity,g} = -\Delta m_g g \tag{2-13}$$

$$F_{friction,g} = -\frac{2 f_L u_g{}^2 \Delta m_g}{D} \tag{2-14}$$

$$F_{pressure,g} = (-\frac{\partial P}{\partial L})\frac{\Delta m_g}{\rho_g} \tag{2-15}$$

where f_L is the gas Fanning friction factor. In the majority of pneumatic transport systems, the flow is in the turbulent regime. Thus the basic friction factor found in single phase flow in pipes is employed to represent the energy loss for the transport gas. A number of different expressions could be used for this gas flow. However, the Koo equation [77] has been recommended by Klinzing [71]:

$$f_L = 0.0014 + 0.125\,\mathrm{Re}^{-0.32} \tag{2-16}$$

The differential masses of particles and fluid can be written respectively as

$$\Delta m_s = (1-\varepsilon)\rho_s \Delta V = (1-\varepsilon)\rho_s A dL \tag{2-17}$$

$$\Delta m_g = \varepsilon \rho_g \Delta V = \varepsilon \rho_g A dL \tag{2-18}$$

Combining these terms results in the basic dynamic equations for the multi-particle analysis. If the linear momentum equation is applied to the differential volume of length ΔL inside the vertical column of constant cross-sectional area, it can be shown that [by combination of equations (2-5) and (2-6)]

$$\frac{-\Delta P}{\Delta L} = \frac{P_{in} - P_{out}}{\Delta L} = \rho_g \varepsilon g + \rho_s (1-\varepsilon) g + \frac{2 f \rho_s (1-\varepsilon) u^2{}_s}{D} + \frac{2 f_L \rho_g \varepsilon u^2{}_g}{D} + (1-\varepsilon)\rho_s \frac{du_s}{dt} + \varepsilon \rho_g \frac{du_g}{dt} \tag{2-19}$$

The first two terms of the right side of this equation are static contributions, whereas the next two are due to wall friction, and the final two terms arise from acceleration. Generally the fluid gravity contribution can be ignored relative to the solid static term. It should be mentioned that a few other formulations exist to describe the overall dynamic energy loss sum in terms of the pressure drop [66]. For example, Govier and Aziz [72] used the mechanical energy balance to arrive at a somewhat similar representation. The hydrostatic term is the same. However, an additional factor due to the kinetic energy term is separated from the frictional term. Weber [61] also presented a similar formulation.

Substituting all of the corresponding terms above into equation (2-19) yields after some rearrangement:

$$\frac{P_{in} - P_{out}}{\Delta L} = \rho_g \varepsilon g + \rho_s (1-\varepsilon) g + 0.057 \sqrt{\frac{g}{D}} \rho_s (1-\varepsilon) u_s + \frac{0.0028 \rho_g \varepsilon u^2{}_g}{D} + \frac{0.25 \rho_g{}^{0.68} \mu^{0.32} \varepsilon u_g{}^{1.68}}{D^{1.32}} + (1-\varepsilon)\rho_s \frac{du_s}{dt} + \varepsilon \rho_g \frac{du_g}{dt} \tag{2-20}$$

Equation (2-20) is the basic equation utilized below to study the distribution of gas-solid flow through identical parallel vertical paths.

2.1.3. Governing Equations for 1-D Two-Phase Flow in Two Identical Vertical Parallel Pipes

Extending from a single channel to two vertical identical parallel channels at identical fluid and particle properties (Figure 2-3), we obtain the following transient equations for each path:

$$\frac{\Delta P_1}{\Delta L} = \frac{P_{in} - P_{out}}{\Delta L} = \rho_g \varepsilon_1 g + \rho_s (1-\varepsilon_1) g + 0.057\sqrt{\frac{g}{D}}\rho_s (1-\varepsilon_1) u_{s1} + \frac{0.0028\rho_g \varepsilon_1 u^2{}_{g1}}{D} + \frac{0.25\rho_g{}^{0.68}\mu^{0.32}\varepsilon_1 u_{g1}{}^{1.68}}{D^{1.32}} + (1-\varepsilon_1)\rho_s \frac{du_{s1}}{dt} + \varepsilon_1 \rho_g \frac{du_{g1}}{dt} \quad (2\text{-}21)$$

$$\frac{\Delta P_2}{\Delta L} = \frac{P_{in} - P_{out}}{\Delta L} = \rho_g \varepsilon_2 g + \rho_s (1-\varepsilon_2) g + 0.057\sqrt{\frac{g}{D}}\rho_s (1-\varepsilon_2) u_{s2} + \frac{0.0028\rho_g \varepsilon_2 u^2{}_{g2}}{D} + \frac{0.25\rho_g{}^{0.68}\mu^{0.32}\varepsilon_2 u_{g2}{}^{1.68}}{D^{1.32}} + (1-\varepsilon_2)\rho_s \frac{du_{s2}}{dt} + \varepsilon_2 \rho_g \frac{du_{g2}}{dt} \quad (2\text{-}22)$$

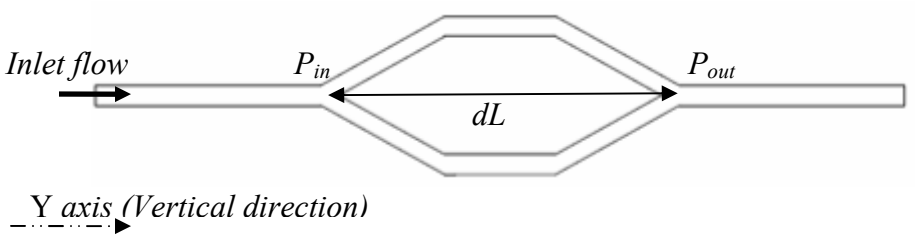

Figure 2-3. Schematic of two identical vertical parallel paths.

2.1.3.1. Steady-State Solution

If one considers only the steady state so that the time-derivative terms are ignored, and assuming an equal pressure drop in both channels [$\Delta P_1 = \Delta P_2$ in equation (2-21) and (2-22)], one obtains:

$$\rho_g g(\varepsilon_1 - \varepsilon_2) + \rho_s g(\varepsilon_2 - \varepsilon_1) + 0.057\sqrt{\frac{g}{D}}\rho_s \left(u_{s1}(1-\varepsilon_1) - u_{s2}(1-\varepsilon_2)\right) + \frac{0.0028\rho_g}{D}(\varepsilon_1 u^2{}_{g1} - \varepsilon_2 u^2{}_{g2}) + \frac{0.25\rho_g{}^{0.68}\mu^{0.32}}{D^{1.32}}(\varepsilon_1 u_{g1}{}^{1.68} - \varepsilon_2 u_{g2}{}^{1.68}) = 0 \quad (2\text{-}23)$$

In addition, gas and solids continuity give volumetric flow rate of

$$Q_{g1} = \gamma Q_{gt} = A\varepsilon_1 u_{g1} \quad (2\text{-}24)$$

$$Q_{g2} = (1-\gamma)Q_{gt} = A\varepsilon_2 u_{g2} \tag{2-25}$$

$$Q_{s1} = \sigma Q_{st} = A(1-\varepsilon_1)u_{s1} \tag{2-26}$$

$$Q_{s2} = (1-\sigma)Q_{st} = A(1-\varepsilon_2)u_{s2} \tag{2-27}$$

where γ and σ are the fractions of the gas and solids flows, respectively, passing through channel 1. Note that for a uniform distribution of gas and solids γ=σ=0.5.

Yang [67] determined the various parts of the steady-state dynamic equation of the particle, and obtained the particle velocity as:

$$u_s = u_g - u_{t0}\left(1+\frac{2fu_s^{\ 2}}{gD}\varepsilon^{4.7}\right)^{0.5} \tag{2-28}$$

Applying Yang's correlation for two identical parallel vertical paths yields:

$$u_{s1} = u_{g1} - u_{t0}\left(1+\frac{0.057u_{s1}\varepsilon_1^{\ 4.7}}{\sqrt{gD}}\right)^{0.5} \tag{2-29}$$

$$u_{s2} = u_{g2} - u_{t0}\left(1+\frac{0.057u_{s2}\varepsilon_2^{\ 4.7}}{\sqrt{gD}}\right)^{0.5} \tag{2-30}$$

where u_{t0} is the single particle settling (or terminal) velocity in an undisturbed fluid.

The equations for two parallel paths are summarized in Table 2-2. Equations (2-23) to (2-27), (2-29) and (2-30) constitute seven non-linear algebraic equations, but there are eight unknowns (γ, σ, u_{g1}, u_{s1}, ε_1, u_{g2}, u_{s2} and ε_2). Hence there is one extra degree of freedom (as pointed out in Chapter 1), unless we can invoke an extra condition, such as pressure drop minimization. Note, however, that the uniform condition (where $\gamma = \sigma =$

0.5; $u_{g1} = u_{g2}$; $u_{s1} = u_{s2}$; and $\varepsilon_1 = \varepsilon_2$) satisfies all seven equations and hence always represents one solution. Whether this solution is stable or unstable is considered below.

Table 2-2. System of equations for distribution of gas-solid through two parallel paths.

Expression	Equation No.
$\rho_g g(\varepsilon_1-\varepsilon_2)+\rho_s g(\varepsilon_2-\varepsilon_1)+0.057\sqrt{\frac{g}{D}}\rho_s\left(u_{s1}(1-\varepsilon_1)-u_{s2}(1-\varepsilon_2)\right)$ $+\frac{0.0028\rho_g}{D}(\varepsilon_1 u^2{}_{g1}-\varepsilon_2 u^2{}_{g2})+\frac{0.25\rho_g{}^{0.68}\mu^{0.32}}{D^{1.32}}(\varepsilon_1 u_{g1}{}^{1.68}-\varepsilon_2 u_{g2}{}^{1.68})=0$	(2-23)
$Q_{g1}=\gamma Q_{gt}=A\varepsilon_1 u_{g1}$	(2-24)
$Q_{g2}=(1-\gamma)Q_{gt}=A\varepsilon_2 u_{g2}$	(2-25)
$Q_{s1}=\sigma Q_{st}=A(1-\varepsilon_1)u_{s1}$	(2-26)
$Q_{s2}=(1-\sigma)Q_{st}=A(1-\varepsilon_2)u_{s2}$	(2-27)
$u_{s1}=u_{g1}-u_{t0}\left(1+\frac{0.057u_{s1}\varepsilon_1{}^{4.7}}{\sqrt{gD}}\right)^{0.5}$	(2-29)
$u_{s2}=u_{g2}-u_{t0}\left(1+\frac{0.057u_{s2}\varepsilon_2{}^{4.7}}{\sqrt{gD}}\right)^{0.5}$	(2-30)

Solution for one case study: In order to solve equations (2-23) to (2-27), (2-29) and (2-30), γ is chosen as a variable to be defined. We are then left with seven non-linear algebraic equations and seven unknowns (σ, u_{g1}, u_{s1}, ε_1, u_{g2}, u_{s2} and ε_2). A vertical cylindrical pipe is selected with a ΔL= 610 mm height and 38 mm diameter. Other operating conditions (constants of equations) are summarized in Table 2-3.

The iterative Newton-Raphson method was used to solve this set of equations. The convergence was highly sensitive to the initial guess for seven unknowns, because of non-linearity of the equations. After marching for different γ values (0 to 1), Table 2-4 was obtained.

Table 2-3. Defined operating conditions (20°C and 101.3 kPa).

Gas	
Type	Air
Density (kg/m^3)	1.225
Viscosity (kg/m.s)	1.79E-05
Inlet velocity (m/s)	20
Solids	
Type	Glass Beads
Density (kg/m^3)	2500
Particle size (μm)	30
Terminal velocity[1] (m/s)	0.68
Volume fraction, α_s (%)=1-ε	10

Table 2-4 represents all steady state gas-solid distribution solutions for the specific system defined through two vertical identical parallel pipes. Clearly, the equal distribution (γ=σ=0.5) is one solution, but other distributions also satisfy the equal pressure balance through the paths. In other words, this model predicts clearly that in addition to equal distribution of gas-solid flow through the parallel paths, many other non-uniform distributions (with different σ and γ values) of multi-phase flow through the different branches can satisfy the pressure drop and continuity requirements[2].

Figures 2-4 and 2-5 plot the data from Table 2-4. Figure 2-4 shows the effect of unequal distribution of gas-solid flow on the pressure drop of the system. The uniform distribution with exactly half of gas and half of solids flow passing through each of separate paths gives the lowest pressure drop, consistent with the predictions by Grace et al. [18], as presented in Chapter 1. Hence, if energy minimization is applicable, one might expect the uniform flow distribution to be the solution found in practice.

---

[1] Calculated from: $$u_{t0} = \left(\frac{4D_s(\rho_s - \rho_g)g}{3C_{D\infty}\rho_g} \right)^{0.5}$$

[2] Note that there is no solution for γ equal to 0 or 1. Physically, in these two conditions one of the paths will contain no gas (so there will be no pressure drop) and consequently, the entire gas flow will pass through the other branch (resulting in a pressure drop in that path). Therefore the pressure balance criterion cannot be satisfied. Also, considering γ=1, the denominator of equation (2-23) would be zero and the impossibility of this case is clear mathematically.

Although the penalty of mal-distribution of phases results in more energy consumption (higher pressure drop) for the system, the pressure drop difference between the uniform distribution and most of the non-uniform solutions is small. For example, the difference between the pressure drops of the uniform distribution and the γ=0.7 solution is only 4.5%. Therefore, based on empirical findings of mal-distribution of gas-solid systems presented in Chapter 1, it would appear the energy minimization may not be applicable, so that non-uniform distributions may be favoured in practice. Thus, instability analysis is needed to find whether or not the equal distribution is stable and the degree of stabilities of the other solutions.

Table 2-4. Steady state solutions of distribution of gas-solid flows through two vertical identical parallel pipes (ΔL= 610 mm, D=38 mm).

γ	σ	u_{g1} (m/s)	u_{s1} (m/s)	ε_1	u_{g2} (m/s)	u_{s2} (m/s)	ε_2	ΔP (Pa)
0.05	0.09	1.38	0.70	0.72	21.13	20.13	0.90	4427
0.10	0.19	2.59	1.89	0.77	19.89	18.90	0.91	4003
0.15	0.26	3.73	3.01	0.81	18.73	17.75	0.91	3737
0.20	0.32	4.83	4.09	0.83	17.61	16.64	0.91	3554
0.25	0.36	5.91	5.16	0.85	16.52	15.57	0.91	3425
0.30	0.39	6.98	6.20	0.86	15.44	14.51	0.91	3332
0.35	0.42	8.04	7.25	0.87	14.37	13.46	0.90	3266
0.40	0.45	9.10	8.28	0.88	13.31	12.42	0.90	3223
0.45	0.48	10.15	9.31	0.89	12.26	11.38	0.90	3197
0.50	0.50	11.20	10.35	0.89	11.20	10.35	0.89	3189
0.55	0.52	12.26	11.38	0.90	10.15	9.31	0.89	3197
0.60	0.55	13.31	12.42	0.90	9.10	8.28	0.88	3223
0.65	0.58	14.37	13.46	0.90	8.04	7.25	0.87	3266
0.70	0.61	15.44	14.51	0.91	6.98	6.20	0.86	3332
0.75	0.64	16.52	15.57	0.91	5.91	5.16	0.85	3425
0.80	0.68	17.61	16.64	0.91	4.83	4.09	0.83	3555
0.85	0.74	18.73	17.75	0.91	3.73	3.01	0.81	3737
0.90	0.81	19.89	18.90	0.91	2.59	1.89	0.77	4003
0.95	0.91	21.13	20.13	0.90	1.38	0.70	0.72	4427

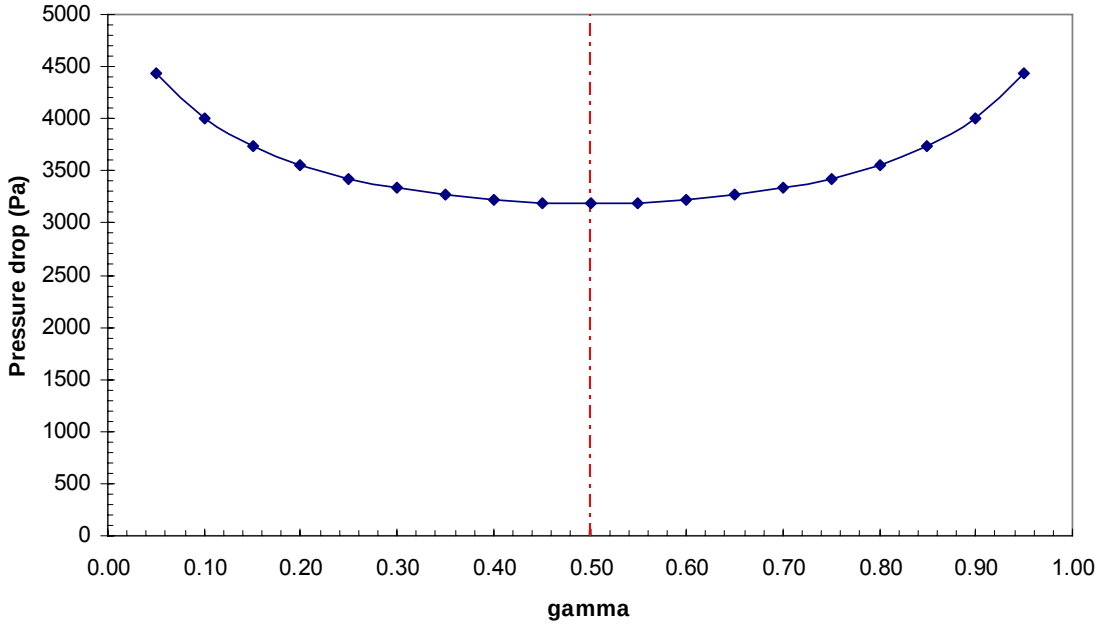

Figure 2-4. Effect of mal-distribution on pressure drop of the system for conditions in Table 2-3.

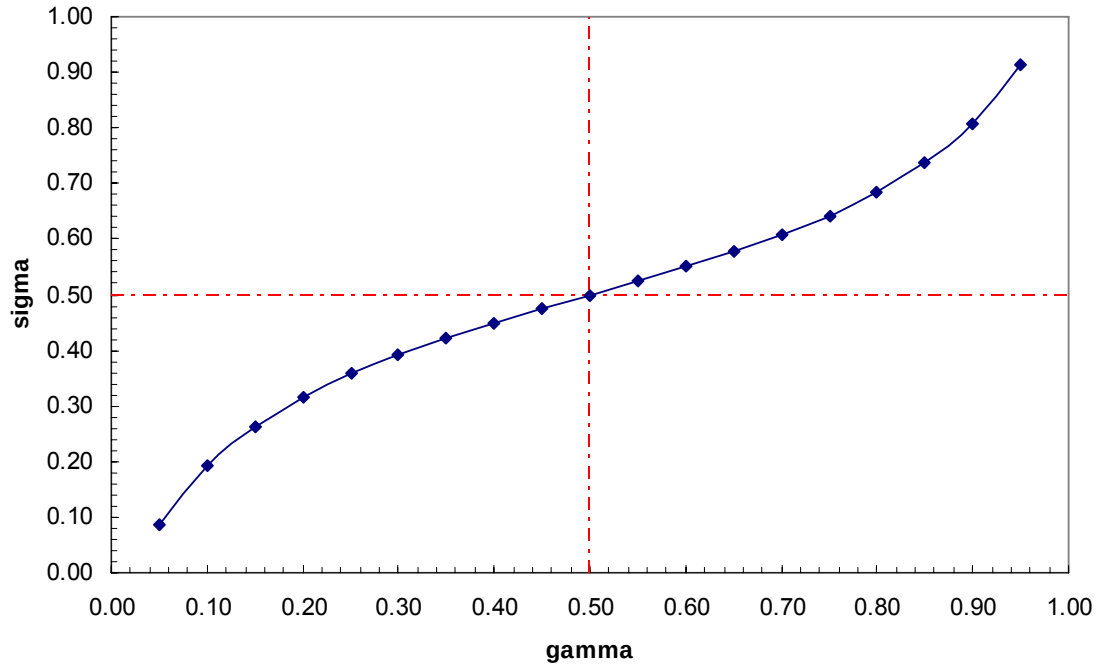

Figure 2-5. Relationship between gas and solids distribution parameters for steady-state solutions of governing equations for conditions in Table 2-3.

Figure 2-5 and Table 2-4 show that the branch with more gas and solids content also has higher gas and solid velocities than the branch with the lower flow. It is interesting to consider how the system can provide equal pressure drop in both branches when there is more gas and more solids in one branch than the other. Figures 2-6 and 2-7 help to provide the answer; Figure 2-6 represents the ratio of solid to gas flow rate in each pipe as a function of volumetric gas portion in branch 1. Consider the case where more flow is going to branch 1. Thus, according to Figure 2-6 by going far from equal distribution point (right hand side of γ=0.5), the solid-to-gas ratio in branch 1 is almost constant; however, the solid-to-gas ratio in branch 2 increases. In other words, as shown by Figure 2-7, in order to keep the pressure drop balance, the line with low gas and solids (branch 2) has lower volumetric void fraction (higher ratio of solid to gas) causing enough extra pressure drop to compensate for the higher velocities and flow rates, and hence higher frictional losses, in branch 1.

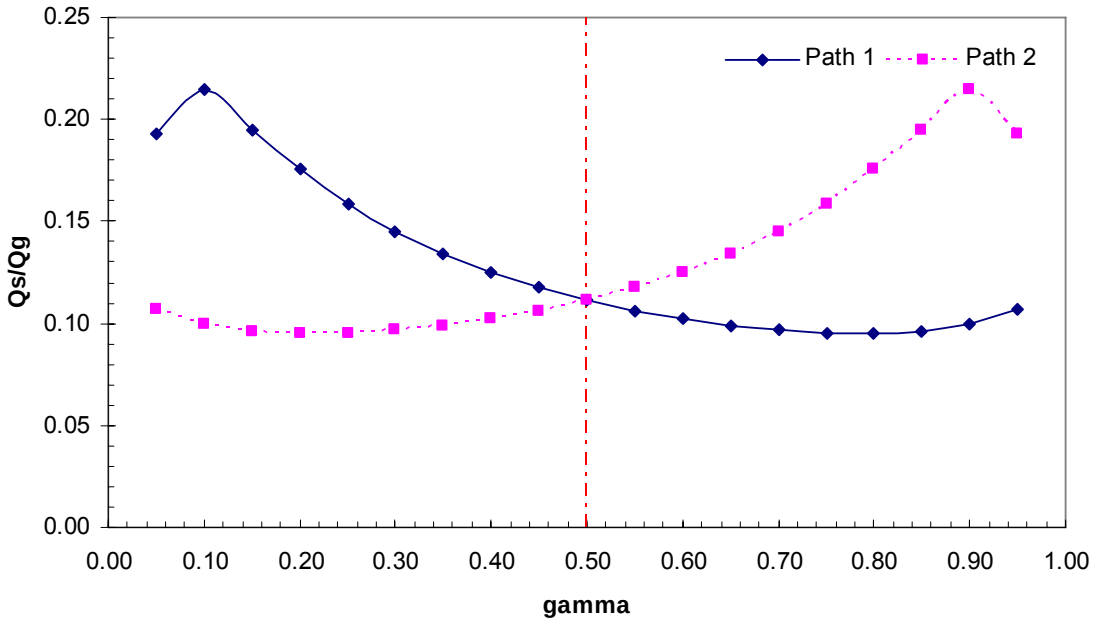

Figure 2-6. Solid distribution pattern for conditions in Table 2-3.

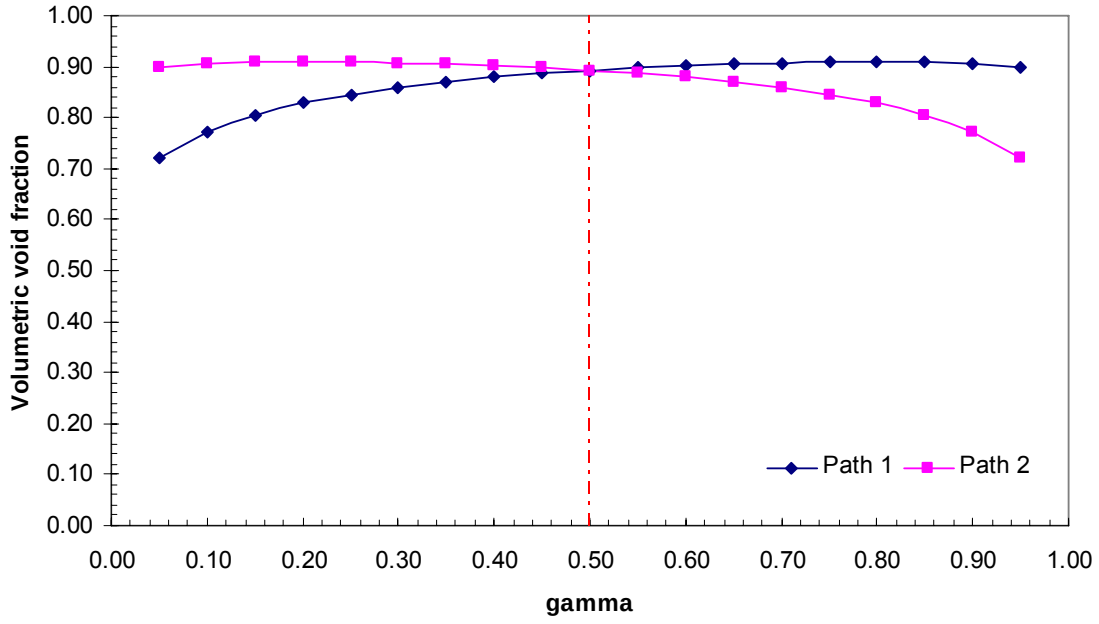

Figure 2-7. Voidage distribution pattern for conditions in Table 2-3.

2.1.4. Governing Equations for 1-D Two-Phase Flow in *N* Identical Vertical Parallel Pipes

Extension of equation (2-20) leads to an equation of motion for each of *N* vertical identical pipes in parallel is

$$\frac{-\Delta P_i}{\Delta L} = \frac{P_{in} - P_{out}}{\Delta L} = \rho_g \varepsilon_i g + \rho_s (1-\varepsilon_i) g + 0.057\sqrt{\frac{g}{D}}\rho_s (1-\varepsilon_i) u_{si} + \frac{0.0028\rho_g \varepsilon_i u^2{}_{gi}}{D} + \frac{0.25\rho_g{}^{0.68}\mu^{0.32}\varepsilon_i u_{gi}{}^{1.68}}{D^{1.32}} + (1-\varepsilon_i)\rho_s \frac{du_{si}}{dt} + \varepsilon_i \rho_g \frac{du_{gi}}{dt}, \quad i = 1...N \tag{2-31}$$

Based on the same approach as in Section 2.1.3.1, the system of equations for the steady-state motion of gas-solid flow through *N* parallel paths is summarized in Table 2-5.

Table 2-5. System of equations for distribution of gas-solid through *N* parallel paths.

Expression	Equation No.
$\rho_g g(\varepsilon_1-\varepsilon_2-...-\varepsilon_N)+\rho_s g(\varepsilon_N-\varepsilon_{N-1}-...-\varepsilon_1)+$ $0.057\sqrt{\frac{g}{D}}\rho_s\left(u_{s1}(1-\varepsilon_1)-u_{s2}(1-\varepsilon_2)-...-u_{sN}(1-\varepsilon_N)\right)+$ $\frac{0.0028\rho_g}{D}(\varepsilon_1 u^2{}_{g1}-\varepsilon_2 u^2{}_{g2}-...-\varepsilon_N u^2{}_{gN})+$ $\frac{0.25\rho_g{}^{0.68}\mu^{0.32}}{D^{1.32}}(\varepsilon_1 u_{g1}{}^{1.68}-\varepsilon_2 u_{g2}{}^{1.68}-...-\varepsilon_N u_{gN}{}^{1.68})=0$	(2-32)
$Q_{gi}=\gamma_i Q_{gt}=A\varepsilon_i u_{gi},\ i=1...N$	(2-33)
$Q_{si}=\sigma_i Q_{st}=A(1-\varepsilon_i)u_{si},\ i=1...N$	(2-34)
$u_{si}=u_{gi}-u_{t0}\left(1+\frac{0.057u_{si}\varepsilon_i{}^{4.7}}{\sqrt{gD}}\right)^{0.5},\ i=1...N$	(2-35)

As noted in Chapter 1, Grace et al. [18] analysed the degrees of freedom for a system of *N* parallel paths by considering the gas and solid mass balances. There are 2*N* unknowns and (*N*-1) constraints, so that the system with two phases and *N* parallel paths has (*N*+1) degrees of freedom. Therefore we could obtain an infinite number of solutions by choosing different parameters as degree of freedoms. Again equal distribution for each of the *N* paths clearly satisfies all the equations.

2.2. STABILITY ANALYSIS – ANALYTICAL APPROACH

A wide range of possible steady-state solutions can be obtained as discussed in the previous section. The uniform solution has a minimum pressure drop and consequently, it might be assumed that the system selects this solution. However, experimental investigations suggest that other distribution patterns may occur in practice. Therefore, it is important to investigate the stability of the steady-state solutions.

2.2.1. Linear Stability Analysis for a Single Pipe

For one-dimensional gas and solids flow we have:

$$Q_g = u_g A\varepsilon \tag{2-36}$$

$$Q_s = u_s A(1-\varepsilon) \tag{2-37}$$

We can also write

$$Q_g = kQ_s \tag{2-38}$$

where k is a flow coefficient. From the above expressions, it is possible to rearrange equation (2-20) as a function of solids flow rate. For the time-dependent terms of equation (2-20), one can obtain:

$$(1-\varepsilon)\rho_s \frac{du_s}{dt} + \varepsilon\rho_g \frac{du_g}{dt} = \frac{(1-\varepsilon)\rho_s}{A} \frac{d(\frac{Q_s}{(1-\varepsilon)})}{dt} + \frac{\varepsilon\rho_g}{A} \frac{d(\frac{kQ_s}{\varepsilon})}{dt} \tag{2-39}$$

All of the derivatives of equation (2-39) should be calculated one by one. Applying the chain rule for the right-hand side terms of equation (2-39) yields:

$$\frac{(1-\varepsilon)\rho_s}{A} \frac{d(\frac{Q_s}{(1-\varepsilon)})}{dt} = \frac{\rho_s}{A}\frac{dQ_s}{dt} + \frac{\rho_s Q_s}{A(1-\varepsilon)}\frac{d\varepsilon}{dt} \tag{2-40}$$

$$\frac{\varepsilon\rho_g}{A} \frac{d(\frac{kQ_s}{\varepsilon})}{dt} = \frac{\rho_g k}{A}\frac{dQ_s}{dt} - \frac{\rho_g kQ_s}{A\varepsilon}\frac{d\varepsilon}{dt} + \frac{\rho_g Q_s}{A}\frac{dk}{dt} \tag{2-41}$$

After substitution of the above expressions into equation (2-20), the final expression for the pressure drop of a single vertical pipe as a function of solid flow rate can be obtained as:

$$\frac{\Delta P}{\Delta L} = \frac{P_{in} - P_{out}}{\Delta L} = f(Q_s, \varepsilon, k) + (\frac{\rho_s + \rho_g k}{A})\frac{dQ_s}{dt} + (\frac{\rho_s Q_s}{A(1-\varepsilon)} - \frac{\rho_g k Q_s}{A\varepsilon})\frac{d\varepsilon}{dt} + \frac{\rho_g Q_s}{A}\frac{dk}{dt} \tag{2-42}$$

where $f(Q_s,\varepsilon,k)$ is given by:

$$f(Q_s, \varepsilon, k) = \rho_g \varepsilon g + \rho_s (1-\varepsilon) g + 0.057\sqrt{\frac{g}{D}}\frac{\rho_s}{A}Q_s + \frac{0.0028\rho_g k^2 Q^2{}_s}{DA^2\varepsilon} + \frac{0.25\,\mathrm{Re}^{-0.32}\,\rho_g k^2 Q_s{}^2}{DA^2\varepsilon} \tag{2-43}$$

As mentioned above, the idea of linearized stability analysis is to study the behaviour of the system by introducing a small perturbation to see whether it grows, remains unchanged or decreases exponentially with time. A linear stability analysis is next performed on the steady-state solutions.

Introducing a small perturbation in the solid flow rate, q_s, around the steady-state solution $Q_{s,0}$, and applying Taylor expansion for each term yields:

$$P_{in} = P_{in,0} + \frac{dP_{in}}{dQ_s}q_s \tag{2-44}$$

$$f(Q_s, \varepsilon, k) = f_0(Q_s, \varepsilon, k) + \frac{df(Q_s, \varepsilon, k)}{dQ_s}q_s \tag{2-45}$$

$$\frac{dQ_s}{dt} = \frac{d(Q_{s,0} + q_s)}{dt} = \frac{dq_s}{dt} \tag{2-46}$$

$$\frac{d\varepsilon}{dt} = \frac{d(\varepsilon_0 + \frac{d\varepsilon}{dQ_s} q_s)}{dt} = \frac{d\varepsilon}{dQ_s}\frac{dq_s}{dt} \tag{2-47}$$

$$\frac{dk}{dt} = \frac{d(k_0 + \frac{dk}{dQ_s} q_s)}{dt} = \frac{dk}{dQ_s}\frac{dq_s}{dt} \tag{2-48}$$

Here $P_{in,0}$, $f_0(Q_s, \varepsilon, k)$, $Q_{s,0}$, ε_0 and k_0 are the corresponding steady-state parameters. Also it is assumed that the effect of solid perturbation on output pressure (P_{out}) is negligible. After substitution of Taylor expanded terms into equation (2-42), the following equation for the perturbation variable q_s is obtained:

$$\frac{1}{\Delta L}\frac{dP_{in}}{dQ_s} q_s = \frac{df(Q_s, \varepsilon, k)}{dQ_s} q_s + T\frac{dq_s}{dt} \tag{2-49}$$

where

$$T = \left[(\frac{\rho_s + \rho_g k}{A}) + \left((\frac{\rho_s Q_s}{A(1-\varepsilon)} - \frac{\rho_g k Q_s}{A\varepsilon}) \frac{d\varepsilon}{dQ_s} \right) + \left((\frac{\rho_g Q_s}{A}) \frac{dk}{dQ_s} \right) \right] \tag{2-50}$$

Since $f(Q_s, \varepsilon, k)$ is a function of three variables, Q_s, ε and k, the chain rule yields:

$$\frac{df(Q_s, \varepsilon, k)}{dQ_s} = \frac{\partial f(Q_s, \varepsilon, k)}{\partial Q_s} + \frac{\partial f(Q_s, \varepsilon, k)}{\partial \varepsilon}\frac{\partial \varepsilon}{\partial Q_s} + \frac{\partial f(Q_s, \varepsilon, k)}{\partial k}\frac{\partial k}{\partial Q_s} \tag{2-51}$$

The first term on the right side of equation (2-51), $\frac{\partial f(Q_s, \varepsilon, k)}{\partial Q_s}$, can be obtained by differentiation. The same method can be used to calculate $\frac{\partial f(Q_s, \varepsilon, k)}{\partial \varepsilon}$ and $\frac{\partial f(Q_s, \varepsilon, k)}{\partial k}$,

but because of the complexity, numerical differentiation with a very small step size (δ) is also useful. Centric differentiation[1] can be used to calculate $\frac{\partial \varepsilon}{\partial Q_s}$ and $\frac{\partial k}{\partial Q_s}$.

An exponential model is considered for the perturbation parameter so that

$$q_s = \delta_s e^{\lambda t} \tag{2-52}$$

where δ_s is the perturbation amplitude and λ is a semi-eigenvalue (or growth factor). The sign of λ determines the stability of solution. For $\lambda<0$ the solution will be stable and the perturbation term will shrink and disappear as time passes. A more negative value of λ causes faster disappearance of the perturbation. At $\lambda=0$, the perturbation is neutral (i.e. it neither grows nor shrinks), but since the perturbation does not grow and it is assumed that the perturbation amplitude is very small, a system with $\lambda=0$ can be considered stable as well. On the other hand, for $\lambda>0$, q_s grows exponentially and the solution is unstable.

Substituting equation (2-52) into (2-49) and solving for the eigenvalue yields:

$$\lambda = \frac{\frac{dP_{in}}{dQ_s} - \Delta L \frac{df(Q_s, \varepsilon, k)}{dQ_s}}{\Delta L T} \tag{2-53}$$

For this case study, T is greater than zero. The condition for stability, $\lambda \le 0$ requires that

$$\frac{dP_{in}}{dQ_s} \le \Delta L \frac{df(Q_s, \varepsilon, k)}{dQ_s} \tag{2-54}$$

[1] Centric differentiation (three point estimation) is one of the numerical differentiation methods as follow:

$$f'(x) = \frac{f(x+h) - f(x-h)}{2h}$$

More generally:

$$f'(x) = \frac{f(x+h_2) - f(x-h_1)}{h_1 + h_2}$$

Based on equation (2-42), since $f(Q_s, \varepsilon, k)$ is equal to the steady-state pressure drop of the system divided by ΔL, the above condition is always satisfied for a single pipe and the system is always stable.

2.2.2. Linear Stability Analysis for Two Identical Vertical Parallel Pipes

A similar approach is followed for two parallel channels. Based on equations (2-21) and (2-22), considering two vertical pipes and perturbing the solid flow rates yield:

$$\frac{dP_{in}}{dQ_{st}}(q_{s1}+q_{s2})-\Delta L\frac{df_1(Q_{s1},\varepsilon_1,k_1)}{dQ_{s1}}q_{s1}-\Delta LT_1\frac{dq_{s1}}{dt}=0 \tag{2-55}$$

$$\frac{dP_{in}}{dQ_{st}}(q_{s1}+q_{s2})-\Delta L\frac{df_2(Q_{s2},\varepsilon_2,k_2)}{dQ_{s2}}q_{s2}-\Delta LT_2\frac{dq_{s2}}{dt}=0 \tag{2-56}$$

where

$$T_1=\left[\left(\frac{\rho_s+\rho_g k_1}{A}\right)+\left(\left(\frac{\rho_s Q_{s1}}{A(1-\varepsilon_1)}-\frac{\rho_g k_1 Q_{s1}}{A\varepsilon_1}\right)\frac{d\varepsilon_1}{dQ_{s1}}\right)+\left(\left(\frac{\rho_g Q_{s1}}{A}\right)\frac{dk_1}{dQ_{s1}}\right)\right] \tag{2-57}$$

$$T_2=\left[\left(\frac{\rho_s+\rho_g k_2}{A}\right)+\left(\left(\frac{\rho_s Q_{s2}}{A(1-\varepsilon_2)}-\frac{\rho_g k_2 Q_{s2}}{A\varepsilon_2}\right)\frac{d\varepsilon_2}{dQ_{s2}}\right)+\left(\left(\frac{\rho_g Q_{s2}}{A}\right)\frac{dk_2}{dQ_{s2}}\right)\right] \tag{2-58}$$

$$f_1(Q_{s1},\varepsilon_1,k_1)=\rho_g\varepsilon_1 g+\rho_s(1-\varepsilon_1)g+0.057\sqrt{\frac{g}{D}}\frac{\rho_s}{A}Q_{s1}+\frac{0.0028\rho_g k_1{}^2 Q^2{}_{s1}}{DA^2\varepsilon_1}+\frac{0.25\,\mathrm{Re}_1^{-0.32}\,\rho_g k_1{}^2 Q_{s1}{}^2}{DA^2\varepsilon_1} \tag{2-59}$$

$$f_2(Q_{s2},\varepsilon_2,k_2)=\rho_g\varepsilon_2 g+\rho_s(1-\varepsilon_2)g+0.057\sqrt{\frac{g}{D}}\frac{\rho_s}{A}Q_{s2}+\frac{0.0028\rho_g k_2{}^2 Q^2{}_{s2}}{DA^2\varepsilon_2}+\frac{0.25\,\mathrm{Re}_2^{-0.32}\,\rho_g k_2{}^2 Q_{s2}{}^2}{DA^2\varepsilon_2} \tag{2-60}$$

An approach similar to that for a single path can be used to calculate $\frac{df_1(Q_{s1},\varepsilon_1,k_1)}{dQ_{s1}}$ and $\frac{df_2(Q_{s2},\varepsilon_2,k_2)}{dQ_{s2}}$, yielding

$$\frac{df_1(Q_{s1},\varepsilon_1,k_1)}{dQ_{s1}}=\frac{\partial f_1}{\partial Q_{s1}}+\frac{\partial f_1}{\partial \varepsilon_1}\frac{\partial \varepsilon_1}{\partial Q_{s1}}+\frac{\partial f_1}{\partial k_1}\frac{\partial k_1}{\partial Q_{s1}} \tag{2-61}$$

$$\frac{df_2(Q_{s2},\varepsilon_2,k_2)}{dQ_{s2}}=\frac{\partial f_2}{\partial Q_{s2}}+\frac{\partial f_2}{\partial \varepsilon_2}\frac{\partial \varepsilon_2}{\partial Q_{s2}}+\frac{\partial f_2}{\partial k_2}\frac{\partial k_2}{\partial Q_{s2}} \tag{2-62}$$

Likewise for perturbation variables, q_{s1} and q_{s2}, we have:

$$q_{s1}=\delta_{s1}e^{\lambda t} \tag{2-63}$$

$$q_{s2}=\delta_{s2}e^{\lambda t} \tag{2-64}$$

where $q_s=q_{s1}+q_{s2}$. Substitution of equations (2-63) and (2-64) into (2-55) and (2-56) yields:

$$\frac{dP_{in}}{dQ_{st}}(\delta_{s1}+\delta_{s2})-\Delta L\frac{df_1(Q_{s1},\varepsilon_1,k_1)}{dQ_{s1}}\delta_{s1}-\Delta L T_1\lambda\delta_{s1}=0 \tag{2-65}$$

$$\frac{dP_{in}}{dQ_{st}}(\delta_{s1}+\delta_{s2})-\Delta L\frac{df_2(Q_{s2},\varepsilon_2,k_2)}{dQ_{s2}}\delta_{s2}-\Delta L T_2\lambda\delta_{s2}=0 \tag{2-66}$$

The system would again be stable if $\lambda\le 0$. The eigenvalues are the solutions of the following determinant, known as the second order characteristic polynomial:

$$\begin{vmatrix} \frac{dP_{in}}{dQ_{st}} - \Delta L \frac{df_1(Q_{s1},\varepsilon_1,k_1)}{dQ_{s1}} - \Delta L T_1 \lambda & \frac{dP_{in}}{dQ_{st}} \\ \frac{dP_{in}}{dQ_{st}} & \frac{dP_{in}}{dQ_{st}} - \Delta L \frac{df_2(Q_{s2},\varepsilon_2,k_2)}{dQ_{s2}} - \Delta L T_2 \lambda \end{vmatrix} = 0 \qquad (2\text{-}67)$$

Equation (2-67) is a quadratic equation for λ resulting in two values. The eigenvalues can be found numerically by determining dP_{in}/dQ_{st}, $df_1\ (Q_{s1},\ \varepsilon_1,\ k_1)\ /dQ_{s1}$, $df_2\ (Q_{s2},\ \varepsilon_2,\ k_2)\ /dQ_{s2}$, T_1 and T_2 for each steady-state solution (e.g. from Table 2-4). Since we seek the sign of eigenvalues and their magnitude is not important for stability analysis, it is better to find a mathematical way to determine the eigenvalue sign without calculating their values. The Routh-Hurwitz stability criterion is utilized in this regard. The main concept of Routh-Hurwitz stability criterion is presented briefly in Appendix B.

2.2.2.1. Stability Analysis Results

As mentioned above, the idea is to subject the system (steady-state solutions) to small perturbations of the solid flow rate. In this section, it is proposed to implement the stability idea on the specific steady-state solutions presented in Table 2-4 above. Two approaches can be followed:

A. Application of Routh-Hurwitz stability criterion:

The Routh-Hurwitz stability criterion[1] is applied to find the sign of the eigenvalues of the steady-state solutions presented in Table 2-4. Recall that for $\lambda \leq 0$, the system is stable, whereas for $\lambda > 0$, we have an unstable solution.

Based on determinant (2-67), for the system with two vertical identical parallel paths, the characteristic polynomial is second order with:

$$a_2\lambda^2 + a_1\lambda + a_0 = 0 \qquad (2\text{-}68)$$

[1] Refer to Appendix B

where

$$a_2 = (\Delta L)^2 T_1 T_2 \tag{2-69}$$

$$a_1 = \left((\Delta L)^2 \frac{df_1}{dQ_{s1}} - \Delta L \frac{dP_{in}}{dQ_{st}} \right) T_2 + \left((\Delta L)^2 \frac{df_2}{dQ_{s2}} - \Delta L \frac{dP_{in}}{dQ_{st}} \right) T_1 \tag{2-70}$$

$$a_0 = -\Delta L \frac{dP_{in}}{dQ_{st}} \left(\frac{df_1}{dQ_{s1}} + \frac{df_2}{dQ_{s2}} \right) + (\Delta L)^2 \left(\frac{df_1}{dQ_{s1}} \cdot \frac{df_2}{dQ_{s2}} \right) \tag{2-71}$$

The corresponding Routh-Hurwitz table is:

$$\begin{vmatrix} a_2 & a_0 \\ a_1 & 0 \\ a_0 & 0 \end{vmatrix} \tag{2-72}$$

Both T_1 and T_2 are greater than zero[1]. Also since total input gas and solids flow rate is constant, at the limit $dP_{in}/dQ_{st} \rightarrow -\infty$[2]. Hence for all steady-state solutions, a_2 and a_1 are always greater than zero. Therefore the sign of a_0 determines whether or not the system is stable. Based on the Routh-Hurwitz algorithm, for each steady-state solution, if the sign of a_0 is positive, all corresponding eigenvalues are less than zero and the system is stable.

From Equations (2-42) and (2-43), it can be understood that $\Delta L.f_i\ (Q_{si},\ \varepsilon_i,\ k_i)$ is equal to the steady-state pressure drop of the system [$\Delta P_i = \Delta L.f_i\ (Q_{si},\ \varepsilon_i,\ k_i)$]. Therefore for two parallel paths, *Total pressure drop* $= \Delta P_1 = \Delta P_2 = \Delta L.f_1\ (Q_{s1},\ \varepsilon_1,\ k_1) = \Delta L.f_2\ (Q_{s2},\ \varepsilon_2,\ k_2)$. Thus it can be shown easily that:

$$\frac{d(Total\ pressure\ drop)}{dQ_{s1}} = \Delta L \frac{df_1(Q_{s1}, \varepsilon_1, k_1)}{dQ_{s1}} \tag{2-73}$$

[1] Based on numerical computation of T_1 and T_2 using equations (2-57) and (2-58).
[2] Pustylnik et al. [15] reached the same result in gas-liquid system. Refer to Appendix A for more details.

$$\frac{d(Total\ pressure\ drop)}{dQ_{s2}} = \Delta L \frac{df_2(Q_{s2}, \varepsilon_2, k_2)}{dQ_{s2}} \tag{2-74}$$

Figure 2-8 shows the steady-state total pressure drop of the system defined in Section 2.1.3.1 as a function of solid flow rates through paths 1 and 2. Because of the symmetry of the system, the mirror projection of a data point in path 1 will have a corresponding point in path 2. For example if one chooses 'Point A' in Figure 2-8 as a representative of path 1, the related point in path 2 will be 'Point B'. Both paths 1 and 2 have the common region at the 'uniform distribution' point. It can be easily obtained that for the entire mal-distributed steady-state solutions, $df_1/dQ_{s1} = - df_2/dQ_{s2}$, whereas for the uniform steady-state solution, $df_1/dQ_{s1} = df_2/dQ_{s2} = 0$.

Therefore for the mal-distributed solutions ($\gamma \neq 0.5$), the first term of equation (2-71) is zero. Also because of the symmetry in Figure 2-8, the second term of a_0 is always negative and thus, $a_{0,\ unequal\ distribution} < 0$. Therefore all of the unequal steady-state solutions of the case study are unstable solutions.

On the other hand, for the uniform distribution solution ($\gamma = 0.5$), both the first and second terms of equation (2-71) are zero, and therefore, $a_{0,\ equal\ distribution} = 0$. Based on 'Special Case 2' of Appendix B, in these cases all of the zero elements of the corresponding row [third row of expression (2-72)] should be replaced by the coefficients of the differentiated auxiliary polynomial[1].

Therefore the new Routh-Hurwitz table for the uniform distribution solution becomes

$$\begin{vmatrix} a_2 & a_0 \\ a_1 & 0 \\ a_1 & 0 \end{vmatrix} \tag{2-75}$$

[1] For this case the auxiliary polynomial is: $a_1\lambda = 0$

Since all elements of the first columns of the above table are positive, the eigenvalue of the uniform distribution solution is the root of the auxiliary polynomial that is λ=0. Therefore, the uniform distribution of gas-solid flow is the only stable case among all the steady-state solutions.

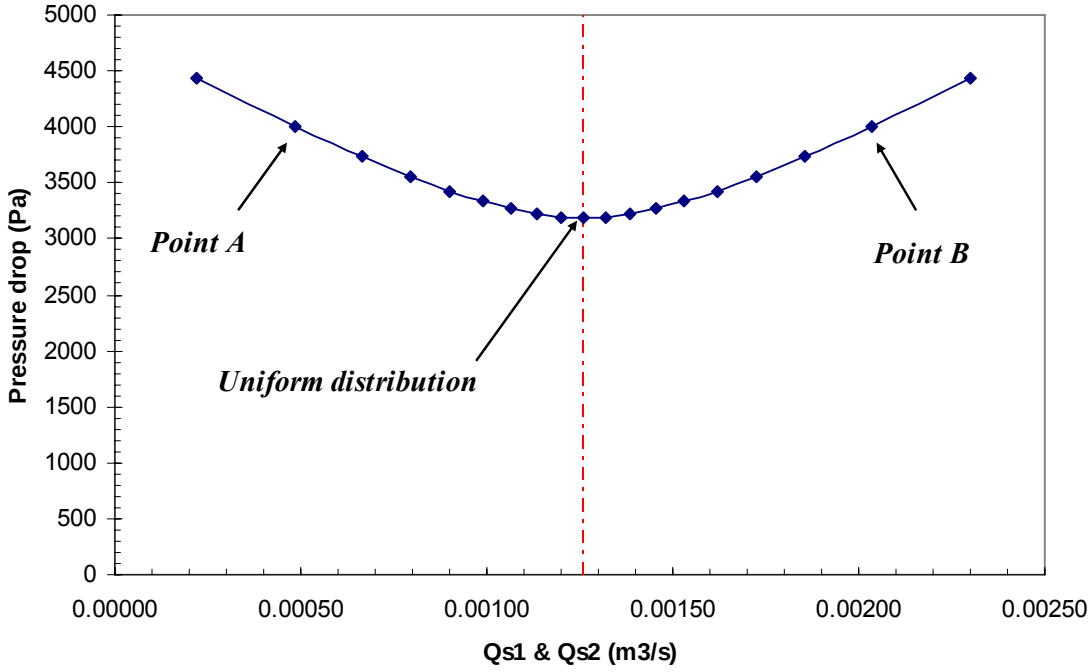

Figure 2-8. Pressure drop of system where properties are given in Table 2-3 as a function of solid flow rates through paths 1 and 2.

B. General approach for stability of uniform distribution steady-state solution:

As presented in the previous section, the Routh-Hurwitz algorithm can be used to examine the stability of the system (for uniform and non-uniform solutions) and it was found that the only stable solution is the uniform one. For the uniform distribution solution, an alternative approach is also applicable as follows.

If we just consider stability of the equal distribution solution, it should be possible to propose a general correlation for the stability criterion. According to equations (2-59) and (2-60), since for the uniform distribution $\varepsilon_1=\varepsilon_2$, $k_1=k_2$ and $Q_{s1}=Q_{s2}$, it can be easily proven that:

$$f_1(Q_{s_1}) = f_2(Q_{s_2}) \tag{2-76}$$

$$T_1 = T_2 \tag{2-77}$$

Therefore by substituting the above relationships in expression (2-67), the following general stability criterion (eigenvalues) for the equal distribution solution of two identical parallel paths is

$$\begin{cases} \lambda_1 = \dfrac{2\dfrac{dP_{in}}{dQ_{st}} - \Delta L \dfrac{df_1}{dQ_{s1}}}{\Delta L T} \\ \lambda_2 = \dfrac{-\dfrac{df_2}{dQ_{s2}}}{2T} \end{cases} \tag{2-78}$$

This condition of stability is satisfied if all of the eigenvalues are equal or less than zero (Note that the denominators of both terms above are greater than zero):

$$\begin{cases} 2\dfrac{dP_{in}}{dQ_{st}} - \Delta L \dfrac{df_1}{dQ_{s_1}} \le 0 \\ -\dfrac{df_2}{dQ_{s_2}} \le 0 \end{cases} \tag{2-79}$$

Since in our cases, the inlet total gas flow rate is constant, dP_{in}/dQ_{st} approaches $-\infty$, and the first stability condition is always satisfied. Thus, the only condition for stability of the uniform distribution solution (γ=0.5) for two parallel paths is that:

$$-\frac{df_i}{dQ_{si}} \le 0,\ i = 1 or\ 2 \tag{2-80}$$

Again, as discussed in part *A* above of this section, for an equal distribution solution both $-df_1/dQ_{s1}$ and $-df_2/dQ_{s2}$ are equal to zero. Therefore using this general approach, the uniform distribution solution is the stable solution.

In summary, there are two methods for determining the stability of solutions. The Routh-Hurwitz method is applicable for stability examination of all steady-state solutions (both equal and unequal distributions), whereas, approach *B* can be used for stability determination, but is limited to the uniform distribution solution. Both methods demonstrate that for the defined case study, the only steady-state stable solution is the uniform distribution of multi-phase flow through parallel paths, while all mal-distributed solutions are unstable.

2.2.3. Stability Analysis for *N* Identical Vertical Parallel Pipes

Once steady-state solutions are obtained, the stability of the solutions is analyzed using equation (2-49) for each path:

$$\frac{dP_{in}}{dQ_{st}}(q_{s1}+...+q_{sN})-\Delta L\frac{df_i(Q_{si},\varepsilon_i,k_i)}{dQ_{si}}q_{si}-\Delta LT_i\frac{dq_{si}}{dt}=0,\ i=1...N \tag{2-81}$$

where

$$T_i=\left[(\frac{\rho_s+\rho_g k_i}{A})+\left((\frac{\rho_s Q_{si}}{A(1-\varepsilon_i)}-\frac{\rho_g k_i Q_{si}}{A\varepsilon_i})\frac{d\varepsilon_i}{dQ_{si}}\right)+\left((\frac{\rho_g Q_{si}}{A})\frac{dk_i}{dQ_{si}}\right)\right],\ i=1...N \tag{2-82}$$

$$\begin{aligned}f_i(Q_{si},\varepsilon_i,k_i)&=\rho_g\varepsilon_i g+\rho_s(1-\varepsilon_i)g+0.057\sqrt{\frac{g}{D}}\frac{\rho_s}{A}Q_{si}+\\&\frac{0.0028\rho_g k_i{}^2Q^2{}_{si}}{DA^2\varepsilon_i}+\frac{0.25\,\mathrm{Re}_i^{-0.32}\rho_g k_i{}^2Q_{si}{}^2}{DA^2\varepsilon_i},\ i=1...N\end{aligned} \tag{2-83}$$

Substituting $\delta_{si}e^{\lambda t}$ for perturbation variables (q_{si}) yields:

$$\frac{dP_{in}}{dQ_{st}}(\delta_{s1}+...+\delta_{sN})-\Delta L\frac{df_i(Q_{si},\varepsilon_i,k_i)}{dQ_{si}}\delta_{si}-\Delta LT_i\lambda\delta_{si}=0,\ i=1...N \tag{2-84}$$

The system is stable for $\lambda \leq 0$. The eigenvalue is a solution of the characteristic polynomial

$$a_i\lambda^i + a_{i-1}\lambda^{i-1} + ... + a_1\lambda + a_0 = 0,\ i = 1...N \tag{2-85}$$

that is the simplified format of determinant

$$\begin{bmatrix} \frac{dP_{in}}{dQ_{st}} - \frac{df_1}{dQ_{s1}} - \Delta LT_1\lambda & \frac{dP_{in}}{dQ_{st}} & \cdots & \frac{dP_{in}}{dQ_{st}} \\ \frac{dP_{in}}{dQ_{st}} & \frac{dP_{in}}{dQ_{st}} - \frac{df_2}{dQ_{s2}} - \Delta LT_2\lambda & \frac{dP_{in}}{dQ_{st}} & \frac{dP_{in}}{dQ_{st}} \\ \cdots & & \cdots & \cdots \\ \frac{dP_{in}}{dQ_{st}} & \frac{dP_{in}}{dQ_{st}} & \cdots & \frac{dP_{in}}{dQ_{st}} - \frac{df_N}{dQ_{sN}} - \Delta LT_N\lambda \end{bmatrix} \begin{bmatrix} \delta_1 \\ \delta_2 \\ . \\ . \\ . \\ \delta_N \end{bmatrix} = 0 \tag{2-86}$$

Again the sign of the eigenvalues [roots of equation (2-85)] can be determined using the Routh-Hurwitz stability criterion. Also the same approach as presented in part *B* of Section 2.2.2.1 can also be used to find the stability of uniform distribution solution:

According to equation (2-83), considering an even distribution solution for *N* paths, it is easily proven that

$$f_1(Q_{s_1}) = f_2(Q_{s_2}) = ... = f_N(Q_{sN}) \tag{2-87}$$

$$T_1 = T_2 = ... = T_N \tag{2-88}$$

Therefore by considering the above relationship in expression (2-86), the following eigenvalues can be obtained:

$$\begin{cases} \lambda_1 = \dfrac{N\dfrac{dP_{in}}{dQ_{st}} - \Delta L\dfrac{df_i}{dQ_{si}}}{\Delta LT} \\ \lambda_i = \dfrac{-\dfrac{df_i}{dQ_{si}}}{2T} \end{cases}, \; i = 2...N \tag{2-89}$$

The condition of stability is satisfied if all eigenvalues are equal or less than zero; i.e.

$$\begin{cases} N\dfrac{dP_{in}}{dQ_{st}} - \Delta L\dfrac{df_i}{dQ_{s_i}} < 0 \\ -\dfrac{df_i}{dQ_{s_i}} < 0 \end{cases}, \; i = 2...N \tag{2-90}$$

Since the inlet total solid flow rate is constant, dP_{in}/dQ_{st} approaches $-\infty$, and the first stability condition is always satisfied. Thus, the only condition for stability of uniform distribution solution for N parallel paths is:

$$-\frac{df_i}{dQ_{si}} < 0, \; i = 1...N \tag{2-91}$$

2.3. DISCUSSION AND CONCLUSION OF THE ANALYTICAL STUDIES

In Section 2.1, the distribution of gas-solid flow through vertical identical parallel pipes was modeled analytically based on equality of pressure drop through all paths. It was demonstrated that several steady-state gas-solid distribution solutions including the uniform distribution can satisfy the pressure drop balance condition.

The next issue to be addressed was the stability of the steady-state solutions. Based on perturbation of the solid flow rate, instability analysis was performed. For one defined

case study (Table 2-3), it was obtained that the only steady-state stable solution is the uniform distributed one, whereas all mal-distributed solutions are unstable.

One can question based on the proposed model, whether there are any cases where the uniform distribution solution is unstable or where some mal-distributed solutions are stable? Based on the symmetric behaviour of the system about the uniform distribution solution, (e.g. see Figure 2-4 or Figure 2-8), any mal-distributed solution can be stable if and only if the corresponding data point in its 'pressure drop vs. solid flow rate' plot (like Figure 2-8) has zero slope amount (d *(Total pressure drop)*$/ dQ_{si} = df_i\,(Q_{si}, \varepsilon_i, k_i)/dQ_{si} = 0$). In other words, the only solutions that are stable are ones where the local or general pressure drop reaches a minimum or maximum.

Based on some studies for different operating conditions (e.g. the concentration of solid, inlet velocity, etc) and physical dimensions, it was found in all cases that the only steady-state solution was where the pressure drop reached a minimum, i.e. the uniform distribution solution. Thus, it is appears that uniformity is favoured for different operating conditions and dimensions for gas-solid flow through identical vertical parallel paths.

Note finally that the stability analysis leads to a conclusion consistent with the energy minimization approach explained by Grace et al. [18] and presented in Chapter 1. In all cases, the solution with the minimum pressure drop (minimum energy consumption) is the uniformly distributed one, and stability analysis also suggests that the stable solution is the one with a minimum pressure drop.

2.4. MODELING - NUMERICAL APPROACH

An analytical model and stability analysis for pneumatic conveying of gas-solid flow through identical vertical paths was presented in the previous section. Since the purpose

of this work was to perform stability analysis by perturbing the solid flow rate, the most pragmatic and simplest approach (1-D model) was pursued. Although a 1-D model is an acceptable approach, it is of interest to study the behaviour of the system in 2-D and 3-D space using computational fluid dynamics. FLUENT 6.2.16 commercial software was used in this regard.

2-D and 3-D steady-states CFD studies were performed for gas-solid two-phase flow through a vertical 'Y branch'. Also by perturbing the solid flow rate, stability analysis was performed. The final result of numerical stability study was then compared with the analytical results of the previous section. Finally, the effect of upstream non-uniformity on the distribution through the bifurcation was investigated in several two-dimensional cases.

2.4.1. Multi-Phase Flow Numerical Simulation

Advances in computational fluid mechanics have provided the basis for further insight into the dynamics of multiphase flows. Currently there are two major approaches for the numerical simulation of multiphase flows: the Euler-Euler approach and the Euler-Lagrange approach (Discrete Phase Model[1]).

In the Lagrangian approach, the fluid phase is treated as a continuum by solving the time-averaged Navier-Stokes equations, while the dispersed phase is solved by tracking a large number of particles through the calculated flow field.

The discrete phase formulation used by FLUENT contains the assumption that the second phase is sufficiently dilute that particle-particle interactions and the effects of the particle volume fraction on the gas phase are negligible. In practice, this implies that the discrete phase must be present at a relatively low volume fraction, usually less than 5%.

[1] DPM

On the other hand, Huber and Sommerfeld [43] demonstrated the importance of simulating particle-wall and particle-particle interactions and the dominant effect that this has on the particle stream. As such, the Lagrangian approach is the most approximate framework to model a dense gas-solid system. Therefore, the Euler-Euler approach was selected for this work.

In the Euler-Euler approach, the different phases are treated mathematically as interpenetrating continua. Since the volume of a phase cannot be occupied by the other phases, the concept of phasic volume fraction (or interpenetrating continua) is introduced. These volume fractions are assumed to be continuous functions of space and time with their sum being one at every position. Conservation equations for each phase are derived to obtain a set of equations, with similar structure for all phases [44].

In FLUENT software, three different Euler-Euler multiphase models are available: a volume of fluid[1] model, a mixture model, and an Eulerian model. The relevant models for our case study are the last two. Once more since the mixture model was proposed for dilute gas-solid simulations, a Eulerian model was selected for this study.

2.4.2. Governing Equations for Eulerian Framework

The Eulerian model is the most complex of the multiphase models in FLUENT. An Eulerian treatment is used for each phase. It solves a set of *n* momentum and continuity equations for each phase. Coupling is achieved through the pressure and interphase exchange coefficients. The FLUENT solution is based on:

- A single pressure is shared by all phases.
- Momentum and continuity equations are solved for each phase.

Conservation of mass: the volume fraction of each phase is calculated from a continuity equation:

[1] VOF

$$\frac{\partial}{\partial t}(\alpha_q \rho_q) + \nabla.(\alpha_q \rho_q \vec{\upsilon_q}) = 0 \qquad (2\text{-}92)$$

where ρ_q , α_q and $\vec{\upsilon_q}$ are the density, volume fraction and velocity of phase q respectively. Note that

$$\alpha_s + \alpha_g = 1 \qquad (2\text{-}93)$$

Conservation of Momentum: Following previous work [45 - 52], FLUENT uses a multi-fluid granular model to describe the flow behaviour of a gas-solid mixture. The solid-phase stresses are derived by analogy between the random particle motion arising from particle-particle collisions. As for a gas, the intensity of the particle velocity fluctuations determines the stresses, viscosity, and pressure of the solid phase.

The conservation of momentum for a gas phase is:

$$\frac{\partial}{\partial t}(\alpha_g \rho_g \vec{\upsilon_g}) + \nabla \cdot (\alpha_g \rho_g \vec{\upsilon_g}^2) = -\alpha_g \nabla p + \nabla \cdot \overline{\overline{\tau_g}} + \alpha_g \rho_g \vec{g} + K_{sg}(\vec{\upsilon_s} - \vec{\upsilon_g}) \qquad (2\text{-}94)$$

where the right-hand side last term results from interphase force. $K_{sg}(=K_{gs})$ is the interphase momentum exchange coefficient and $\overline{\overline{\tau_g}}$ is the gas phase stress-strain tensor:

$$\overline{\overline{\tau_g}} = \alpha_g \mu_g (\nabla \cdot \vec{\upsilon_g} + \nabla \cdot \vec{\upsilon_g}^{\mathrm{T}}) + \alpha_g (\lambda_g - \frac{2}{3}\mu_g) \nabla \cdot \vec{\upsilon_g} \overline{\overline{I}} \qquad (2\text{-}95)$$

Here μ_g and λ_g are the shear and bulk viscosities of the gas phase, respectively.

The conservation of momentum for the solid phase is

$$\frac{\partial}{\partial t}(\alpha_s \rho_s \vec{v_s}) + \nabla \cdot (\alpha_s \rho_s \vec{v_s}^2) = -\alpha_s \nabla p - \nabla p_s + \nabla \cdot \overline{\overline{\tau_s}} + \alpha_s \rho_s \vec{g} + K_{gs}(\vec{v_g} - \vec{v_s}) \qquad (2\text{-}96)$$

The solid stress-tensor, $\overline{\overline{\tau_s}}$, contains shear and bulk viscosities arising from particle momentum exchange due to translation and collision. The shear stress model is not presented in this work.

Since our experimental work (Chapter 3) involves small particles (< 100 μm), lift forces are insignificant compared to drag forces. Therefore this extra term is excluded from the momentum equations. Also the virtual mass force was neglected, since the solids density is much greater than that of the gas.

Several models are available for the interphase momentum exchange coefficient based on different drag coefficient expressions. FLUENT features three gas-solid drag models:

- Syamlal-O'Brien model [53]
- Wen and Yu model [54]
- Gidaspow model [48]

The Syamlal-O'Brien and Wen and Yu models are for dilute gas-solid systems. The Gidaspow model appears to be the most appropriate model for dense gas-solid systems and is used in this study.

In pneumatic conveying, particles are generally suspended in a turbulent gas stream. The *k-ε* model is chosen to describe the effect of turbulent velocity fluctuations. FLUENT has three *k-ε* turbulence model options:

- Mixture turbulence model (applicable for phase density ratio equal to 1)
- Dispersed turbulence model (applicable for dilute multi-phase systems)
- *k-ε* model for each phase (applicable for dense multi-phase systems)

Since simulation of dense system is of interest, the third model was used in this work.

2.4.3. 2 - Dimensional Simulation

2-D CFD modeling was performed on a vertical "Y branch" geometry. The main advantage of two-dimensional numerical modeling is relatively faster computation speed than for three-dimensional simulation because of fewer cells, reducing the number of equations to be solved in each iteration.

2.4.3.1. 2-D Geometry and Mesh Generation

Figure 2-9 shows the geometry and dimensions of the 2-D vertical 'Y branch'. In order to compare the numerical results with the analytical ones, all dimensions were chosen to be the same as in Section 2.1.3.1. Also the dimensions are the same as for the vertical bifurcation section of the experimental facility considered in Chapter 3.

As indicated in Figure 2-9, gas-solid flow can be introduced to the system from the inlet located below the bifurcation. After splitting the multi-phase flow, the recombination pipe joins the parallel paths again and the total flow exits from the outlet section. Based on some CFD runs, it is found that the interactions between two parallel streams at the recombination section may cause local turbulence, increasing the number of iterations needed to achieve convergence. Therefore, as indicated in Figure 2-9, a small infinitesimally thin symmetric baffle was added to reduce re-mixing at the recombination.

The geometry was meshed by GAMBIT 2.2.30 commercial software with 46,080 quadrilateral cells. In order to investigate the behaviour of flow in critical areas accurately, the meshed elements are more populated near the walls and bends. Figure 2-10 shows the meshes at the inlet bifurcation section. The quality of cells was examined by GAMBIT. It was checked that 92% of cells have 'EquiAngle Skew' less than 0.03, and all cells have the 'EquiAngle Skew' lower than 0.16 that is perfectly acceptable [44].

In order to check the symmetry of the geometry and meshed cells in the left and right paths, single-phase air flow with an inlet velocity of 20 m/s was passed through the system. Figure 2-11 shows that the distribution of gas flow is perfectly uniform, confirming that the geometry and cells in the right and left sides were identical.

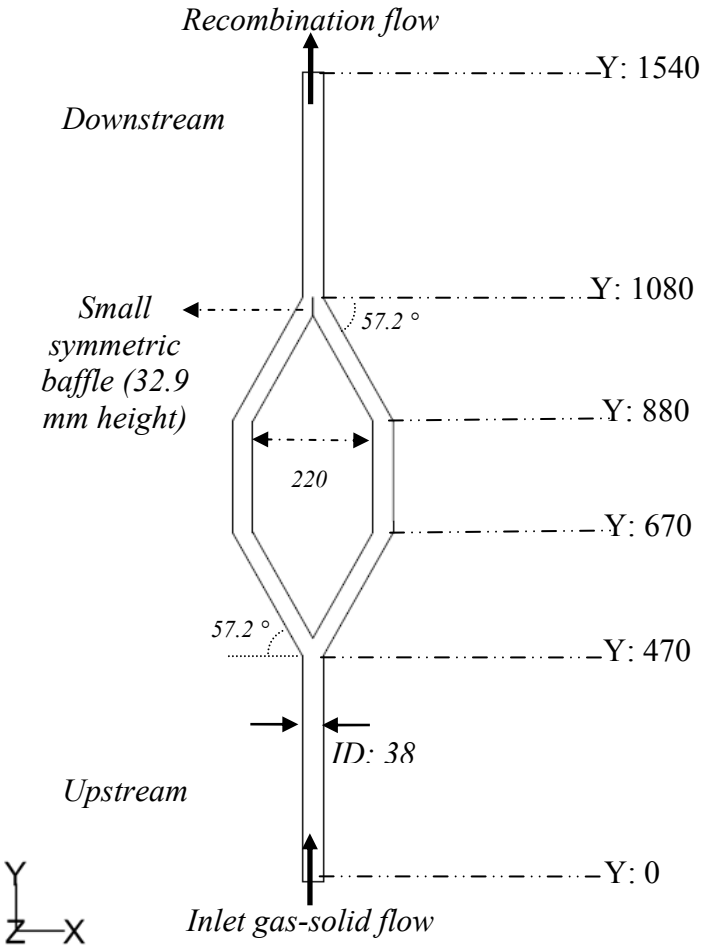

Figure 2-9. Schematic of 2-D 'Y branch' geometry (all dimensions in mm).

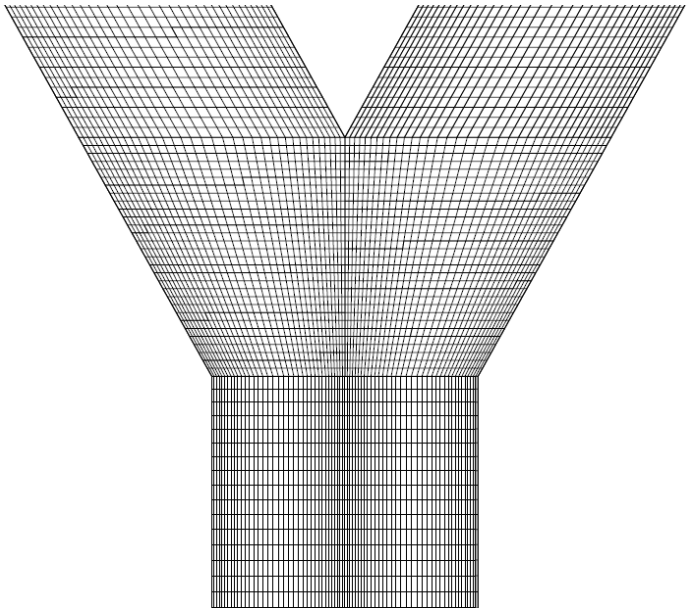

Figure 2-10. Cells in bifurcation section generated by GAMBIT.

2.4.3.2. Model Specification

The material properties and operating conditions are presented in Table 2-6. In order to compare the results with the previous section, all parameters were chosen to be the same as those specified for the case study presented in Section 2.1.3.1.

Table 2-6. Properties and operating conditions for CFD simulation (20°C and 101.3 kPa).

Gas	
Type	Air
Density (kg/m^3)	1.225
Viscosity (kg/m.s)	1.79E-05
Inlet velocity (m/s)	20
Solids	
Type	Glass Beads
Density (kg/m^3)	2500
Particle size (μm)	30
Inlet velocity (m/s)	20
Volume fraction, α_s (%)=1-ε	10

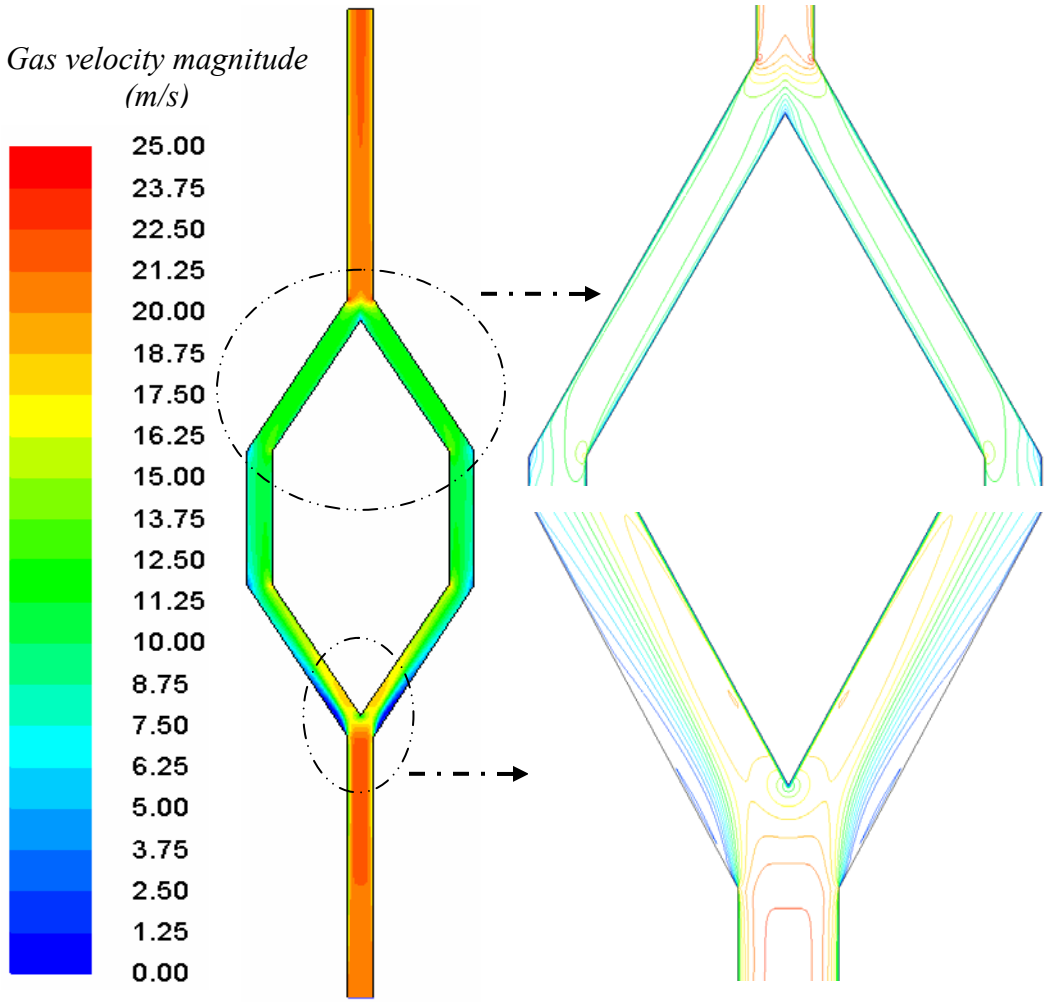

Figure 2-11. Symmetrical distribution of one-phase flow through the parallel paths (inlet velocity: 20 m/s).

2.4.3.3. Steady-State Solution

Steady-state numerical modeling was performed to investigate gas-solid flow through vertical parallel paths. Two criteria can be utilized to establish that a solution has been obtained:

- Magnitude of residuals of different fluid mechanics elements less than a predetermined tolerance level;

- Conservation of mass: magnitude of net mass flow rate[1] less than a predetermined tolerance level.

In many CFD studies, the residuals are acceptable (e.g. less than 1E-4.0), but since the net mass flow rate is far from zero, the iterations should continue until the net flow is very nearly 0.

All of the residuals in our case study were less than 1E-4.0 after 20,000 iterations. However, as shown in Figure 2-12, up to 30,000 iterations, conservation of mass for the steady-state case was not well satisfied. Even after 30,000 iterations, the inset plot on Figure 2-12 shows that the oscillation near zero amount continued and at the limit, the solution tended to zero. The results below were therefore obtained after 90,000 iterations.

The 'Area-weighted average'[2] was selected as a parameter to compare the solid volume fraction in the left and right paths. Figure 2-13 shows the area-weighted volume fraction as a function of numerical iteration for the left and right vertical pipes. It is clear that by extending the numerical computation, both values approach each other.

Figure 2-14 shows the steady-state absolute pressure of the gas-solid mixture through the vertical 'Y branch'. There is almost no discrepancy between the same points at different levels of the right and left paths. The total pressure drop calculated numerically through the vertical parallel path is 3476 Pa, whereas the analytical estimation of the pressure drop of the uniform distribution solution in Section 2.1.3.1 was 3189 Pa. These two values are within 8.3% of each other.

[1] Net mass flow rate = Outlet total mass flow rate – Inlet total mass flow rate

[2] The Area-weighted average of a quantity is computed by dividing the summation of the product of the selected field variable and the cross-sectional area by the total area of the surface [44]:

$$\frac{1}{A}\int \phi dA = \frac{1}{A}\sum_{i=1}^{n} \phi_i \left|A_i\right|$$

where φ is the corresponding quantity.

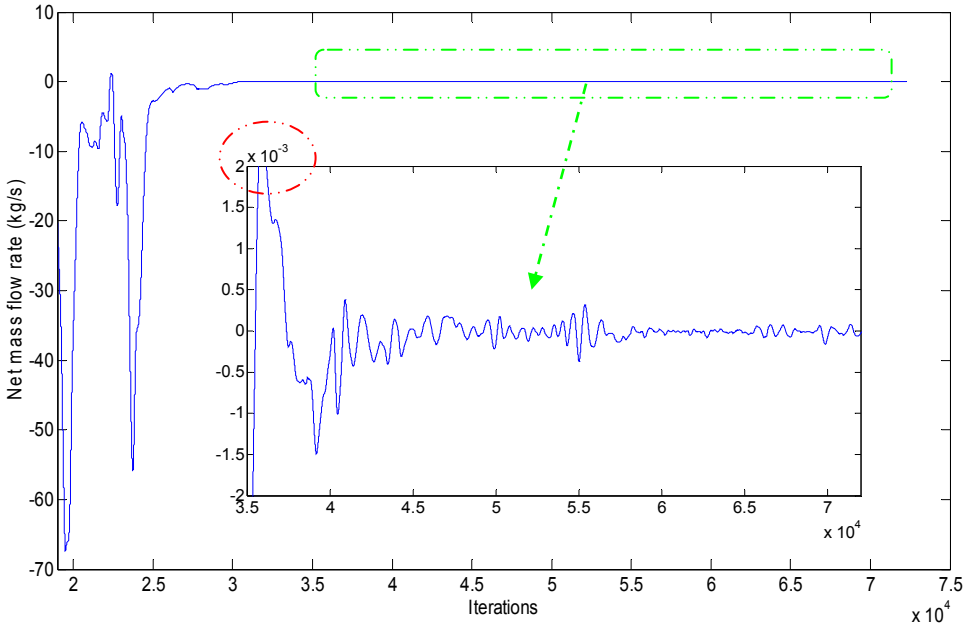

Figure 2-12. Approach of net mass flow rate to zero. Conditions as in Table 2-6.

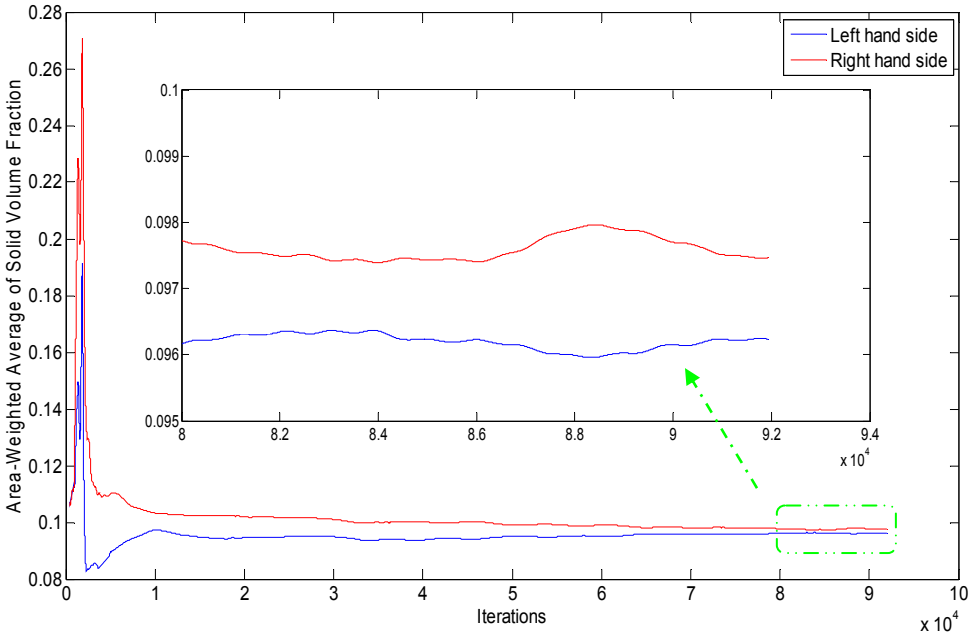

Figure 2-13. Solid volume fraction approach for right and left paths vs. numerical iterations. Conditions as in Table 2-6.

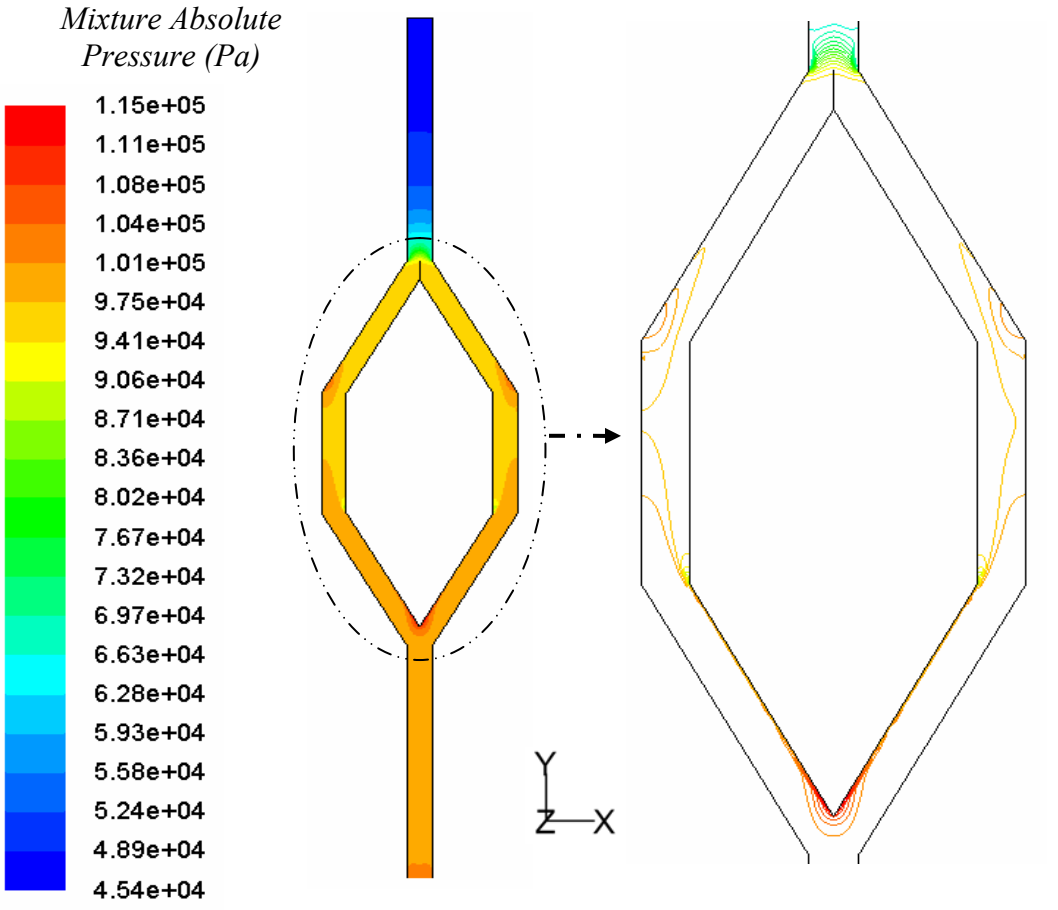

Figure 2-14. Steady-state contours of gas-solid mixture absolute pressure through the system. Conditions as in Table 2-6.

Figure 2-15 shows the gas volume fraction and gas velocity magnitude through the parallel paths. The distribution of gas flow is uniform, with no discrepancy visible. It is apparent that when the gas flow is distributed uniformly, the solid flow splits equally as well. Figure 2-16 corresponds to the distribution of solid volume fraction through the identical parallel paths. The distribution of particles through the vertical 'Y branch' is clearly uniform. Also the solid velocity is almost identical between the left and right pipes, as shown in Figure 2-17. In both cases the effect of the small interface wall located at the recombination section, on preventing the formation of local turbulence between the right and left streams is notable.

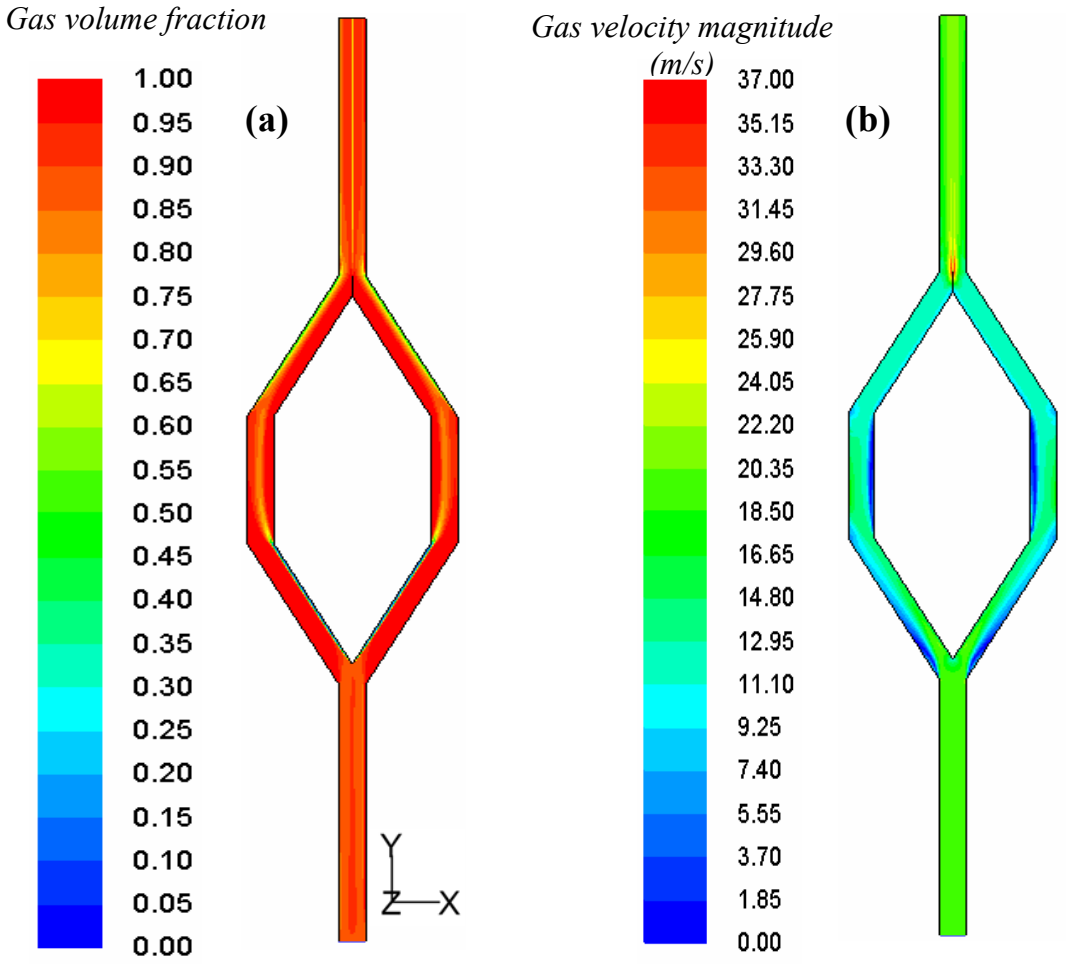

Figure 2-15. Contours of (a) gas volume fraction, and (b) gas velocity magnitude. Conditions as in Table 2-6.

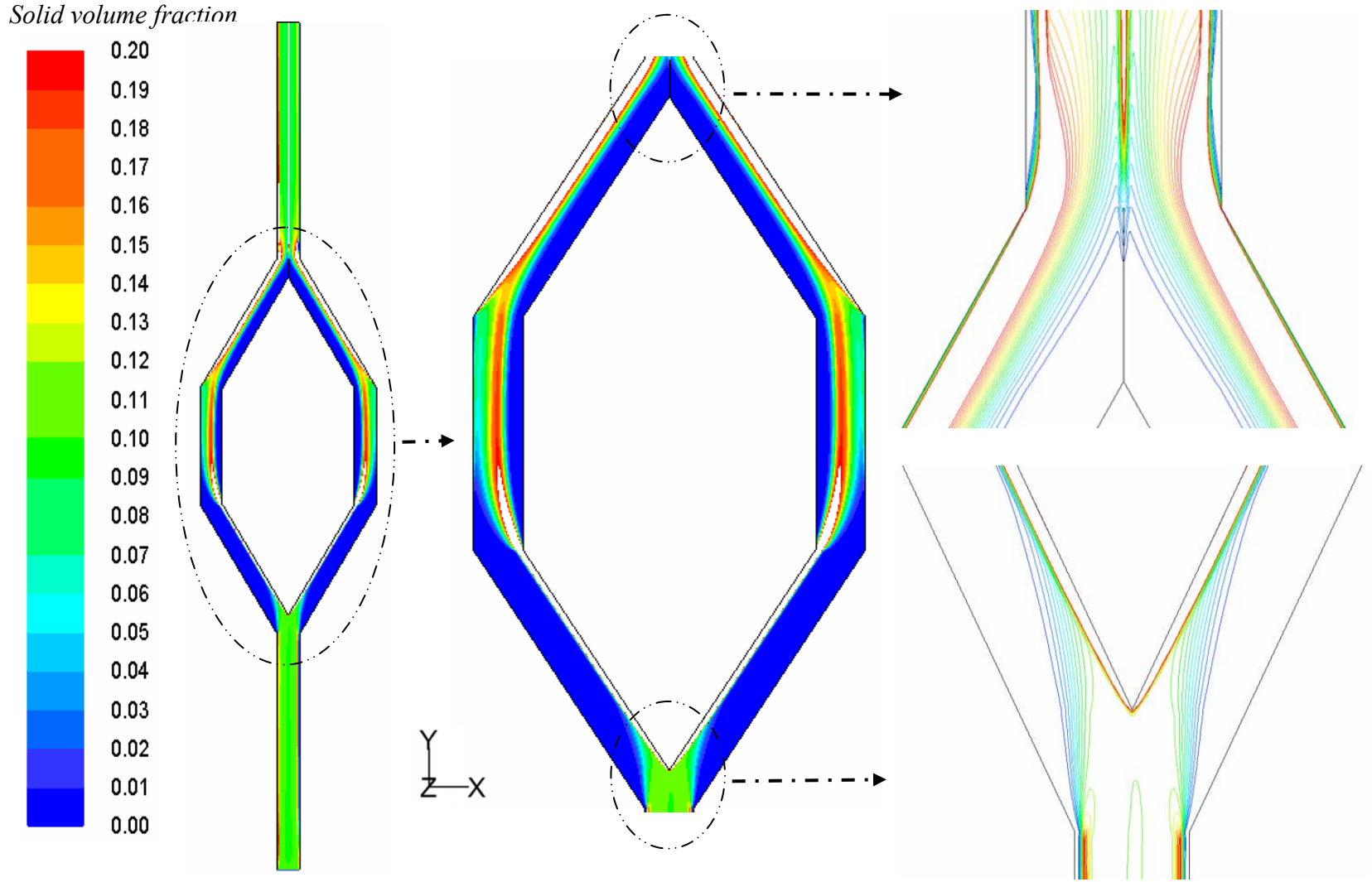

Figure 2-16. Steady-state contours of solid volume fraction for conditions of Table 2-6 (White colour corresponds to volume fractions > 0.2).

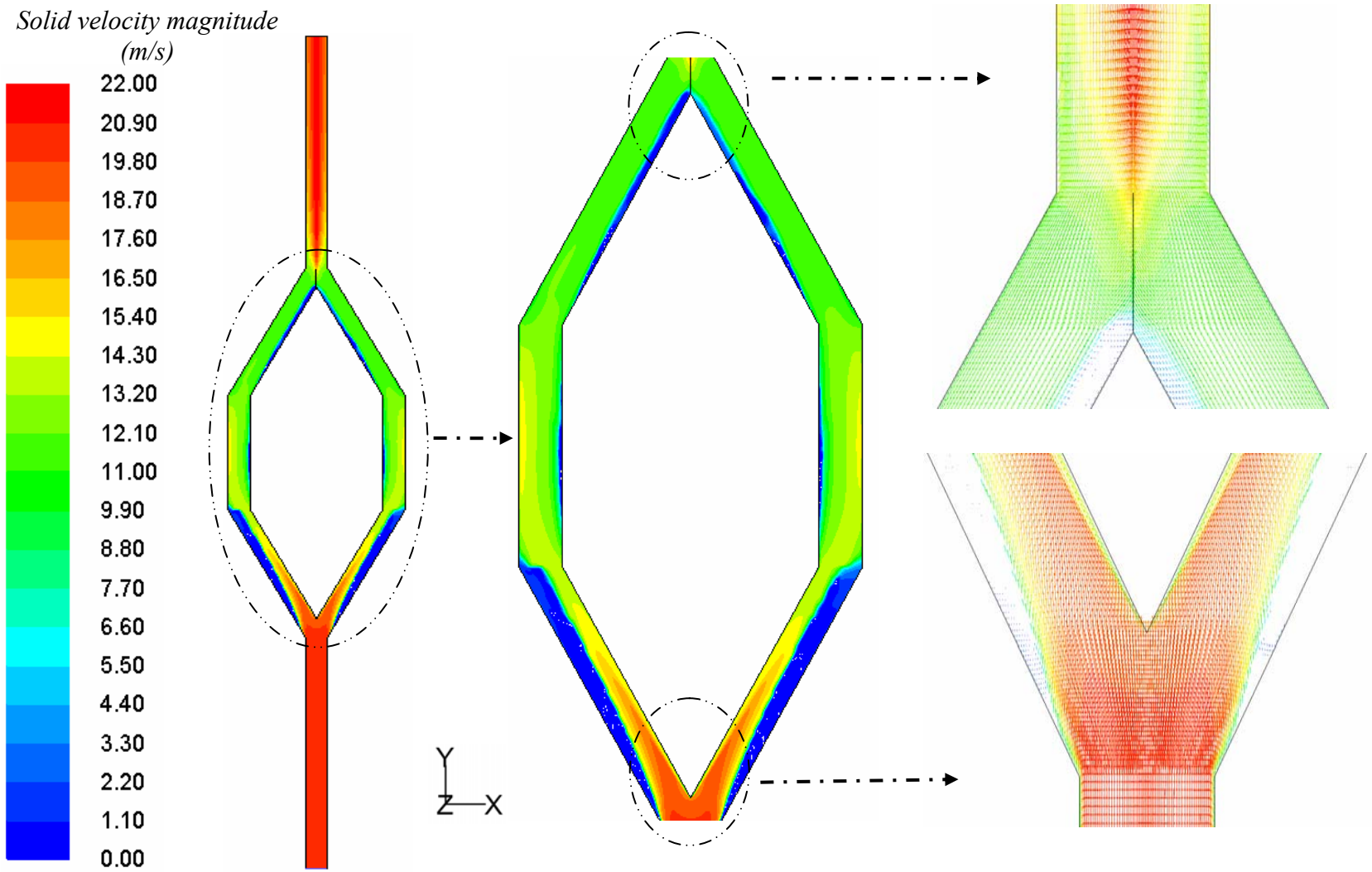

Figure 2-17. Steady-state solid velocity contours and vectors. Conditions as in Table 2-6.

2.4.4. 3 - Dimensional Simulation

3-D simulation is the best way to investigate the behaviour of our case study numerically, since all of the effects of the geometry on the flow are then considered. The main challenge of 3-D CFD simulation is its time-consuming computational operation because of the large number of cells and equations to be solved. Therefore the 3-D simulation was solely focused on investigation of the steady-state distribution and stability of flow through parallel pipes.

2.4.4.1. 3-D Geometry and Mesh Generation

Chapter 3 considers experiments with two identical parallel cyclones. The same geometry and dimensions as the 'Y branch' section of the experimental facility (without the cyclones) was simulated by Gambit 2.2.30 commercial software as shown in Figure 2-18.

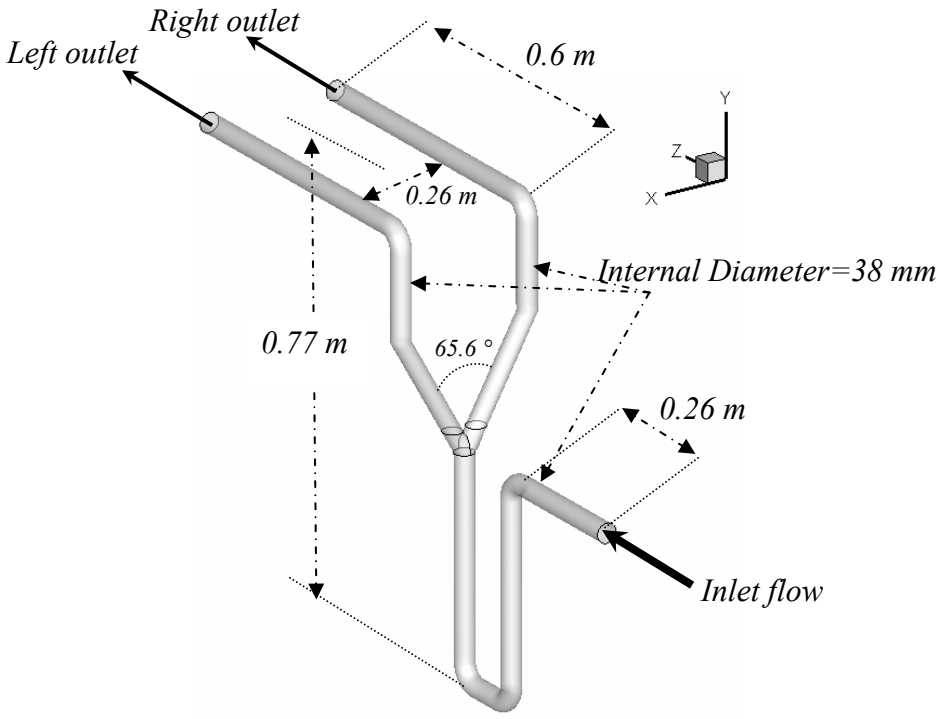

Figure 2-18. 3-D geometry of "Y branch" simulated by Gambit software (cross-sectional plane).

The geometry was meshed by GAMBIT 2.2.30 with 605,172 quadrilateral cells and 196,768 hexahedral cells. Figure 2-19 shows the mesh in the inlet bifurcation section. The quality of cells was examined by GAMBIT. It was checked that 60% of cells have 'EquiAngle Skew' less than 0.2, while the entire cells have the 'EquiAngle Skew' less than 0.35. This is perfectly acceptable [44].

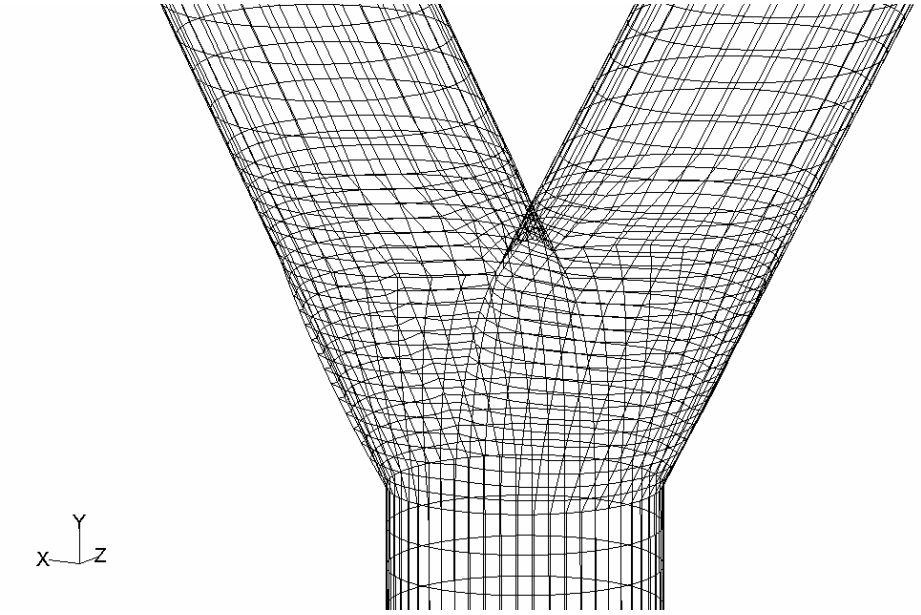

Figure 2-19. 3-D body meshes at inlet bifurcation section.

Similar to the 2-D case, in order to check whether the geometry and meshes in the right and left pipes were identical, air flow through the system without particles was first simulated. Figure 2-20 shows the predicted gas streamlines through the geometry. It is apparent that the gas flow distribution is uniform and that the geometry and cells are symmetrical on the left and right sides.

2.4.4.2. Steady-State Solution

The same operating conditions as the ones presented in Table 2-6 were considered in 3-D simulation. Convergence was deemed to have been reached after 290,000 iterations. All of the fluid residuals were less than 10E-5. Figure 2-21 corresponds to the distribution of

solid volume fraction through the geometry. As expected, the solids concentration is higher in the bends. As shown in Figure 2-22, the steady-state distribution of particles through the vertical 'Y branch' is almost uniform. Also the gas is separated uniformly through the parallel pipes as demonstrated in Figure 2-23. The 3-D results are perfectly consistent with the 2-D simulation.

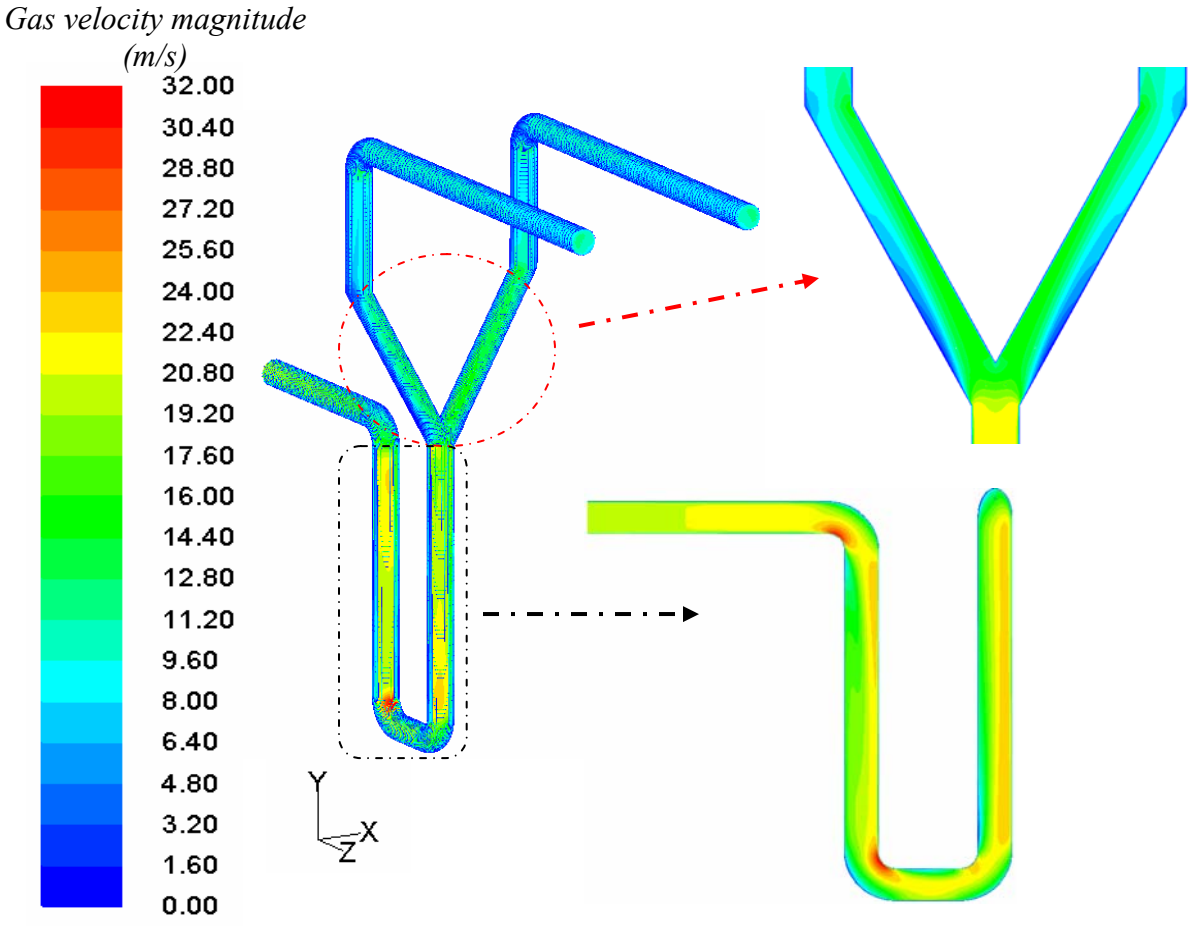

Figure 2-20. Steady-state symmetrical distribution of one-phase air flow through parallel paths (inlet air velocity: 20 m/s).

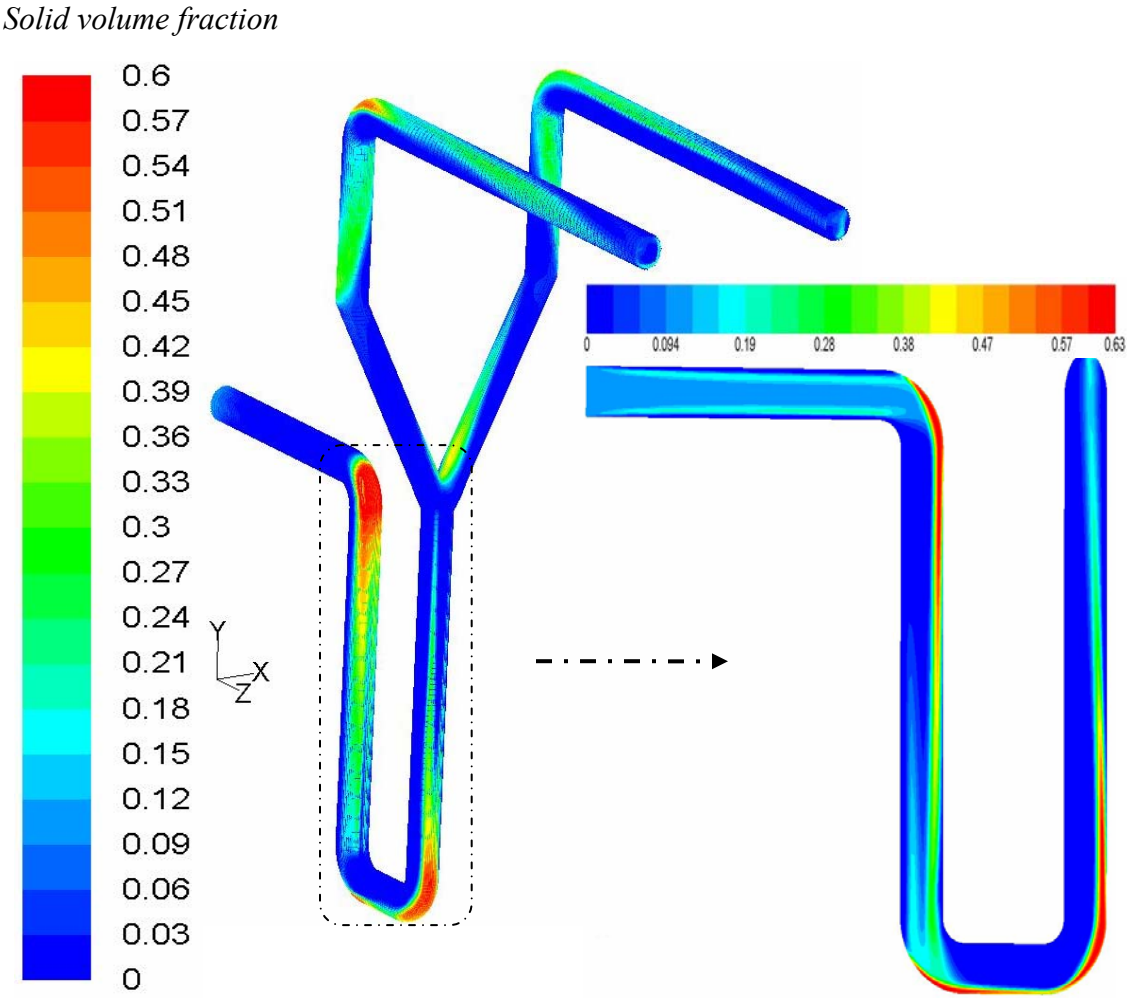

Figure 2-21. Steady-state contours of solid volume fraction for 3-D simulation. Conditions as in Table 2-6.

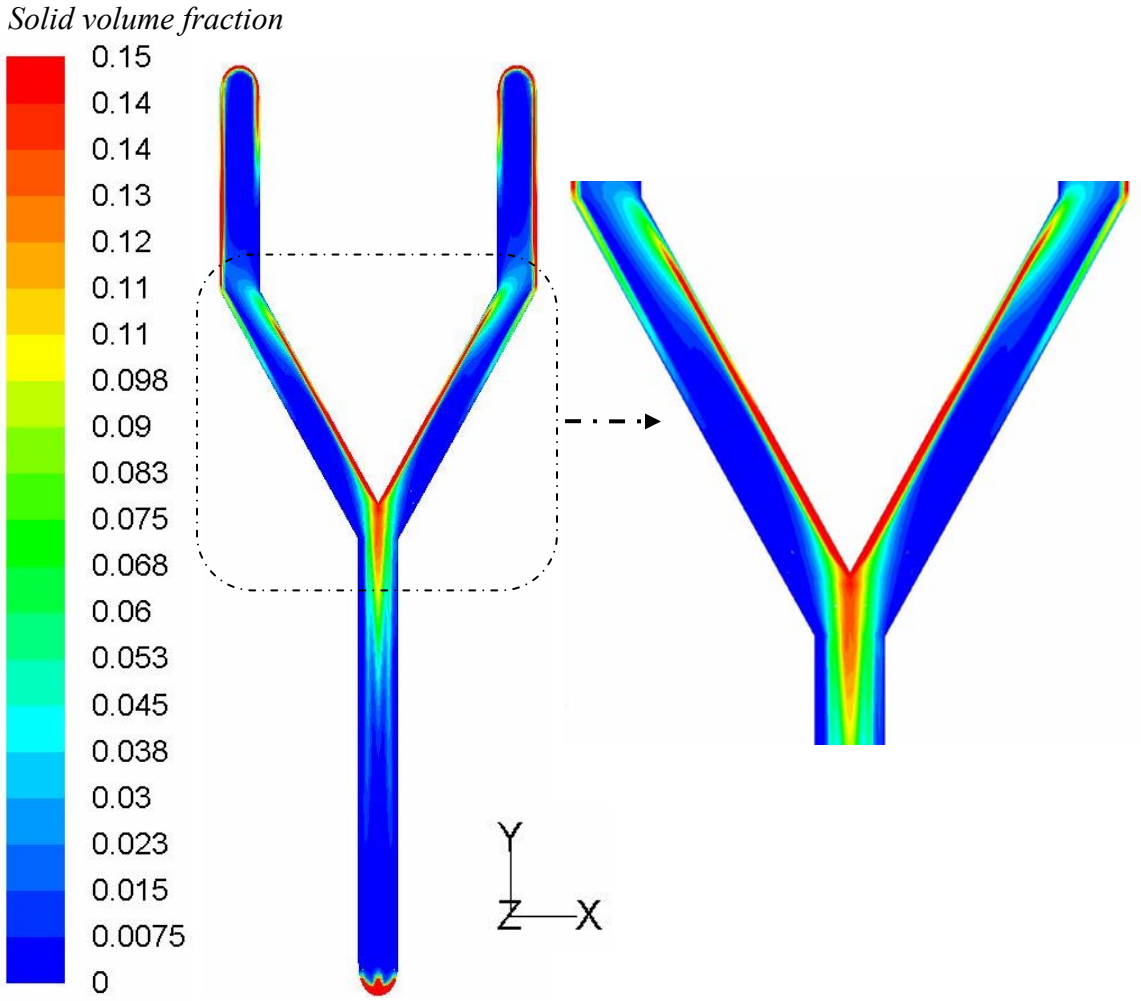

Figure 2-22. Steady-state contours of solid volume fraction at bifurcation for conditions of Table 2-6. Middle plane view.

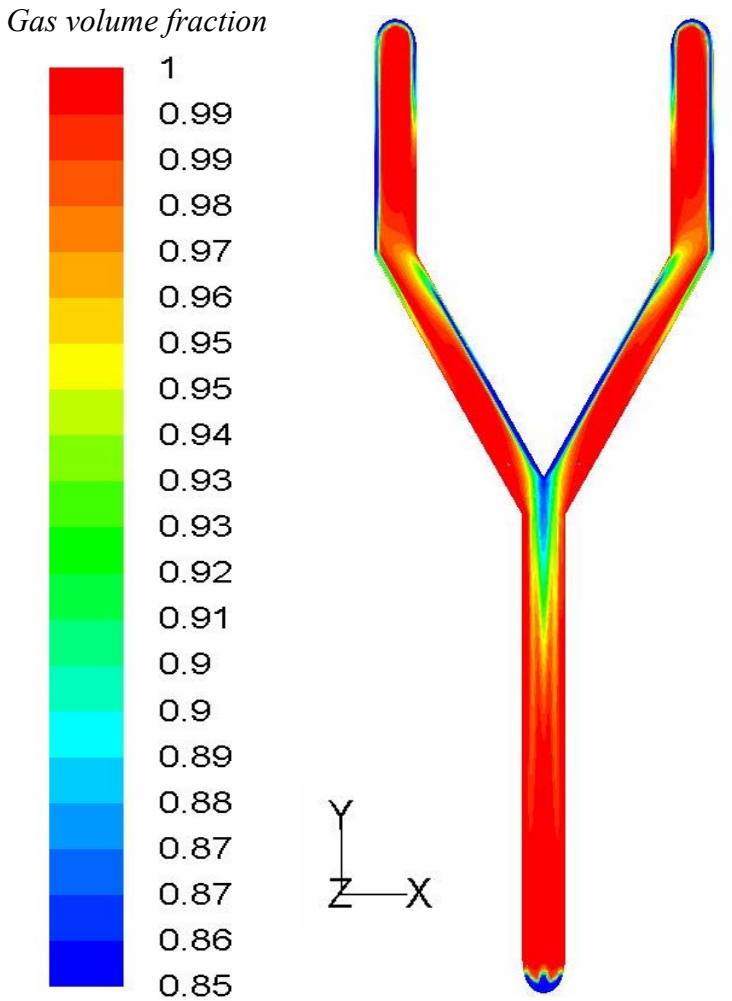

Figure 2-23. Steady-state contours of gas volume fraction at bifurcation for conditions of Table 2-6. Middle plane view.

2.5. STABILITY AND SENSITIVITY ANALYSIS - NUMERICAL APPROACH

2.5.1. Stability Analysis

Two- and three-dimensional CFD studies again indicated that the gas-solid flow was distributed uniformly through the identical parallel paths. As for the analytical approach, the next step was to test the numerical stability of the steady-state uniform solution. A similar approach to perturbation of solid flow rate was utilized in the CFD environment. In order to perturb the system, two methods were used:

1. The system was perturbed by injecting some solids into one of the paths. This can be easily done by changing the bifurcation section boundary condition of one of the paths from 'Wall' to 'Inlet solid flow'.
2. Another method is to partially block one of the paths by defining one of the edges as a 'Wall'.

In order to mal-distribute the multi-phase flow completely, more than 10,000 iterations were carried out for the perturbed condition and after that, the perturbation source was impulsively removed from the system. As for the analytical stability result, it was found numerically that for both the 2-D and 3-D geometries, the stable solution was the uniform distribution solution, since, after removing the imbalance, the flow migrated to an even split through the parallel paths (in 2-D case, after ~3,000 iterations the solution is reached, while ~12,000 iterations were needed for 3-D solution)

2.5.2. Sensitivity Analysis

As described in Chapter 1, there is considerable evidence of mal-distribution of gas-solid flow through vertical parallel pipelines. On the other hand, the above analytical/numerical analyses show that among the many steady-state solutions for the geometries considered, the uniform distribution of both gas and solid flows is a stable solution, with no other stable solutions found.

Recall (from Chapter 1) that in many flow splitting of gas-solid flow applications, several pipeworks and bends are deployed upstream before the bifurcation section. This can form a rope flow and make the main multi-phase stream before the branches non-uniform, as shown in Figure 1-10. Therefore, a sensitivity analysis was performed on the side-to-side of upstream flow to examine its effect on the distribution of the gas-solid flow through the parallel paths. To do this, the upstream inlet flow was divided into two equal parts termed right and left inlet.

Figure 2-24 shows the effect of the side-to-side non-uniformity of the upstream flow on the distribution of gas-solid flow through the 'Y branch'. The volume fraction in the left inlet was kept constant, 0.1, while the volume fraction in the right inlet was decreased gradually from 0.1 to 0. It is apparent that when the upstream flow is non-uniformly distributed (which may be caused by bends) through the main pipe, it will split unequally through the paths, with more solids going through the path with the denser upstream suspension. It is notable that even when the right inlet volume fraction is zero, a few particles are predicted to pass through the right pipe. These results are consistent with the conclusion stated by Cook and Hurworth [97] that the distribution of solids over the cross-section of the pipe, as it approaches the bifurcation, affects the split ratio of material downstream branches. One may question how the system achieves a pressure drop balance in the right and left paths when there is higher volume fraction of solids and gas are passing through the left hand side? The gas velocity contours through the parallel paths for different inlet flow conditions are presented in Figure 2-25. By having more solids in the left-hand side, the gas velocity magnitude in right branch increases to reach the same pressure drop as in the left pipe.

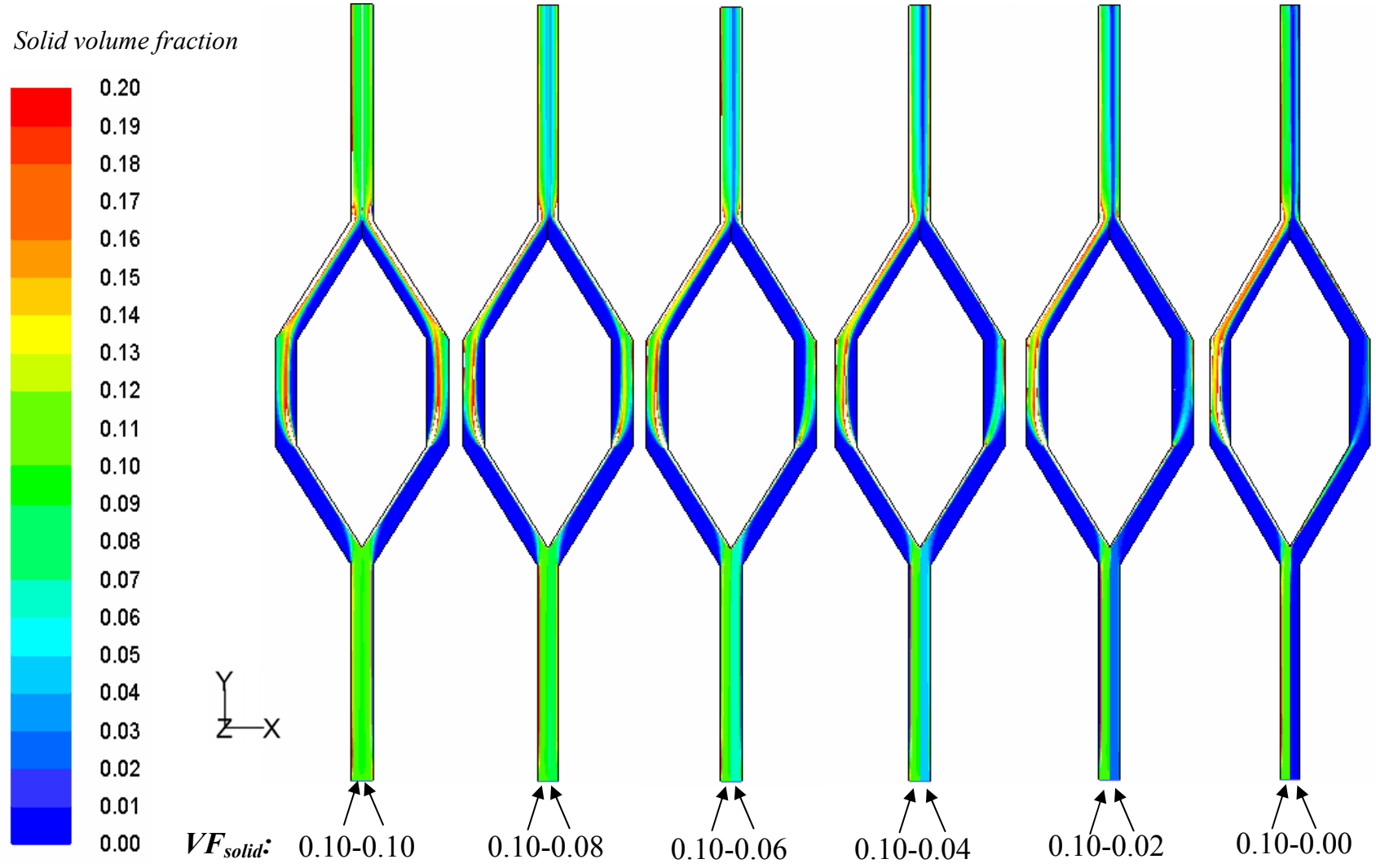

Figure 2-24. Effect of upstream radial distribution on the mal-distribution of solid flow through parallel paths. Other conditions as in Table 2-6.

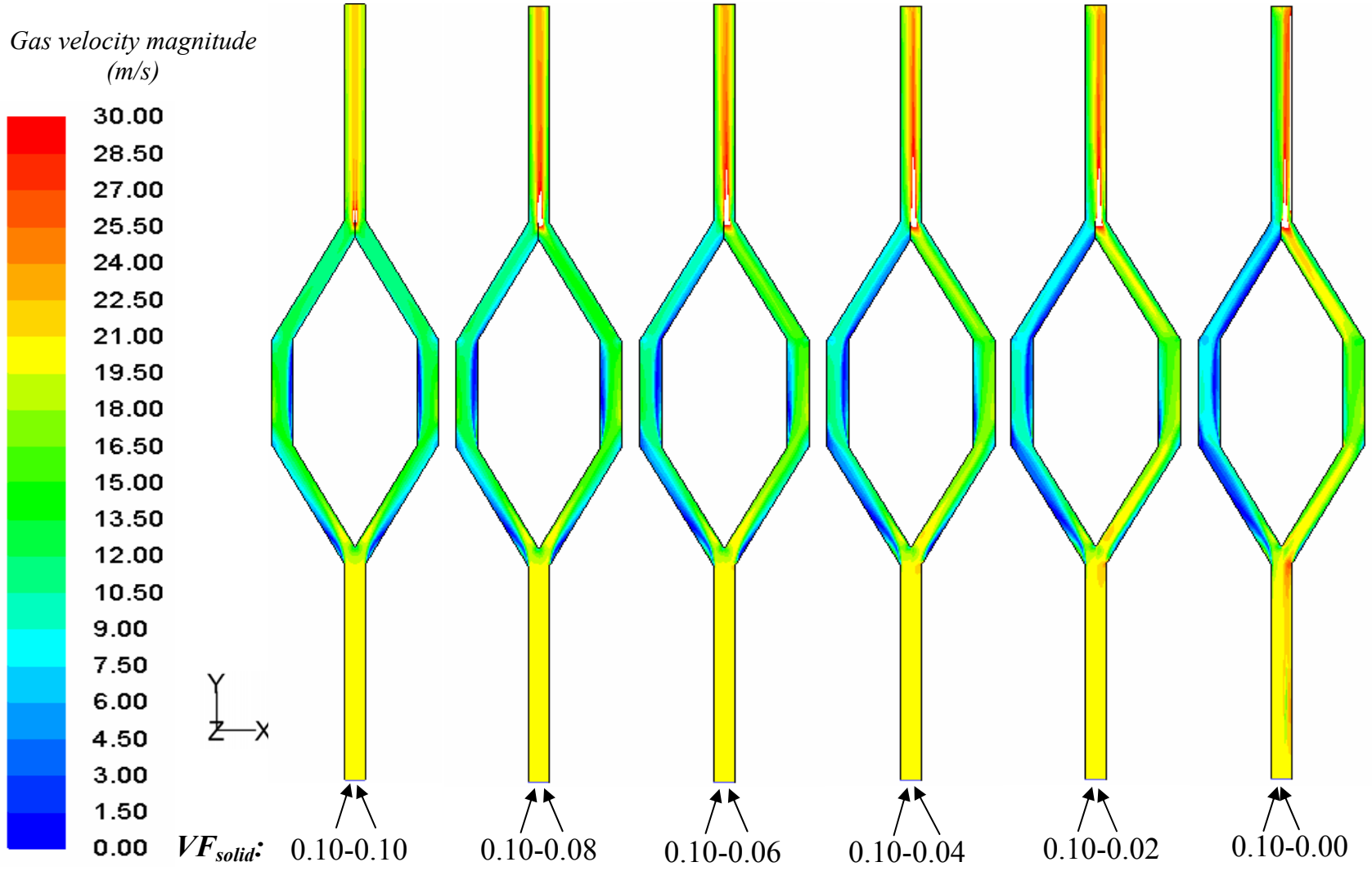

Figure 2-25. Effect of upstream radial distribution on gas velocity through parallel paths. Other conditions as in Table 2-6.

2.6. CONCLUSIONS

Both analytical and numerical analyses suggest that the uniform distribution of gas-solid flow through mostly-vertical identical parallel paths is the only stable solution and any mal-distributed solution have an unstable nature. The energy minimization approach is consistent with the presented results. The analysis was carried out for only one gas (air at atmospheric temperature and pressure) and one particles (30 μm glass beads) at one inlet velocity 20 m/s. However, the qualitative results are likely to apply over much wider range of conditions.

The only way, found in this study that a non-uniform distribution solution can be obtained is when the upstream flow is not distributed uniformly through the main pipe before the bifurcation. Practically, this is due to the rope stream formation generated by pipeworks and bends.

Finally, it should be emphasised that the geometry of each path way may be very important on the distribution and behaviour of the system. In other words, the presented conclusion of this chapter applied only to vertical parallel pipes without any additional unit (e.g. cyclone, reactor) in each path. In the next chapter, the distribution of multi-phase flow through parallel gas-cyclones and the effect of geometry are presented.

Chapter 3. IDENTICAL PARALLEL CYCLONES

Through the fundamental study presented in Chapter 2, the behaviour of gas-solid flow passing identical parallel pipes was indicated. As mentioned in Chapter 1, the parallel path geometry seems to play a significant role in determining the distribution of multi-phase flow through the paths. In this chapter the distribution of gas-solid flow through identical parallel cyclones is studied analytically and experimentally.

3.1. INTRODUCTION

Cyclone separators are very common devices for the removal of the dispersed particles from carrying gases and liquids because of their simple structure, low cost and ease of operation [39]. As explained in Chapter 1, in large circulating fluidized bed combustors and other reactors with high gas-solid flow rates, cyclones are placed in parallel in order to improve collection efficiency. In addition to experimental evidence of mal-distribution of gas-solid flow through parallel cyclones presented in Chapter 1, Figures 3-1 and 3-2 show images of the outlet pipe of six identical parallel cyclones operating inside one of Syncrude's industrial-scale Fluid Coker fluidized bed reactors. During operation of this unit, unequal distribution of multi-phase flow through these six cyclones caused differential fouling among the paths. This differential fouling can form new different internal geometries in each path, changing the distribution of multi-phase flow. Consequently, the overall efficiency of the cyclones decreases and the pressure drop varies. These changes adversely affect the separation of solid particles from the system and the operation of the fluidized bed reactor.

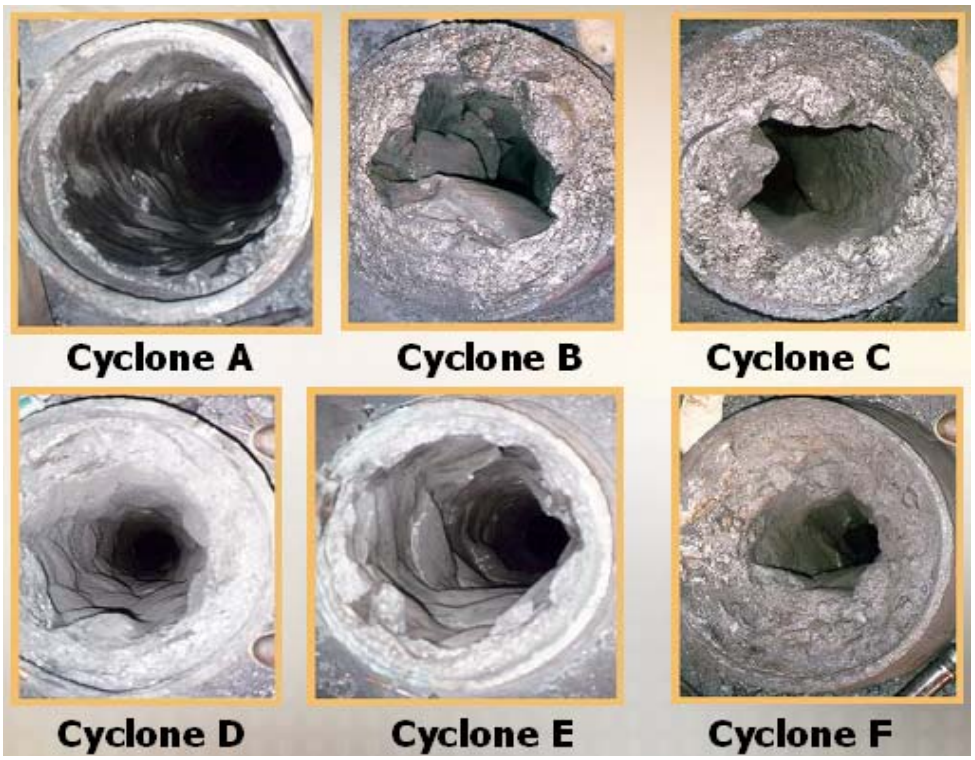

Figure 3-1. Differential fouling at gas outlet tube exit section of identical parallel cyclones inside industrial scale fluidized bed reactor caused by mal-distribution of multi-phase flow.

Figure 3-2. Fouling at gas outlet tube entrance section of one cyclone of identical parallel cyclones inside industrial scale fluidized bed reactor caused by mal-distribution of gas-solid flow compared with clean (unfouled) entrance.

3.2. MODELING

3.2.1. Main Idea of the Model

Pressure drop through the cyclones is a major performance parameter playing a significant role in the process design and control of fluidized bed reactors [39] with internal parallel cyclones. Unequal distribution of flows through the cyclones may also be associated with pressure fluctuations within the system. Answering several key questions would help to provide a better understanding of the distribution:

1. What are the possible distribution patterns of gas and solid volume concentrations for flow through identical parallel cyclones?
2. How can the mal-distribution of gas-solid flow affect the overall pressure drop through the parallel cyclones?
3. Is there an effect of solids loading, inlet gas velocity and other properties on the flow distribution?

In order to predict the possible distributions and their effects on the pressure drop of cyclones, we proceed as follows:

Cyclone pressure drop is a function of geometry and gas and solid flow rates[1]. There are a number of expressions and procedures (mostly empirical) for calculating gas-cyclone pressure drops in the literature [78-84]. For a given geometry, the relationship between cyclone pressure drop and gas and solids flow rates can be written

$$\Delta P_{cyclone} = f(Q_g, Q_s, cyclone\ geometry\ \&\ diameter, gas\ and\ particle\ properties) \quad (3\text{-}1)$$

[1] For very dilute solids flows, the contribution of the solids to pressure drop is commonly ignored.

Thus, different gas and solid flow rates lead to different cyclone pressure drops. In addition, as noted in Chapter 2, gas and solids continuity for one-dimensional fully developed flow through two parallel paths give:

$$m_{g1} = \gamma m_{gt} = A\rho_g u'_{g1} \tag{3-2}$$

$$m_{g2} = (1-\gamma) m_{gt} = A\rho_g u'_{g2} \tag{3-3}$$

$$m_{s1} = \sigma m_{st} = A\rho_s u'_{s1} \tag{3-4}$$

$$m_{s2} = (1-\sigma) m_{st} = A\rho_s u'_{s2} \tag{3-5}$$

where γ and σ are the mass fractions of the gas and solids flows, respectively passing through path 1 and u'_{gi} and u'_{si} are the gas and solids superficial velocities respectively.

It is proposed to calculate the pressure drop of two parallel cyclones for different values of γ and σ (different mixture distributions). Because the net pressure drop must be the same for both paths, the intersection solutions (common region) between different parallel branches delineate the possible distributions. Also, by modeling the pressure drops, the effect of unequal distribution on the pressure drop of the system can be observed. The main idea of the model can be represented by

$$\begin{array}{c} \\ \gamma_1 \\ \gamma_2 \\ \downarrow \\ . \\ . \\ \gamma_n \end{array} \begin{array}{c} \begin{array}{cccccc} \sigma_1 & \sigma_2 & \rightarrow & . & . & \sigma_n \end{array} \\ \begin{bmatrix} \Delta P_{1,1} & \Delta P_{1,2} & . & . & . & \Delta P_{1,n} \\ \Delta P_{2,1} & . & & & & . \\ . & & . & & & . \\ . & & & . & & . \\ . & & & & . & . \\ \Delta P_{n,1} & . & . & . & . & \Delta P_{n,n} \end{bmatrix} \end{array} \tag{3-6}$$

3.2.2. Cyclone Pressure Drop Core Model

In order to implement the above idea, a reliable relationship between cyclone pressure drop and the flows of both gas and solids is needed. There are a number of correlations [78-84] for estimating cyclone pressure drop. However, most of these are empirical and suitable only for very dilute flows through the cyclones. They are not very satisfactory for the more concentrated flows encountered in many fluidized bed processes. In general the cyclone pressure drop falls with increasing solids loading until a turning point is reached, (exhibiting drag reduction phenomenon) [83, 85-88] after which the pressure drop begins to increase. Conventional cyclone pressure drop models do not predict this phenomenon. Therefore, the universal cyclone pressure drop approach of Chen and Shi [39] which considers the cyclone drag reduction effect is selected as an appropriate model for our case study.

Based on this model, the pressure drop across a cyclone includes local losses and frictional losses. The local losses include an expansion loss at the cyclone inlet, ΔP_1, and a contraction loss at the entrance of the outlet tube, ΔP_2. The frictional loss includes a swirling loss due to the friction between the gas flow and the cyclone wall, ΔP_3, and dissipation of gas dynamic energy at the outlet, ΔP_4. The pressure drop is expressed as a summation of these four terms, i.e.

$$\Delta P_{cyclone} = \Delta P_1 + \Delta P_2 + \Delta P_3 + \Delta P_4 \tag{3-7}$$

The overall pressure drop can also be written:

$$\Delta P_{cyclone} = 0.5 \rho_g \xi u_g'^2 \tag{3-8}$$

where ξ is considered to be a drag coefficient for the cyclone, a function of gas flow, solid loading, cyclone dimensions, and cyclone geometry.

In order to present the cyclone drag coefficient correlation, some standard cyclone dimensions should be defined. Figures 3-3 and 3-4 are schematic diagrams of the most common tangential inlet and reverse flow cyclones.

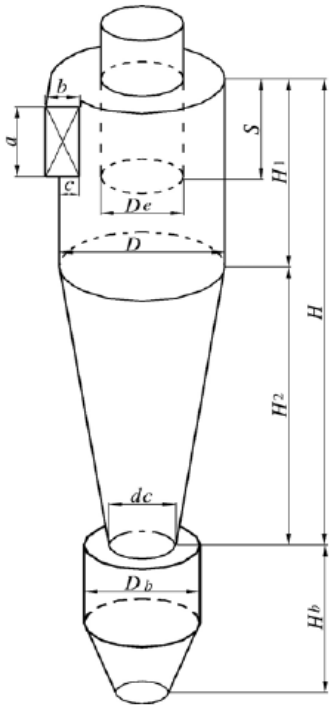

Figure 3-3. Sketch of a reverse flow cyclone separator.

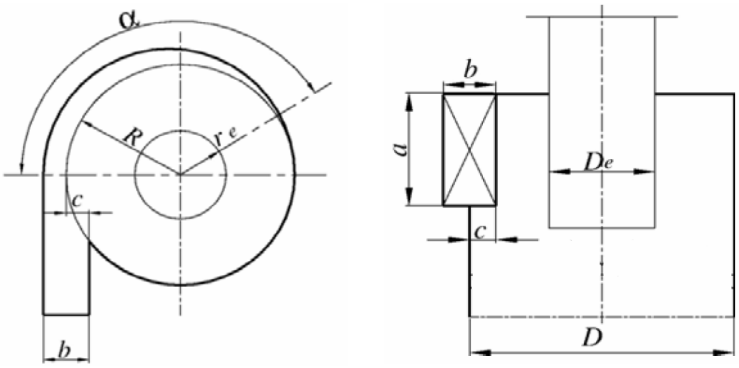

Figure 3-4. Volute inlet.

The cyclone drag coefficient, ξ, for a gas without solids, is given [39] by

$$\xi = \left(1 - \frac{2k_i\tilde{b}}{1+1.33\tilde{b}-\tilde{d}_r}\right)^2 + 1.11 f_0 K_A \tilde{F}_s \tilde{V}_{\theta w}{}^3 \tilde{d}_r^{-1.5n} + \frac{\tilde{V}_{\theta w}^2}{(\tilde{r}_c\tilde{d}_r)^n} + \frac{1}{K_A{}^2(\tilde{d}_r^2-\tilde{r}_c^2)^2} \qquad (3\text{-}9)$$

where k_i is correction coefficient of expansion loss (around 0.3), f_0 is a friction coefficient (0.005 for a steel cyclone), $K_A=\pi D^2/4ab$ (inlet area ratio), $\tilde{b}$ is the dimensionless cyclone inlet width, $\tilde{d}_r$ is the dimensionless cyclone outlet diameter, $\tilde{F}_s$ is the dimensionless area of the contact surface, $\tilde{V}_{\theta w}$ is a dimensionless tangential velocity at radius R, n is the swirl exponent and $\tilde{r}_c$ is the dimensionless radius of the core flow. (Dimensionless parameters are defined in the Nomenclature). $\tilde{r}_c$ has been correlated [39] with a dimensionless diameter of the cyclone outlet, $\tilde{d}_r$, as

$$\tilde{r}_c = 0.38\tilde{d}_r + 0.5\tilde{d}_r{}^2 \qquad (3\text{-}10)$$

In addition, the dimensionless tangential velocity at the cyclone wall is given [39] by

$$\tilde{V}_{\theta w} = \frac{1.11 K_A{}^{-0.21} \tilde{d}_r{}^{0.16}\,\mathrm{Re}^{0.06}}{1+f_0\tilde{F}_s\sqrt{K_A\tilde{d}_r}} \qquad (3\text{-}11)$$

where Re is the cyclone Reynolds number, defined as:

$$\mathrm{Re} = \frac{\rho_g u_g' D}{\mu_g K_A \tilde{d}_r} \qquad (3\text{-}12)$$

The swirl exponent, n, can also be correlated [39] with Re by

$$n = 1 - \exp\left[-0.26\,\mathrm{Re}^{0.12}\left(1+\left|\frac{S-a}{b}\right|\right)^{-0.5}\right] \qquad (3\text{-}13)$$

For dust-laden gases, the cyclone drag coefficient should also be a function of solid loading. Chen and Shi [39] proposed the following equation for cyclone drag coefficient ξ_c, with a dust-laden gas:

$$\xi_c = \left(1+\frac{C_i}{\rho_g}\right)\left(1-\frac{2k_i\tilde{b}}{1+1.33\tilde{b}-\tilde{d}_r}\right)^2 + 1.11 f K_A \tilde{F}_s \tilde{V}'^{\,3}_{\theta w} \tilde{d}_r^{\,-1.5n} + \frac{\tilde{V}'^{2}_{\theta w}}{(\tilde{r}_c\tilde{d}_r)^n} + \frac{1}{K_A^{\,2}(\tilde{d}_r^2-\tilde{r}_c^2)^2} \tag{3-14}$$

where C_i is the inlet dust loading (kg of inlet solid/m^3 inlet gas). Muschelknautz [83] proposed an expression for f:

$$f = f_0(1+3\sqrt{C_i/\rho_g}) \tag{3-15}$$

Based on empirical measurements of Chen and Shi [39], together with Ogawa et al. [89], the following equation is utilized for $\tilde{V}'^{2}_{\theta w}$

$$\tilde{V}'^{2}_{\theta w} = \frac{\tilde{V}^2_{\theta w}}{1+0.35(C_i/\rho_g)^{0.27}} \tag{3-16}$$

3.2.3. Implementation and Results

Using the Chen and Shi [39] cyclone pressure drop correlation, the simple model explained in Section 3.2.1 can be implemented. Two parallel cyclones built for experimental studies are used as reference geometries for this work, as shown in Figure 3-5.

Single-Phase Flow Steady-State Solution: Based on equations (3-8) to (3-13), Figure 3-6 presents the pressure drop of the proposed cyclone for different gas distributions gas alone (air) passes through two identical parallel cyclones for an average inlet gas velocity of 15 m/s. Equality of pressure drops must apply for cyclones 1 and 2. It is obvious that

the only intersection of branch 1 (solid line) with branch 2 (dashed line) is that corresponding to a uniform distribution (γ=0.5). Therefore the uniform distribution is the only possible solution for single phase flow passing through parallel cyclones, and no other solution can be imagined. The same behaviour was found for the geometry considered in Chapter 2.

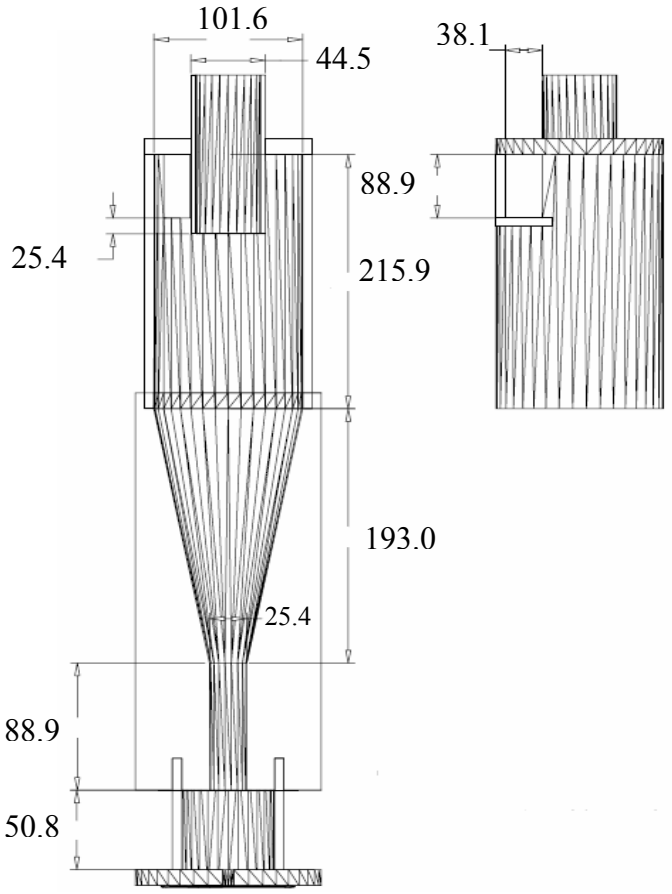

Figure 3-5. Reference cyclone dimensions (all dimensions in mm)

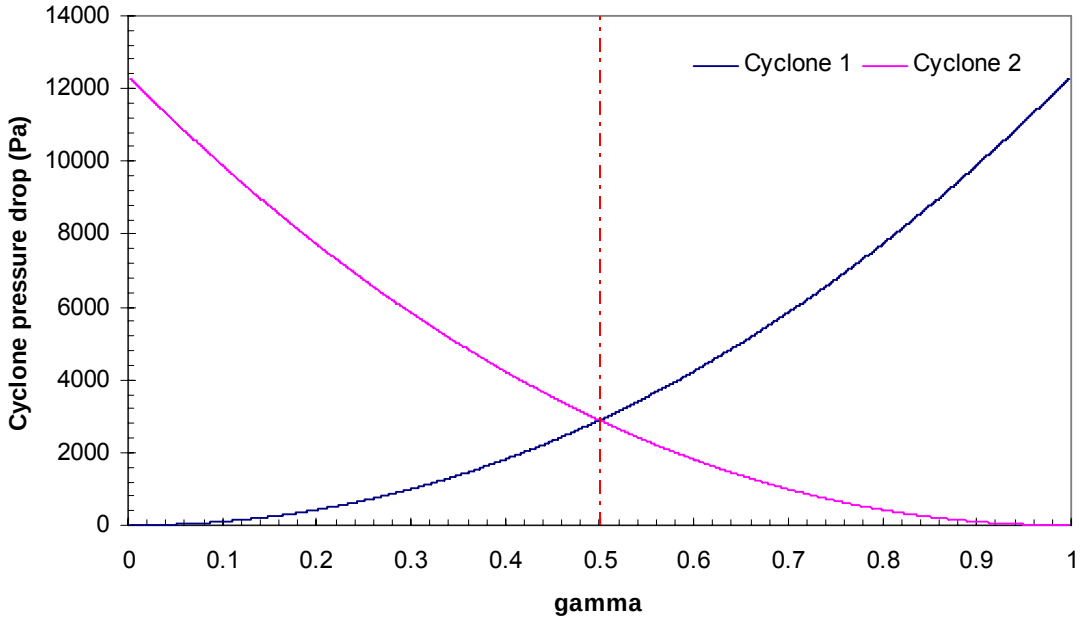

Figure 3-6. Effect of gas (air) alone distribution through two identical parallel cyclones on pressure drop of system (average cyclone inlet velocity: 15 m/s).

Multi-Phase Flow Steady-State Solution: From equations (3-2) to (3-5), the inlet dust loadings (kg/m^3) in cyclones 1 & 2 can be written

$$C_1 = \frac{\rho_g \sigma m_{st}}{\gamma m_{gt}} \tag{3-17}$$

$$C_2 = \frac{\rho_g (1-\sigma) m_{st}}{(1-\gamma) m_{gt}} \tag{3-18}$$

Before predicting the flow distribution for multi-phase flow, it is of interest to observe the drag reduction portrayed by the correlation of Chen and Shi [39]. Figure 3-7 shows the pressure drop for a single cyclone (with reference dimensions as shown in Figure 3-5) and 30 m/s average inlet air velocity. As expected, in very dilute solid concentrations, the cyclone pressure drop decreases because of drag reduction, before increasing. Hence the

Chen and Shi [39] model seems to provide a reasonable approach for estimation of cyclone pressure drops.

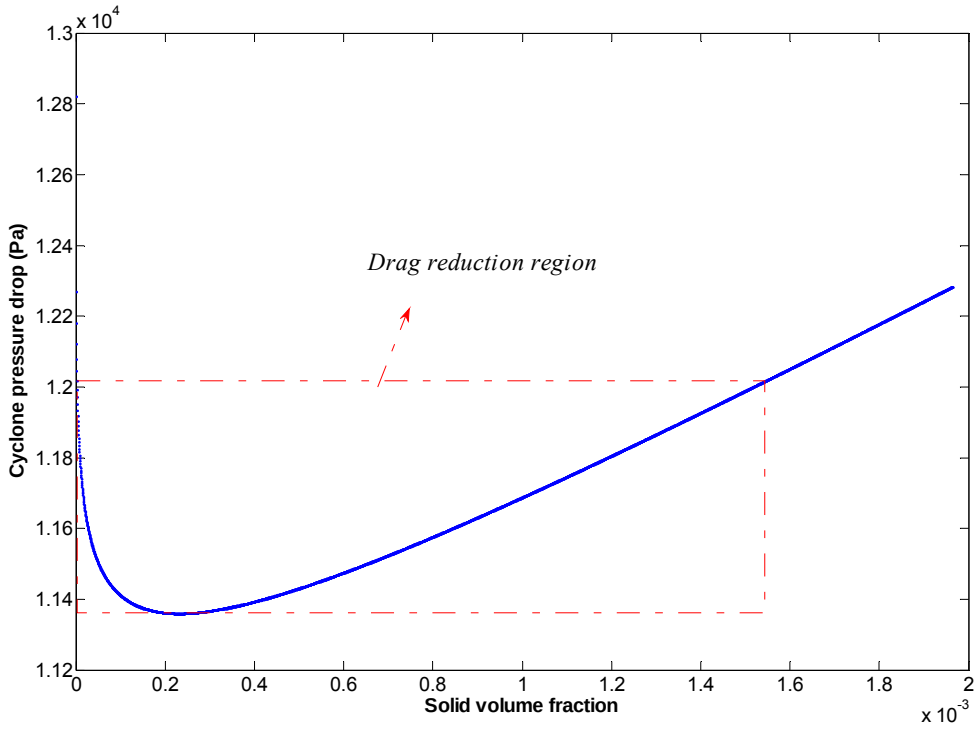

Figure 3-7. Drag reduction at low solid concentrations for pressure drop across cyclone. Cyclone geometry as in Figure 3-5.

Figure 3-8, based on equation (3-6), presents possible gas-solid distributions for two identical parallel cyclones, obtained by setting different γ value and then solving for the other σ and calculating the (matched) pressure drops based on equation (3-14). The operating conditions are presented in Table 3-1. The solid lines are different mixture distribution solutions through path 1, whereas the dashed lines are the corresponding ones through path 2. Colours represent different portions of solids passing through path 1 (i.e. different σ). The solutions are given by the locus of intersection points of the same colour solid (path 1) and dashed (path 2) lines.

Table 3-1. Defined operating conditions (20°C and 101.3 kPa).

Gas	
Type	Air
Density (kg/m^3)	1.225
Viscosity (kg/m.s)	1.79E-05
Average cyclone inlet velocity (m/s)	15
Solids[1]	
Type	Glass Beads
Density (kg/m^3)	2500
Inlet solids volume fraction, α_s (%)=1-ε	20

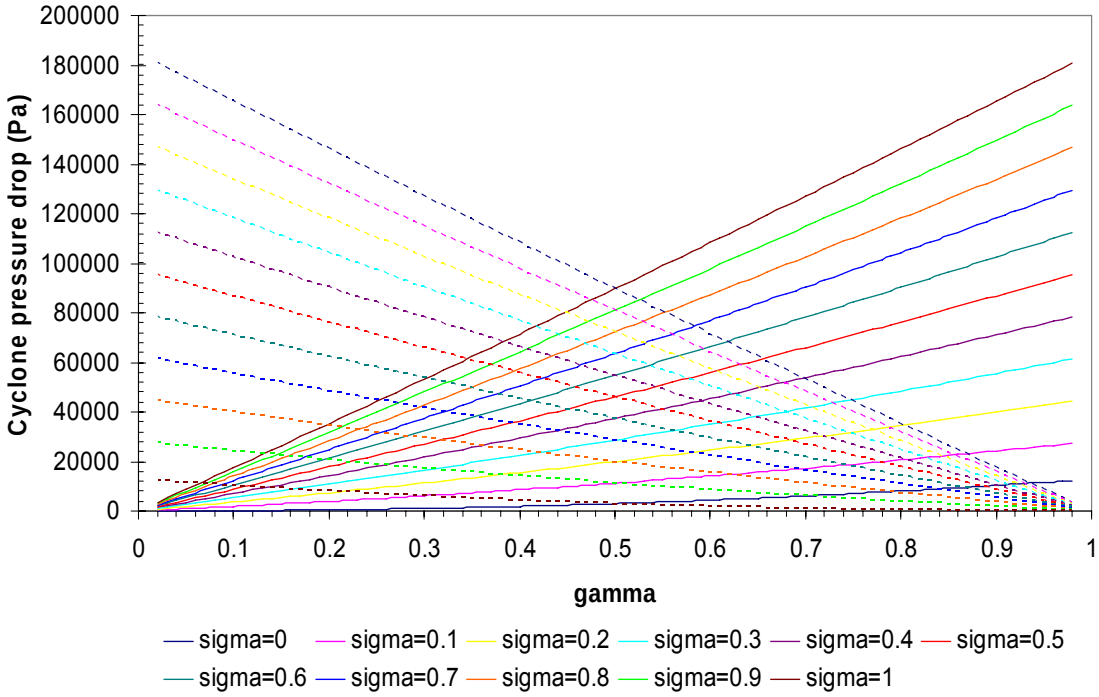

Figure 3-8. Effect of unequal distribution of gas-solid flows though two identical parallel cyclones on pressure drop of system (solid lines: Path 1, dashed lines: Path 2). Cyclone geometry as in Figure 3-5; operating conditions as in Table 3-1.

Figure 3-9 shows a 3D plot of all possible gas-solid distributions through the two parallel cyclones, obtained from Figure 3-8. Based on that and the 2D plot in Figure 3-10, contrary to the case study of 'Y branch' presented in Chapter 2, the uniform distribution

[1] Note that Chen and Shi [39] cyclone model is not explicitly a function of particle diameter. Here the particle diameter is not specified.

of gas-solid flow has a maximum pressure drop through the parallel cyclones for the conditions investigated.

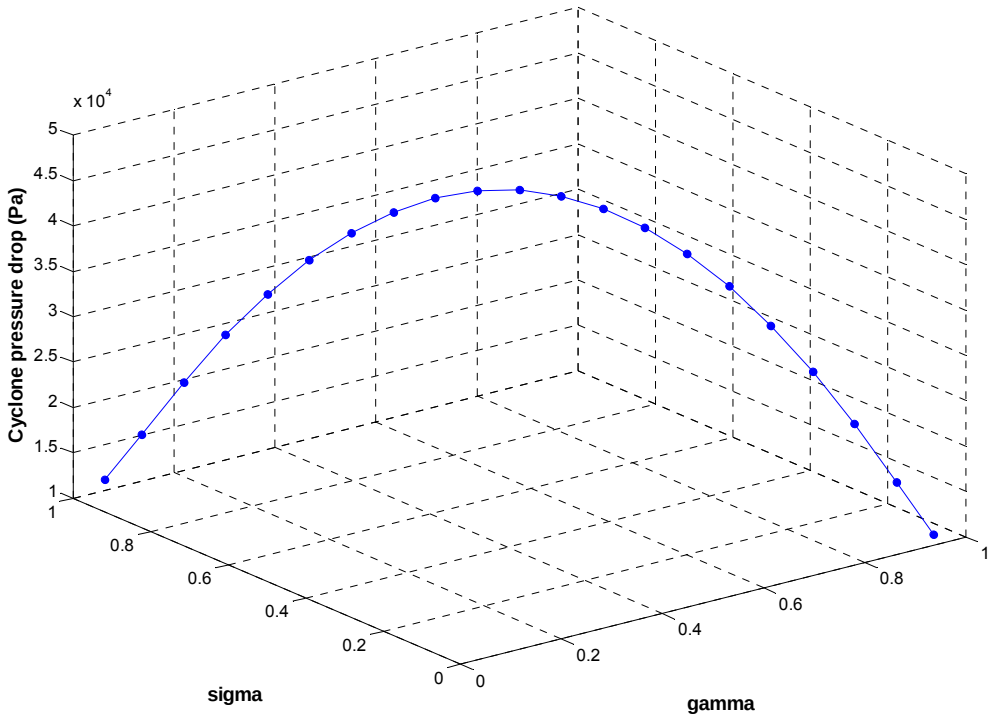

Figure 3-9. Possible gas-solid distribution solutions and its effect on pressure drop of two parallel cyclones. Cyclone geometry as in Figure 3-5; operating conditions as in Table 3-1.

Understanding the mechanism of satisfying the equality of pressure drop through the cyclones helps to rationalize the behaviour of the system. Both Figures 3-9 and 3-11 show that the solutions with more gas passing through path 1 (γ>0.5) have less solids flow through cyclone 1, i.e. σ<0.5, and vice versa for the geometry and total gas and solids flows considered. Also Figure 3-12 shows how the cyclone drag coefficient varies when the gas fractions in cyclones 1 and 2 are varied to satisfy the equal pressure drop criterion. When more gas passes through cyclone 1, more solids are required to pass through cyclone 2 for pressure drop compensation, i.e. to match the pressure drops through the two cyclones.

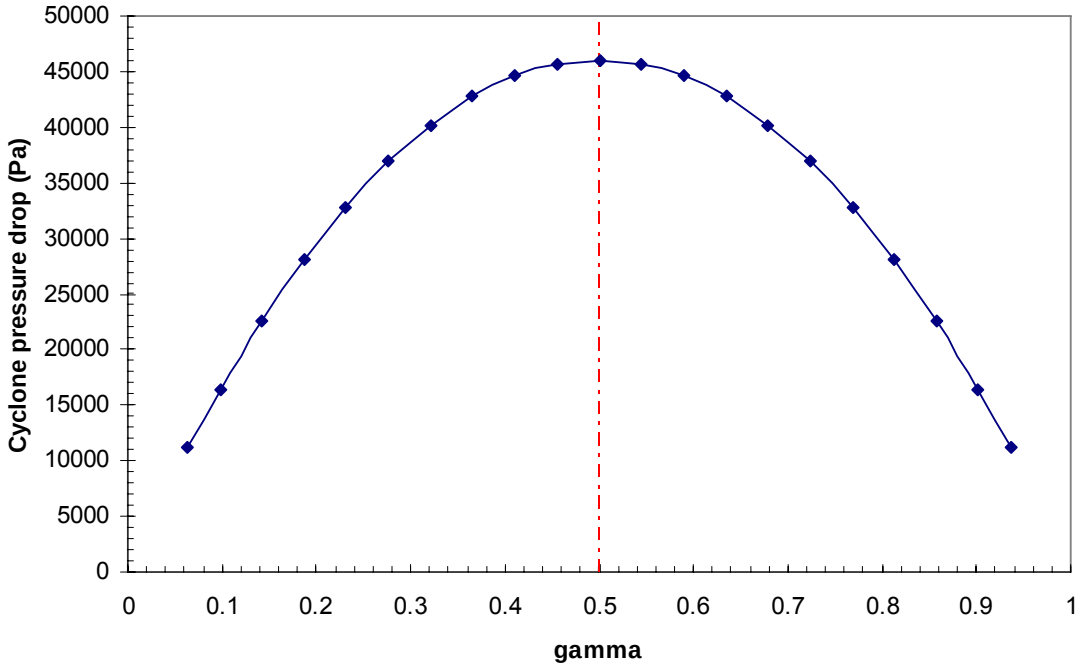

Figure 3-10. Effect of unequal distribution of the gas stream on cyclones pressure drop. Cyclone geometry as in Figure 3-5; operating conditions as in Table 3-1.

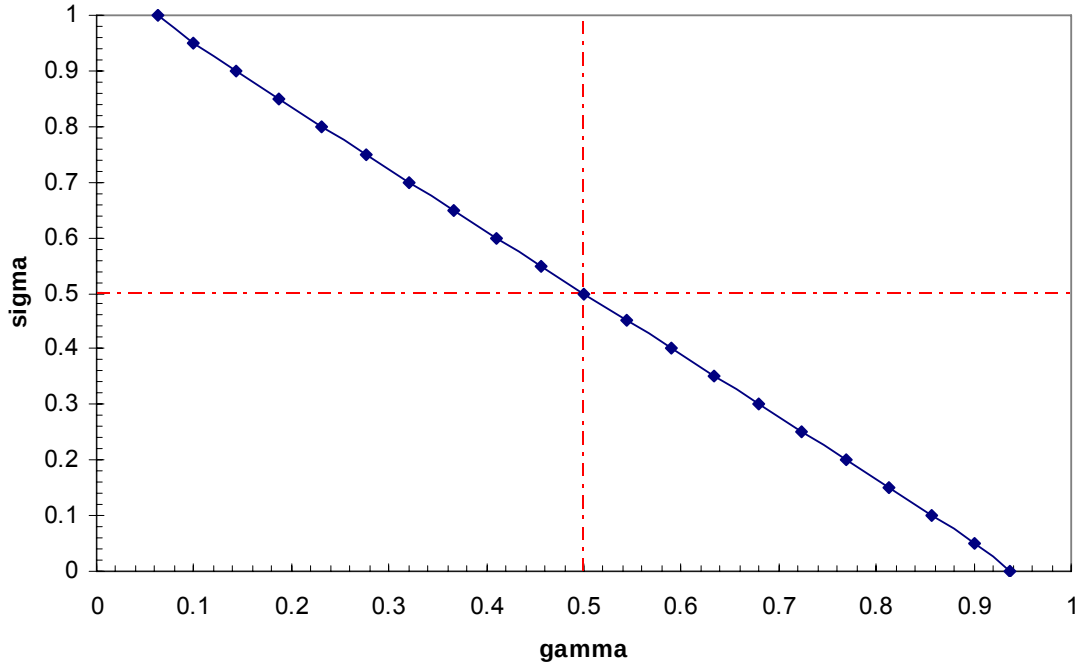

Figure 3-11. Relationship between gas and solids distribution parameters. Cyclone geometry as in Figure 3-5; operating conditions as in Table 3-1.

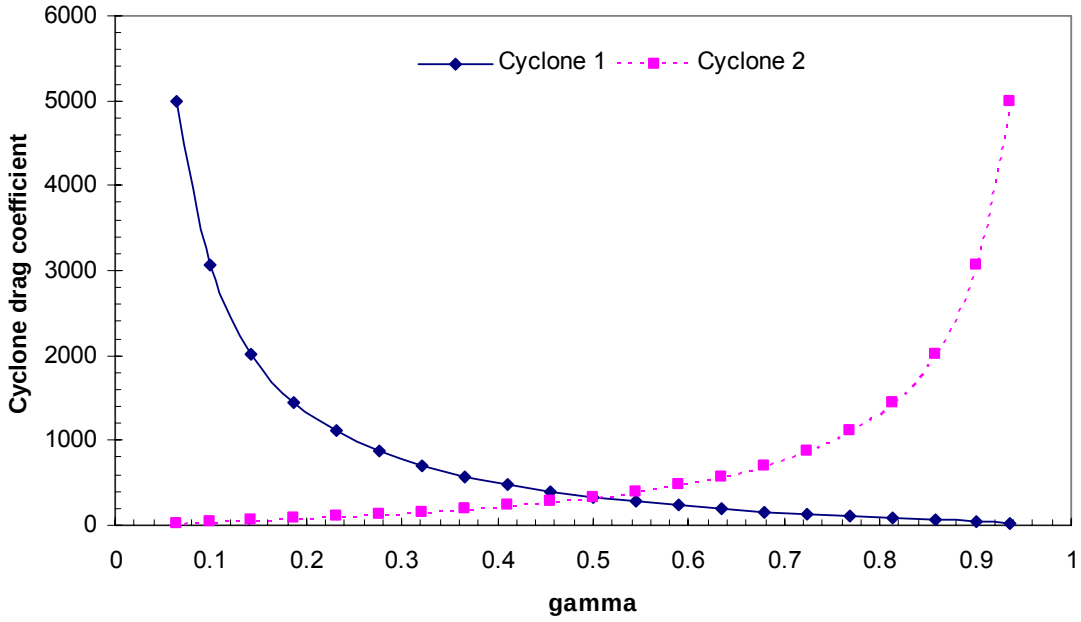

Figure 3-12. Cyclone drag coefficient to satisfy pressure drop balance criterion with varying γ. Cyclone geometry as in Figure 3-5; operating conditions as in Table 3-1.

As pointed out, the pressure drop predicted by Chen and Shi [39] model is a function of both inlet gas velocity and cyclone drag coefficient. Based on the figures, the uniform distribution solution has a higher gas velocity and a lower cyclone drag coefficient than solutions with γ<0.5 (and vice versa for solutions with γ>0.5). The multiplication of these two parameters makes the pressure drop of the uniform distribution solution a maximum. In this case, the uniform distribution of gas-solid flow through identical parallel cyclones consumes maximum energy. Considering the energy minimization approach presented in Chapter 1, this appears to correspond to increased probability of mal-distribution of gas-solids flow through identical parallel cyclones.

3.2.4. Sensitivity Analysis

Based on the proposed cyclone model, another interesting exercise is to predict the behaviour of the system for different solid concentrations. Figure 3-13 shows the effect of mal-distribution of gas stream on pressure drop of identical parallel cyclones for three

inlet solid volumetric concentrations (with the other operating conditions the same as in Section 3.2.3). For all three concentrations, the uniform distribution solution corresponds to maximum pressure drop. It is also clear that when a more dilute mixture is passed through the system, the region of possible non-uniform distribution solutions is more limited. In addition, the cyclone pressure drop varies over a narrower range in more dilute systems.

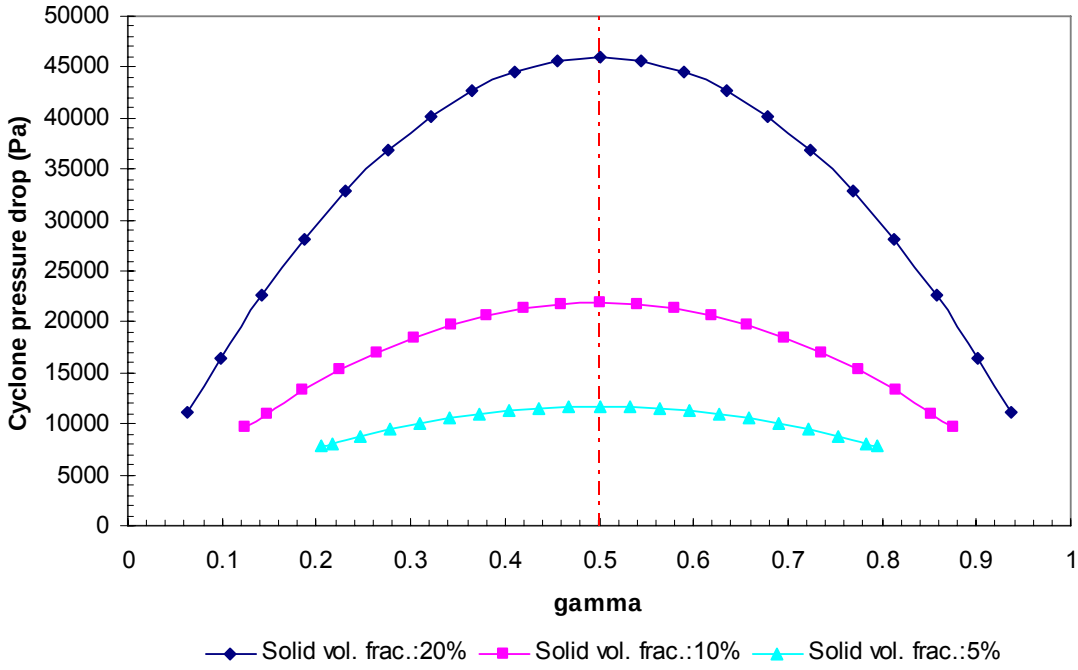

Figure 3-13. Effect of mal-distribution of gas stream on cyclones pressure drop in different inlet solids volumetric concentrations. Cyclone geometry as in Figure 3-5; operating conditions as in Table 3-1.

For more dilute systems, Figure 3-14 shows the pressure drop of the cyclones as a function of γ for a 1% solid inlet volume fraction. Similar to the denser cases presented above, the equal distribution solution has a local maximum pressure drop, but a new type of behaviour is observed; there are two solutions (points A and B in Figure 3-14) with maximum pressure drop. Based on Figure 3-15, there are two turning regions that do not follow the behaviour of the rest of the solutions. Point A is located in the turning region

and has a greater value of γ than its next right side point. Moreover based on Figure 3-16, point A has the highest cyclone drag coefficient among the solutions and the maximum pressure drop through the cyclones. Similarly point B corresponds to no solids in cyclone 1 and maximum overall pressure drop. These two operating points (A and B) are believed to not be relevant in practice as they correspond to all solids travelling through one of the cyclones, something which is probably impossible.

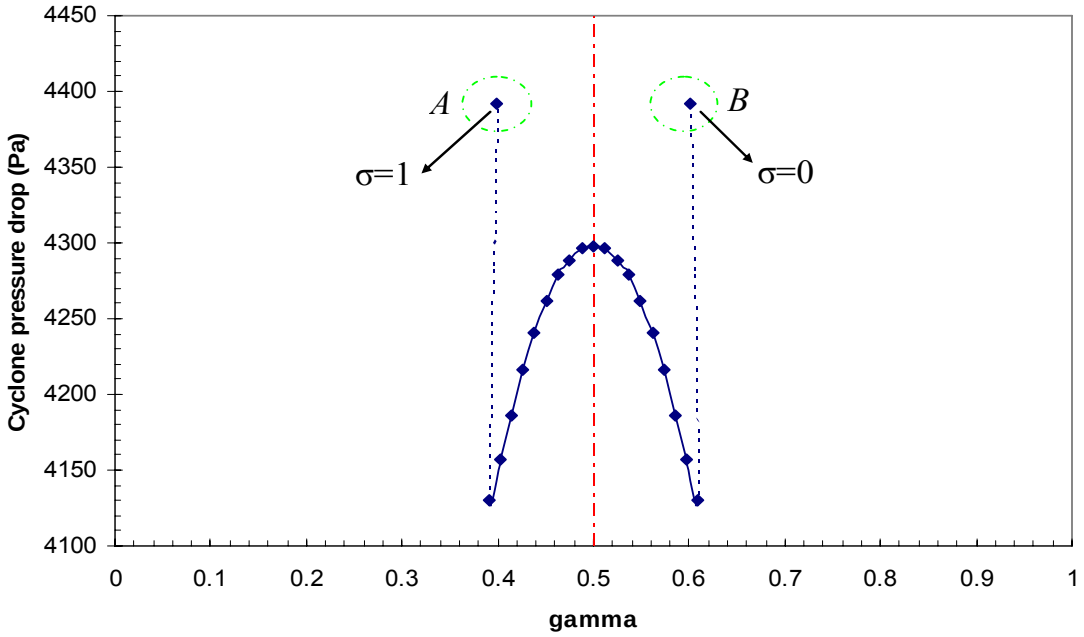

Figure 3-14. Effect of unequal distribution of the gas stream on cyclones pressure drop for 1% solid volume fraction. Cyclone geometry as in Figure 3-5; operating conditions as in Table 3-1.

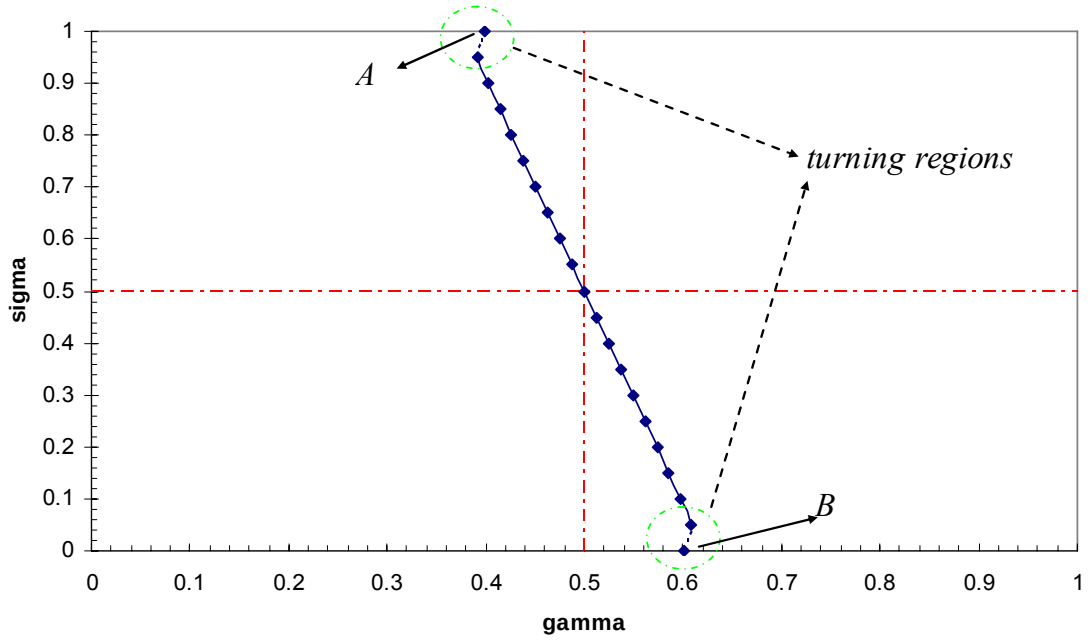

Figure 3-15. The distribution of gas and solid streams through two identical parallel for 1% solid volume fraction. Cyclone geometry as in Figure 3-5; operating conditions as in Table 3-1.

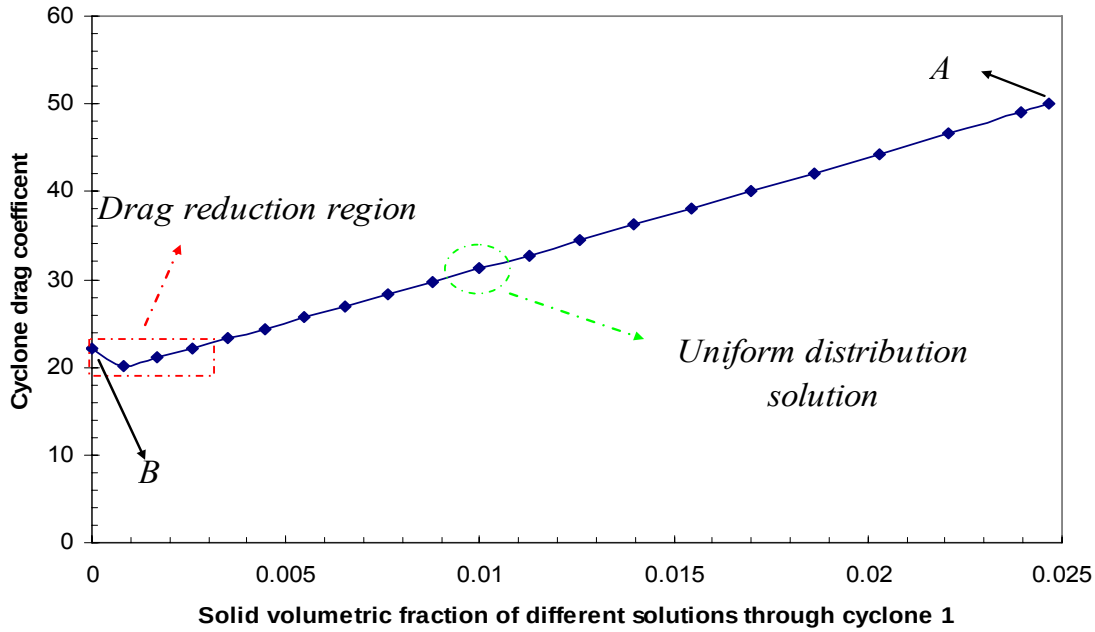

Figure 3-16. Drag reduction through the cyclones for 1% solid volume fraction. Cyclone geometry as in Figure 3-5; operating conditions as in Table 3-1.

As shown in Figure 3-17, by making the system very dilute, the distribution pattern of gas-solid mixture changes and in very dilute cases (0.01% solid volumetric fraction), the mechanism of the distribution of gas-solid flow through the parallel cyclones to reach the same pressure drop in both paths switches to that corresponding to Chapter 2. This means that in very dilute gas-solid flow, solutions with a greater portion of gas in cyclone 1 (γ>0.5) contain more solids flow (σ>0.5) as well. This causes very dilute systems to have a minimum pressure drop corresponding to the uniform distribution solution, as presented in Figure 3-18. Note that based on Figure 3-17, in dense cases (20%, 10% and 5% solids volume fraction) there is no turning region, whereas when the system become more dilute, the turning region arises. That is why the uniform distribution solution has the overall maximum pressure drop in dense cases, whereas there are two points with overall maximum pressure drop in dilute systems.

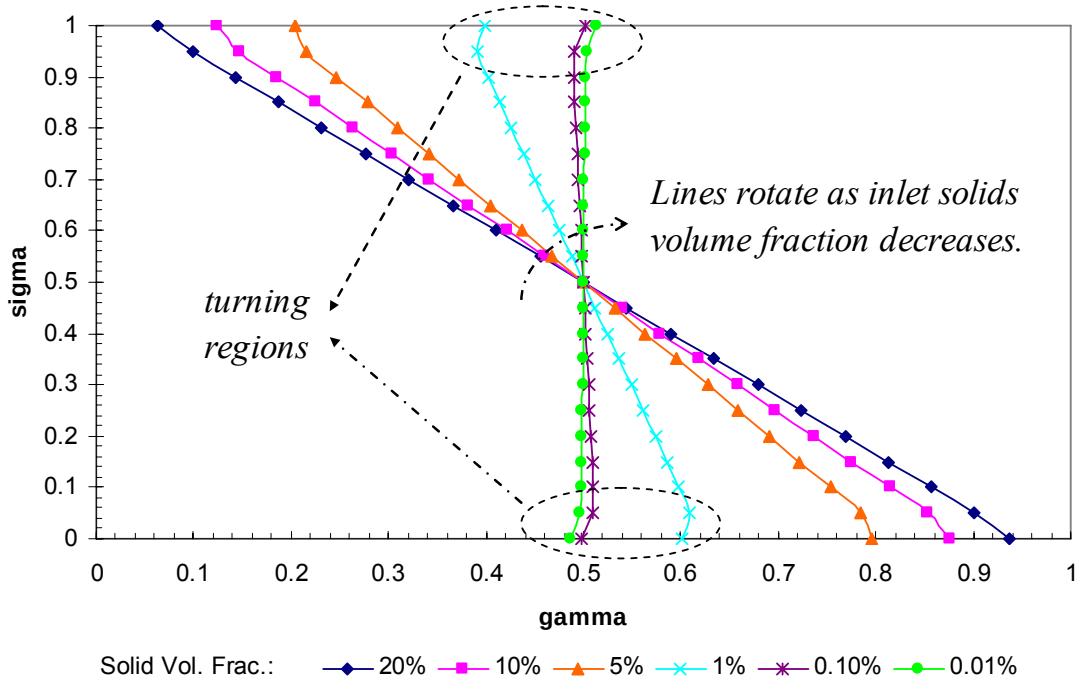

Figure 3-17. The distribution of gas and solid streams through two identical parallel cyclones in different solid volumetric fractions. Cyclone geometry as in Figure 3-5; operating conditions as in Table 3-1.

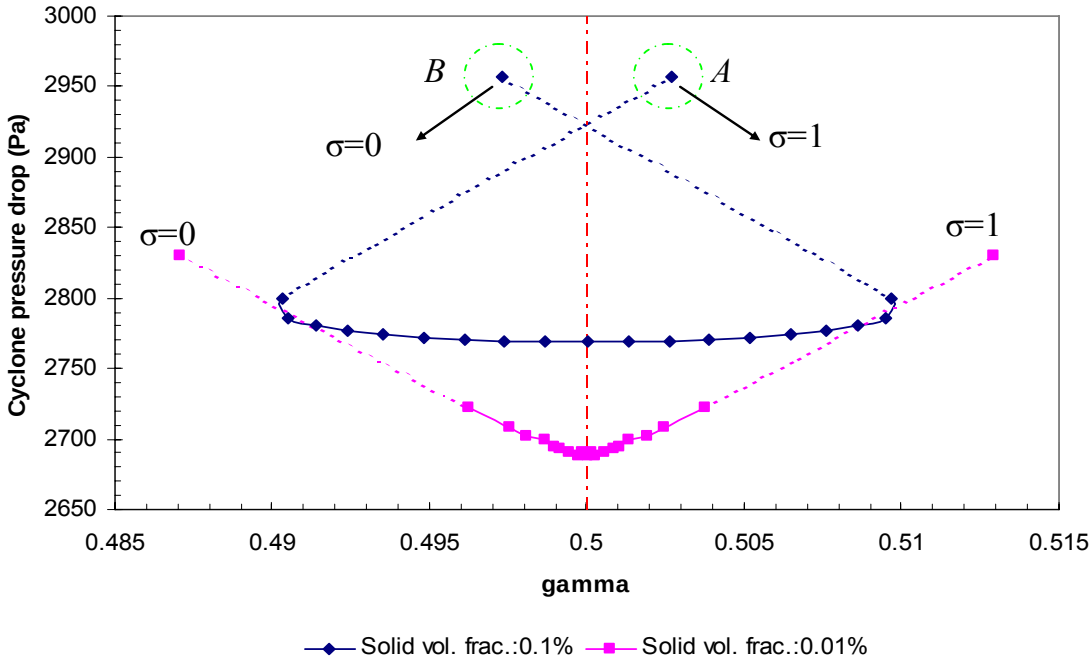

Figure 3-18. Effect of mal-distribution of gas stream through two identical parallel cyclones in dilute systems. Cyclone geometry as in Figure 3-5; operating conditions as in Table 3-1.

Figure 3-18 shows two strange solutions, points A and B, with new behaviour. Based on Figures 3-17 and 3-19, since the corresponding line to the 0.1% solids volume fraction case is very close to the symmetry axis and the turning regions corresponding to points A and B cross the vertical symmetry axis, these two points are special. It is apparent, as presented in Figure 3-20, for α_s=0.0001, an even lower concentration than 0.1% solids volume fraction, the σ-γ line passes the axis of symmetry and the odd behaviour of those two points disappears (as shown in Figure 3-18).

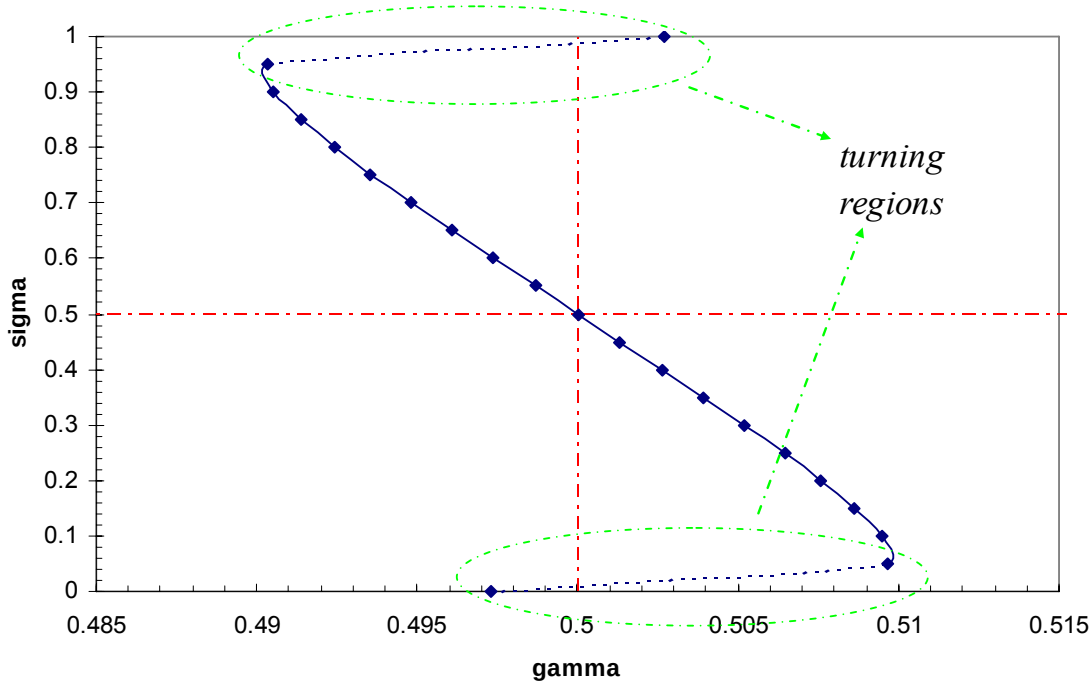

Figure 3-19. σ as a function of γ for 0.001 solid volume fraction case. Other conditions as in Table 3-1.

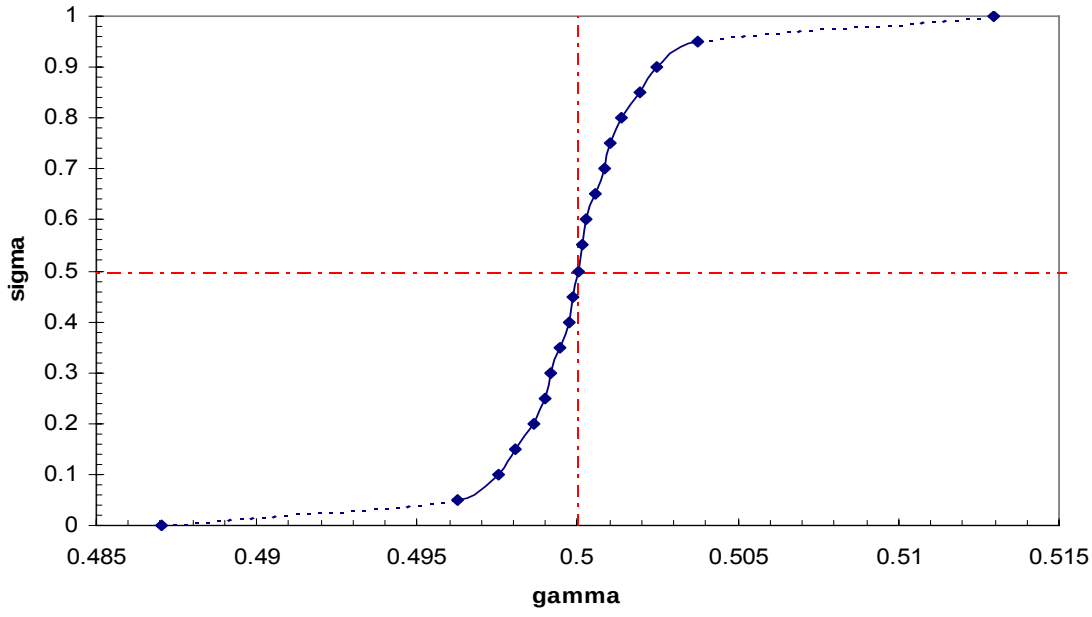

Figure 3-20. σ as a function of γ for 0.0001 solid volume fraction case. Other conditions as in Table 3-1.

3.2.5. Discussion and Conclusions of the Modeling Studies

Dense Systems: Based on the Chen and Shi [39] cyclone correlation, it is shown that a wide array of gas-solid distributions can satisfy the condition of equality of pressure drop through two identical parallel cyclones. A uniform distribution is always one solution. In dense gas-solid multiple cyclone systems, the uniform distribution solution has the greatest pressure drop among the solutions, and the difference between the equal distribution pressure drop and other mal-distributed ones can be very significant. The possibility of the existence of mal-distributed solution is likely to be greater in dense cases. This should be verified experimentally. If energy minimization applies[1], significant mal-distribution is likely to occur in practice, providing an explanation for some of the observations of non-uniformity in practice summarized in Chapter 1.

Dilute Systems: As a system becomes more dilute, the range of mal-distributed solutions becomes narrower and, as presented in Figure 3-18, in very dilute gas-solid systems the solutions are limited to a narrow region near γ=0.5 (uniform distribution). For example, the mal-distributed solutions are limited to the narrow band from $\gamma\approx$0.49 to $\gamma\approx$0.51 in Figure 3-18. In addition, as the system becomes more dilute, drag reduction affects the behaviour of the system and the mechanism of distribution switches to behaviour similar to that for the "Y branch", presented and discussed in Chapter 2. In sufficiently dilute cases, the uniform distribution solution has the minimum cyclone pressure drop. Moreover, there is very little difference between the equal-distribution pressure drop and the unequal ones. In summary, the analyses show that the most favorable distribution solution in dilute cases is likely to be indistinguishable in practice from the uniform distribution of gas-solid flow through identical parallel cyclones.

[1] There is no available transient cyclone pressure drop model in order to perform analytical stability analysis on the steady-state solutions. Therefore energy minimization is applied.

3.3. EXPERIMENTAL STUDY

3.3.1. Experimental Equipment

Limited experimental studies have been done in dilute systems, In order to study the distribution of gas-solid flow through identical parallel paths. An experimental facility with two Plexiglass parallel cyclones was investigated. A photograph of the experimental facility is presented in Figure 3-21. The geometry and dimensions of the Stairmand cyclones are presented in Figure 3-5. As indicated in Figure 3-22 and Figure 3-23, high-pressure air is injected through the system from the bottom, and the gas flow rate is measured by a manually controlled (Visi-Float) flow meter with 2% accuracy (VFC series, Dwyer instruments). The particles are introduced to the system by a solid volumetric screw hopper (100 series, 0-0.0142 m^3/hr, Schenck AccuRate). After the multi-phase gas-solid flow is distributed through the bifurcation, the solids are gathered from the bottom of both parallel cyclones. Also the pressure for each cyclone can be measured at points 1, 2, 3 and 4 in Figure 3-22. The gas flow leaving each of the cyclones can be double separated through two fine dust strainers (CRAFTSMAN) downstream. For the experiments covered in this thesis, since the filters containing porous media were not sufficiently identical, they were removed from the system.

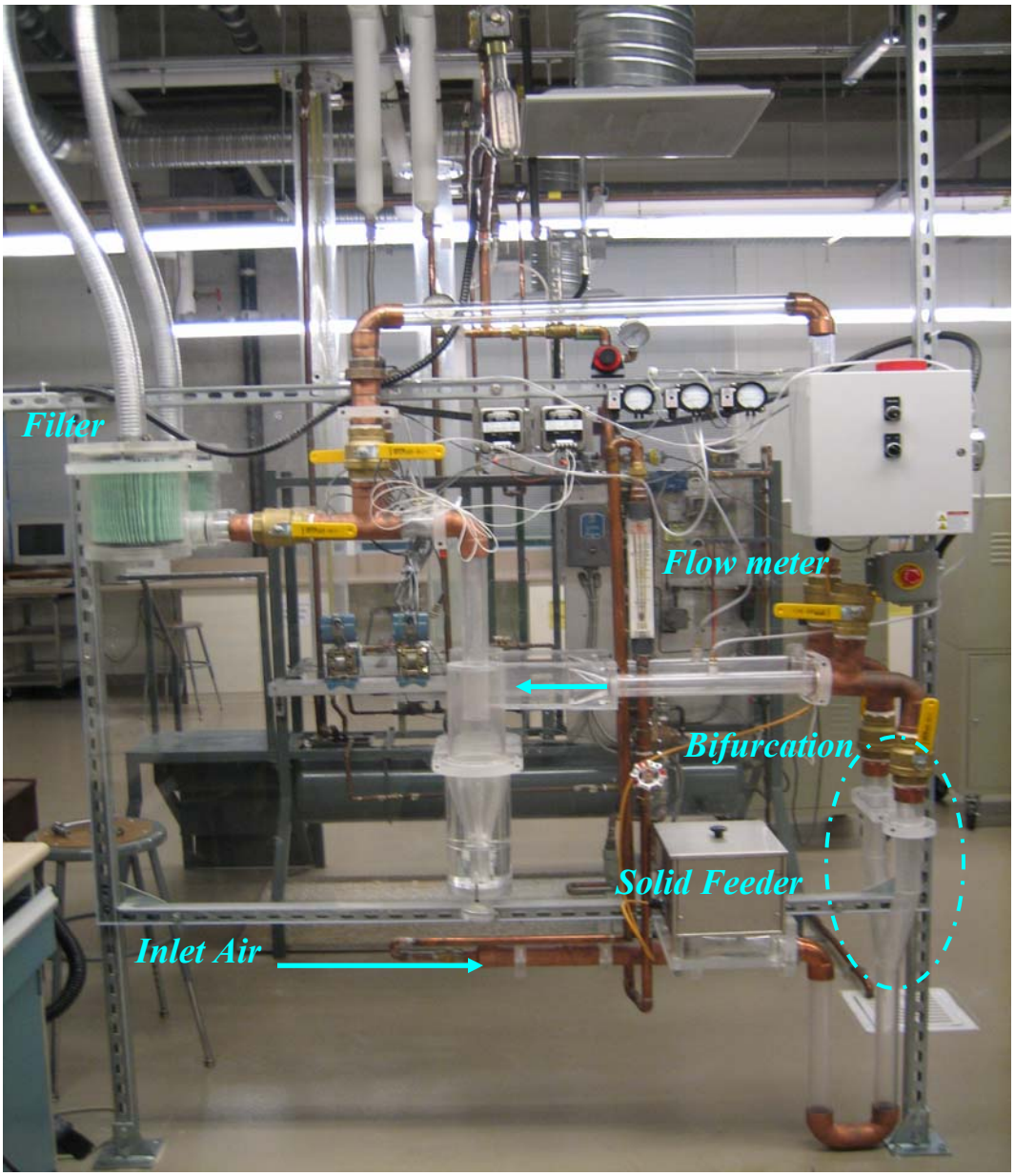

Figure 3-21. Image of equipment set-up containing identical parallel cyclones.

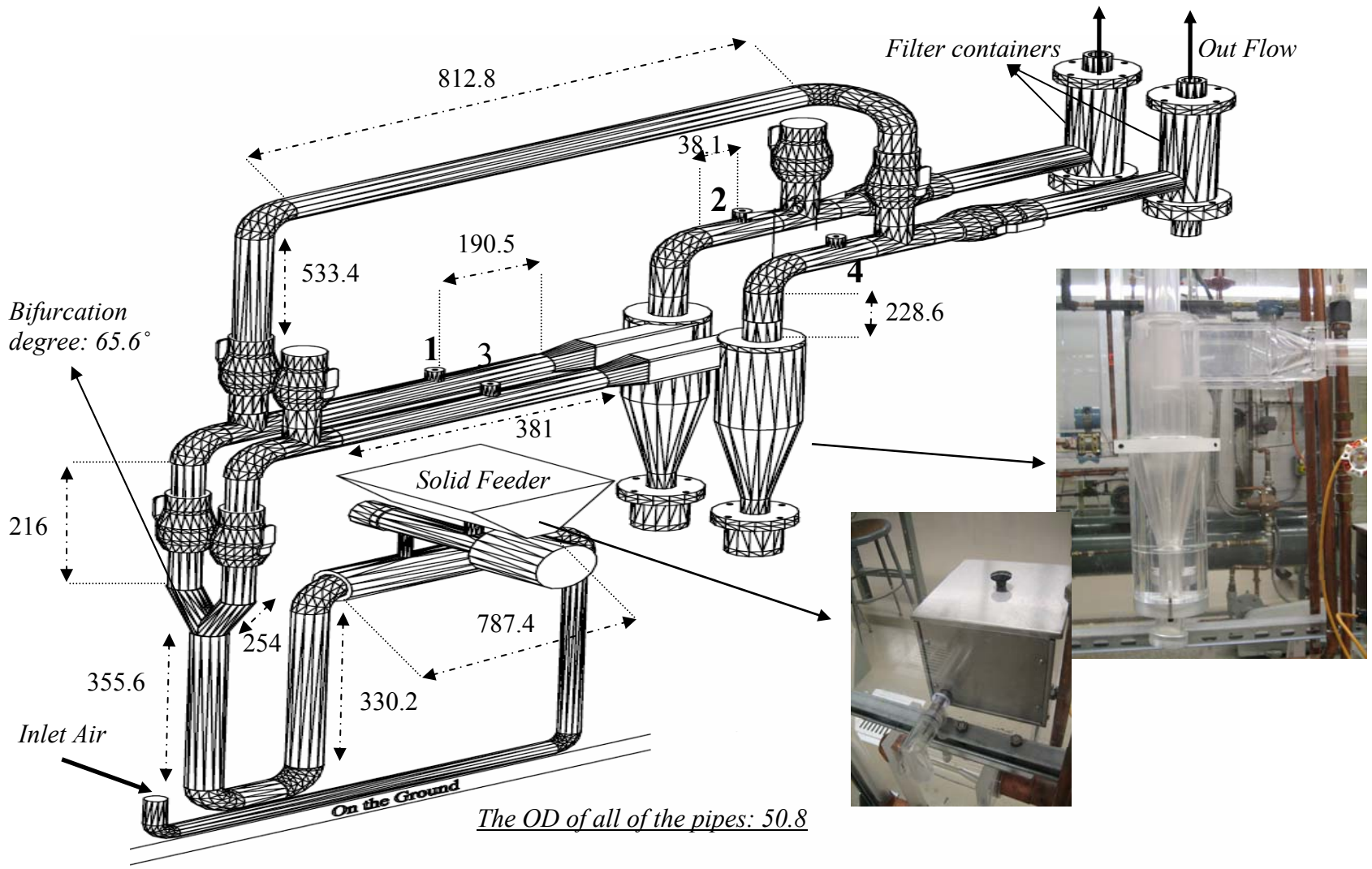

Figure 3-22. Drawing and dimensions of experimental facility (all dimensions in mm). Cyclone geometry as in Figure 3-5.

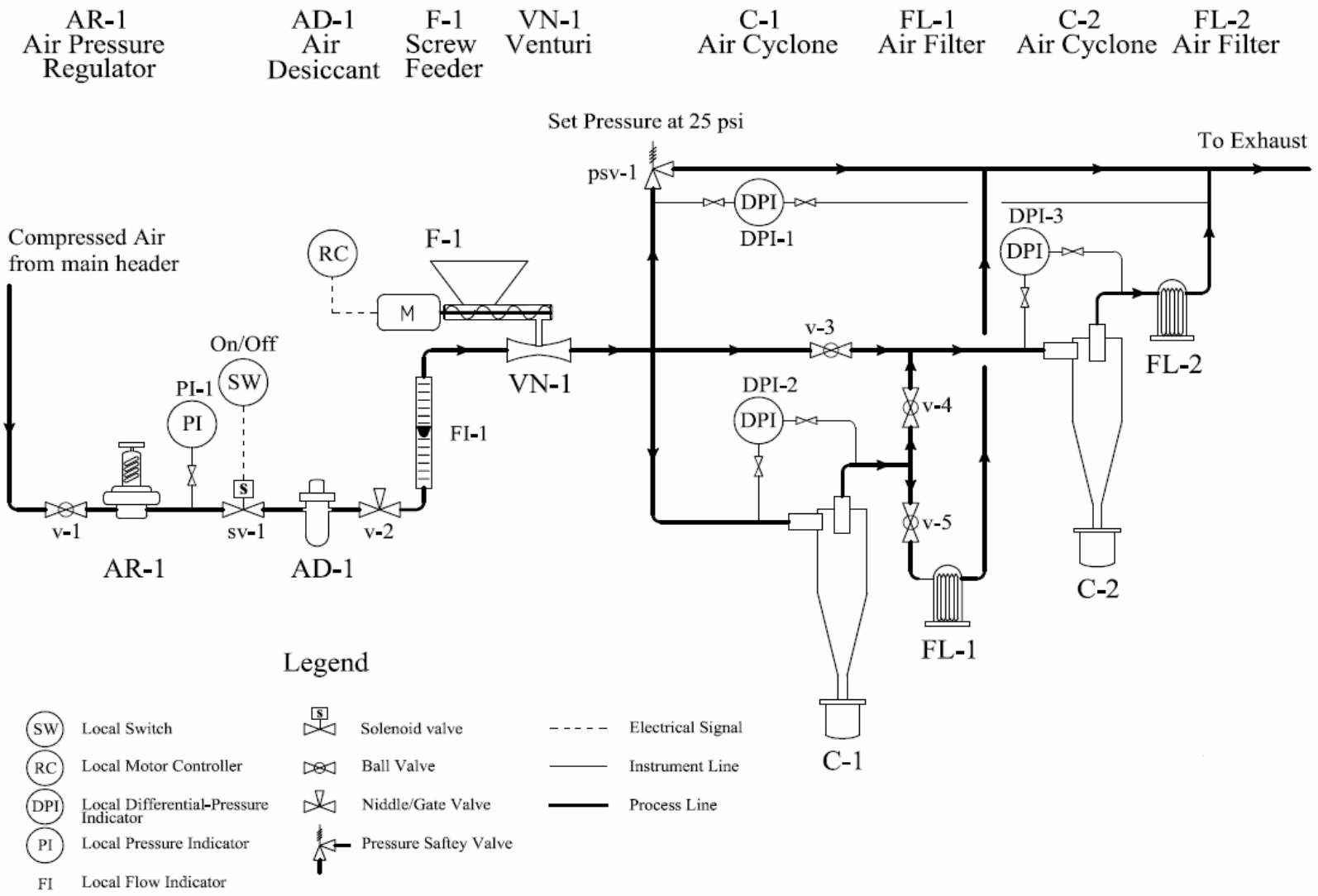

Figure 3-23. Schematic of experimental rig.

3.3.2. Verification of Symmetry

Considerable care was exercised during construction to ensure identical geometry on the right and left side of the bifurcation. It is of interest to check the symmetry of the facility by comparing the pressure drops of the left and right cyclones. To do this, 0.0212 m^3/s pure air was passed through the parallel cyclones and the pressure drop of each was measured by differential pressure transducers. As shown in Figure 3-24, an arithmetic mean pressure drop of cyclone 1 and 2 were virtually the same ($\Delta P_{12,\ mean}$=449 Pa and $\Delta P_{34,\ mean}$=451 Pa). However, since the population of data was distributed over time, a better method to compare the two sets of data is statistical. Hence, the Student t-test was performed, and it was obtained that with 95% confidence level, there was no significant difference between the population means of cyclones 1 and 2, so that the pressure drops across both cyclones were statistically the same[1].

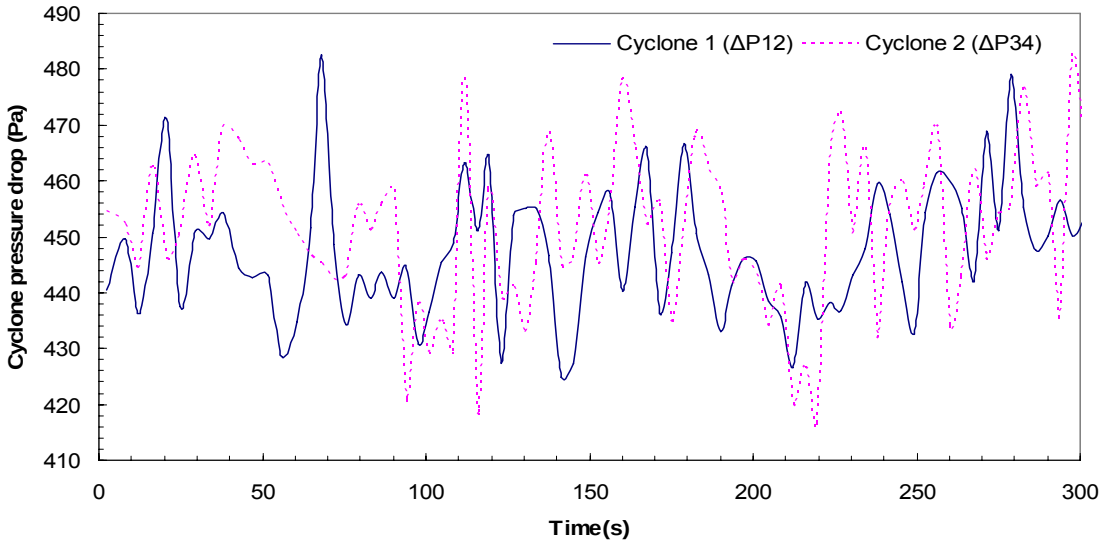

Figure 3-24. Comparison of the pressure drops for parallel cyclones when 0.0212 m^3/s of pure air is passed through the system. Cyclone geometry as in Figure 3-5.

[1] Excel software was used for t-test. As a rule of thumb:

- Probability associated with t-test < 5% → the mean for treatment 1 is significantly different from the mean for treatment 2.
- Probability associated with t-test > 5% → the mean for treatment 1 is not significantly different from the mean for treatment 2 (with 95% confidence level).

If the geometry is symmetrical, passing air through the system should cause points at the same locations on the right and left sides to have the same pressure. Therefore as another pre-processing test, the same locations in right and left sides (point 1 & 3 and 2 & 4 of Figure 3-22) were connected by two differential pressure transducers. As presented in Figures 3-25 and 3-26, the pressure difference between the two points at the same location before the cyclones (points 1 and 3) and those at the corresponding position after the cyclones (point 2 and 4) was very small (In both Figure 3-25 and Figure 3-26, path 1 has 2.3 Pa more pressure drop than path 2, a negligible amount relative to the overall pressure drop of 689.5 kPa). Again this approves that the geometry on the right and left were almost identical.

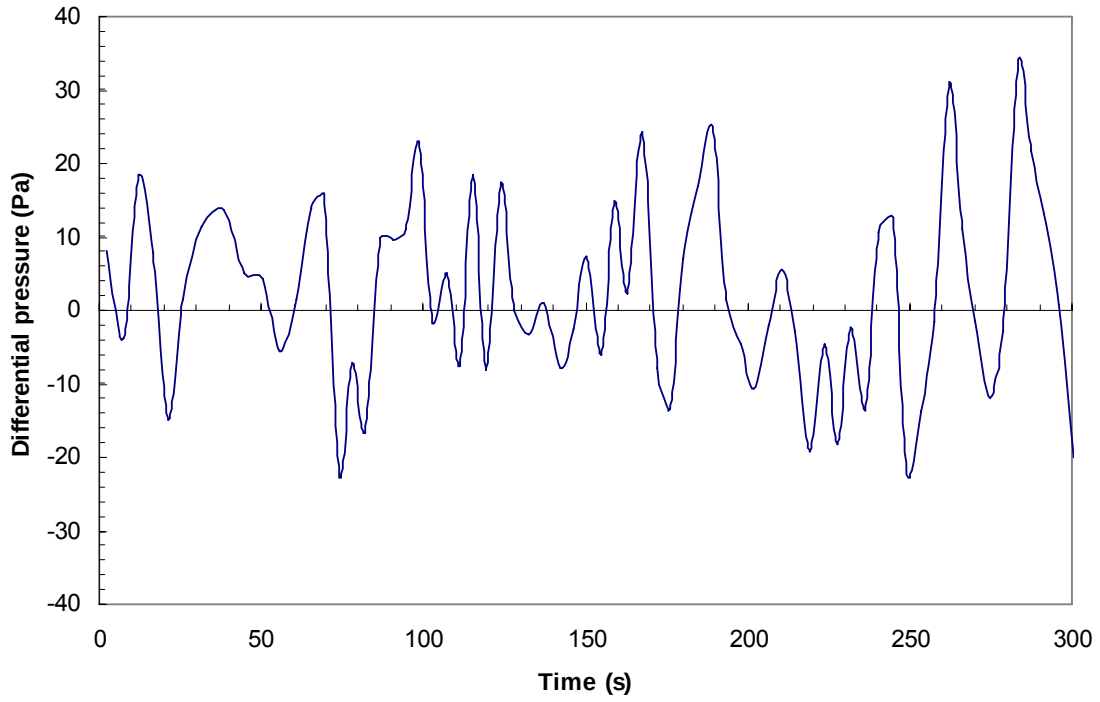

Figure 3-25. Pressure difference between two points at corresponding locations on left and right sides upstream of the cyclones (ΔP_{13}). Cyclone geometry as in Figure 3-5.

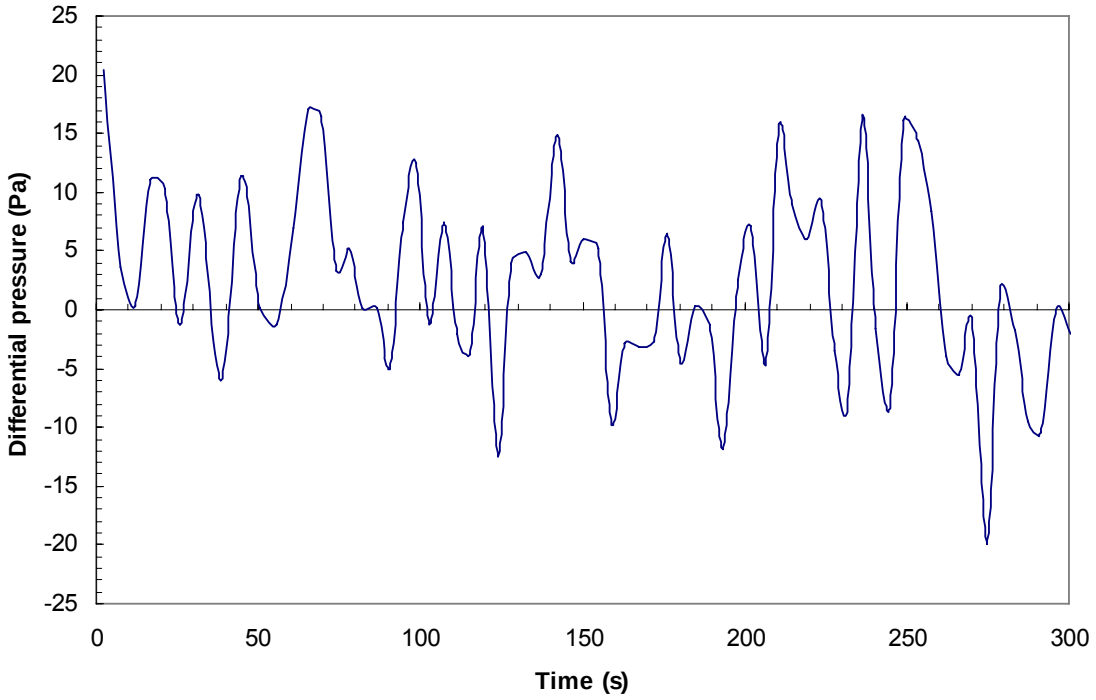

Figure 3-26. Pressure difference between two points at corresponding locations on left and right sides downstream of cyclones (ΔP_{24}). Cyclone geometry as in Figure 3-5.

3.3.3. Experimental Results

3.3.3.1. Steady-State Measurements

Limited experimental studies have been done in dilute gas-solid systems. For the first type of experiment, the dilute gas-solid flow was passed through the two identical parallel cyclones with operating conditions as presented in Table 3-2. The pressure drop of each cyclone was measured dynamically using differential pressure transducers. After 20 minutes of operation, the system was shut down and the solids were retrieved from the bottom of the cyclones and weighed manually. As indicated in Figure 3-27, ten runs were performed with the same operating conditions. Figure 3-27 shows that the distribution of dilute gas-solid flow through identical parallel cyclones was almost uniform. After 20 minutes of operation, cyclone 1 contained 52% of the total solids mass and cyclone 2, 48%. As shown in Figure 3-27, in all 10 runs, each started up from rest, somewhat more

solids passed through cyclone 1 than cyclone 2. This suggests that there may be some small physical differences between paths 1 and 2.

Table 3-2. Experimental operating conditions (20°C and 101.3 kPa).

Gas	
Type	Air
Density (kg/m^3)	1.225
Viscosity (kg/m.s)	1.79E-05
Volumetric flow rate (m^3/s)	0.0212
Solids	
Type	Glass Beads
Density (kg/m^3)	2500
Particle size	U.S. Mesh 80-100
Mass flow rate (kg/s)	0.00025

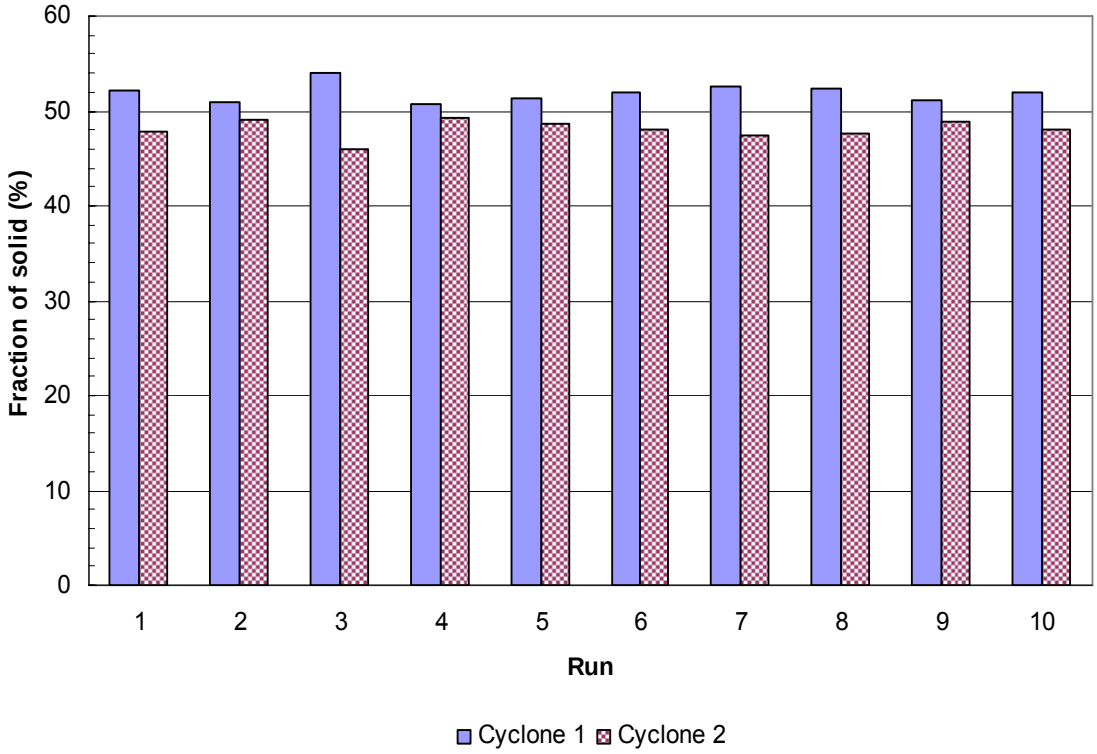

Figure 3-27. Distribution of particles through parallel cyclones in ten runs with identical operating conditions. Cyclone geometry as in Figure 3-5; operating conditions as in Table 3-1.

Figure 3-28 shows the pressure drop across cyclones 1 and 2 as a function of time for run # 2. The student's t-test method shows that during 20 min of the operation, the cyclones pressure drops were statistically equal. The cyclone pressure drop fluctuations for other runs were quite similar to those presented in Figure 3-29.

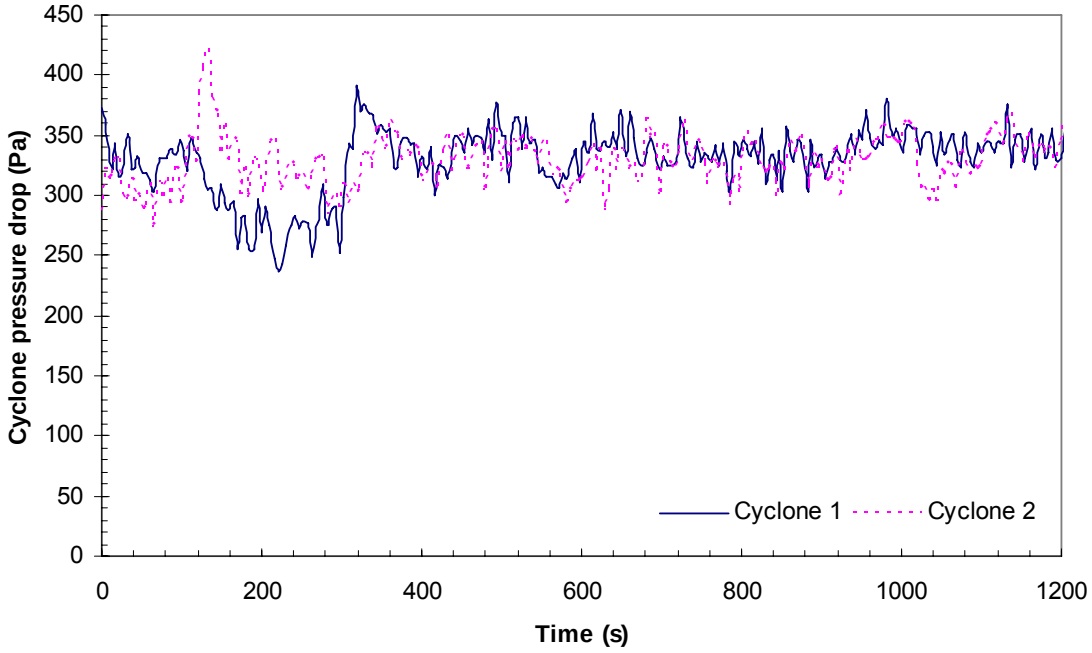

Figure 3-28. Pressure drops through cyclones 1 and 2 for run #2. Cyclone geometry as in Figure 3-5; operating conditions as in Table 3-1.

Using the modeling approach presented in Section 3.2, Figures 3-29, 3-30 and 3-31 show the results of the analytical model for the conditions of this experimental study. Based on the model, since the inlet flow is very dilute, the uniform distribution solution which has the minimum energy consumption is expected to be the most likely solution of the system. Based on Figure 3-29, all possible solutions are limited to the region from $\gamma \approx 0.49$ to $\gamma \approx 0.51$ and the pressure drop difference between the solutions should be no more than 2.3%. Figure 3-30 compares the solid distribution solutions predicted by the model and the ten experimental trials presented above. Based on these ten empirical trials, the region of possible experimental solutions is from $\sigma \approx 0.46$ to $\sigma \approx 0.54$ and there is little discrepancy

between the corresponding pressure drops. This can be taken, when one consider experimental error, to indicate that the energy minimization approach can be applied in the model and that there is good consistency between the empirical measurements and the model predictions. It should be noted that the difference between the average measured cyclone pressure drop and that predicted by the model at uniform distribution solution is 8%.

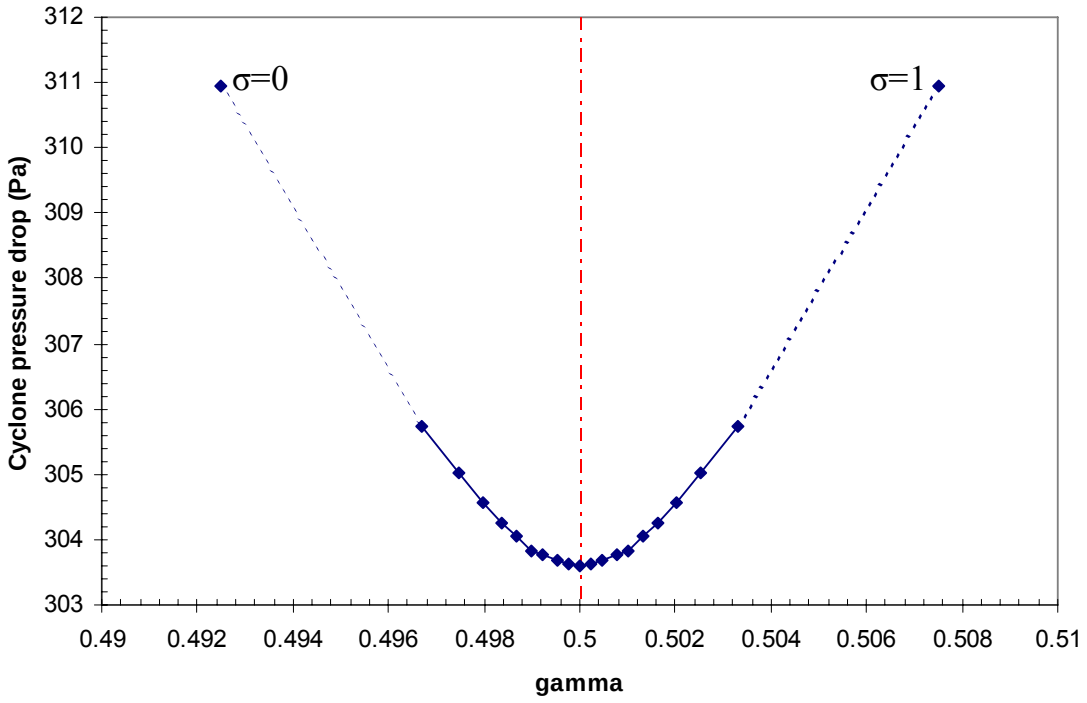

Figure 3-29. Possible gas distribution and pressure drop solutions predicted by cyclone model for conditions of the experimental study. Cyclone geometry as in Figure 3-5; operating conditions as in Table 3-1.

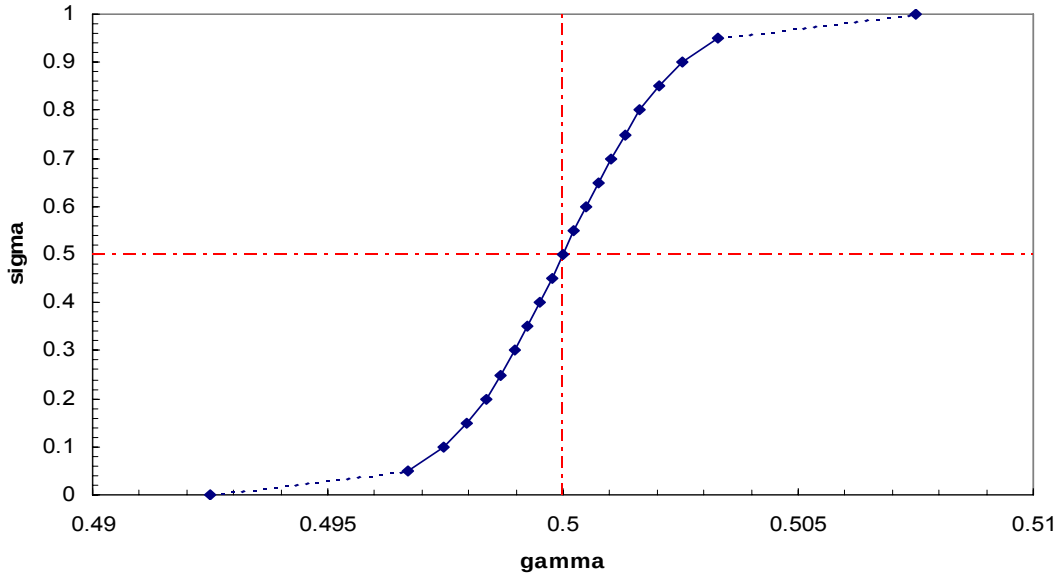

Figure 3-30. Possible gas-solid distributions for the experimental study predicted by cyclone model. Cyclone geometry as in Figure 3-5; operating conditions as in Table 3-1.

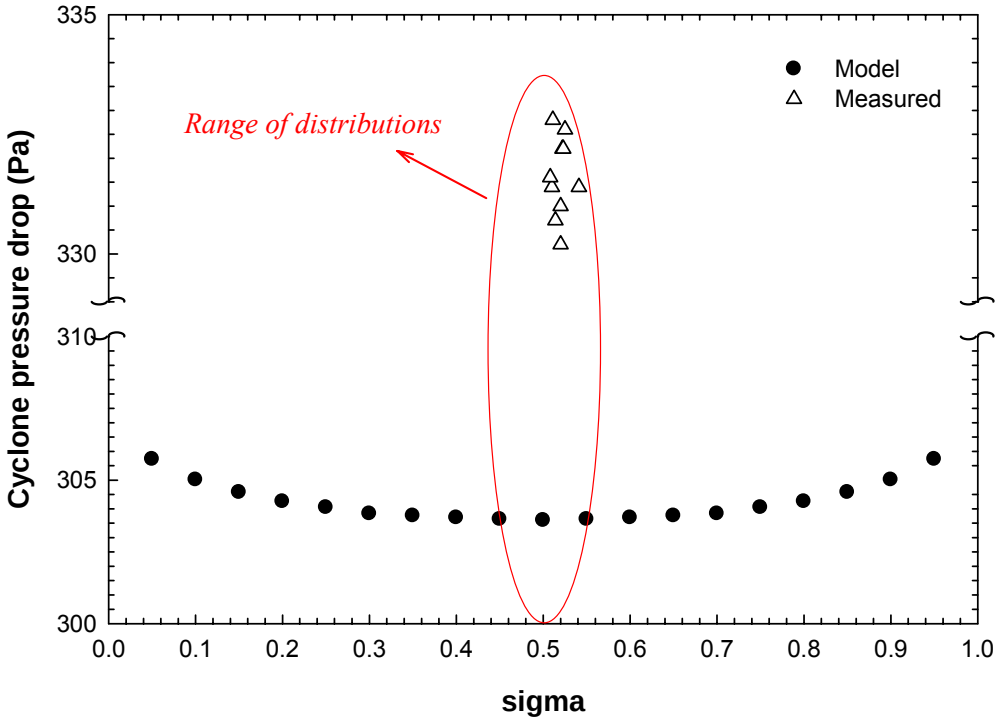

Figure 3-31. Comparison between experimental solid distribution measurements and corresponding solutions predicted by Chen and Shi [39] cyclone model. Cyclone geometry as in Figure 3-5; operating conditions as in Table 3-1.

3.3.3.2. Dynamic Measurements

In the next experimental tests, it was of interest to observe the solids accumulation at the bottom of each cyclone as a function of time. By this means, the dynamic behavior of the distribution of solids through identical parallel cyclones can be investigated. Continuous weighing of particles from each path was made possible by installing load cells at the bottom of both cyclones. However, it was found that the accuracy and stability of the measured data were unacceptable because the load cells are highly sensitive and easily influenced by radial torque generated by particles entering with high momentum. Therefore, a commercial digital balance (EC-2000, 0-2000 gr, Cole-Parmer) with accuracy of 0.01 gr was installed at the bottom of each of the cyclones. Theses scales were connected to the computer and the output data were recorded continuously. Dynamic weighing of the solids in each cyclone was performed with the operating conditions as presented in Table 3-3. The weight of the solids in each path was recorded every 15 s.

Table 3-3. Empirical operating conditions for continuous solids weight measurement (20°C and 101.3 kPa).

Gas	
Type	Air
Density (kg/m^3)	1.225
Viscosity (kg/m.s)	1.79E-05
Flow rate (m^3/s)	0.0212
Solids	
Type	Glass Beads
Density (kg/m^3)	2500
Particle size	U.S. Mesh 80-100
Flow rate (kg/s)	0.00017

Figure 3-32 plots the mass of solids in each cyclone as a function of time. It appears that the solid stream switched from having more through cyclone 2 for the first 400 s to having more solids passing cyclone 1. The differences were, however, small. Also Figure 3-33 displays the cumulative solid fraction distribution as a function of time. Both fractions values converge to nearly σ=0.5. Based on these figures, the system exhibits transient behaviour, but after some time, the system reaches a nearly uniform state. As

above, more solids tend to pass through cyclone 1, likely caused by very small differences in path 1 and 2 geometries. The overall sigma for cyclone 1 is 51%.

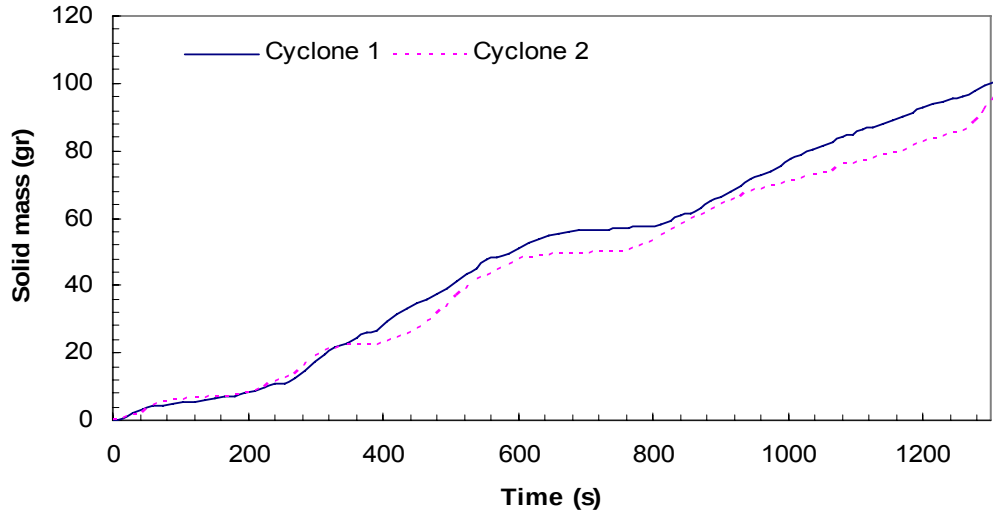

Figure 3-32. Weight of particles as a function of time in each cyclone. Cyclone geometry as in Figure 3-5; operating conditions as in Table 3-1.

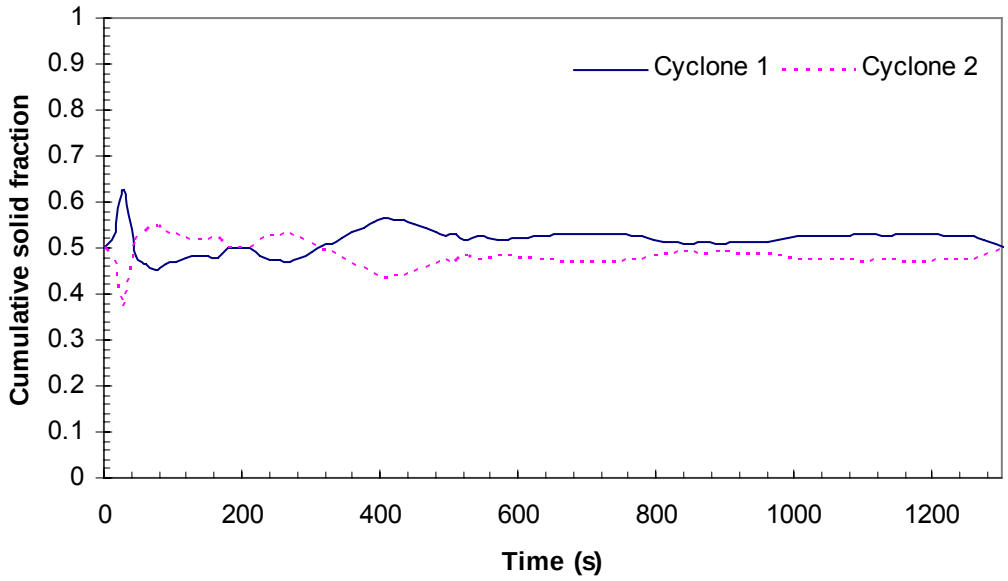

Figure 3-33. Fractional distribution of solids as a function of time for each cyclone. Cyclone geometry as in Figure 3-5; operating conditions as in Table 3-1.

The cyclones pressure drops were also measured, as presented in Figure 3-34. The probability associated with t-test of these two groups of data is 93%. Therefore the pressure drops of the cyclones can be considered to be statistically equal with 95% confidence level.

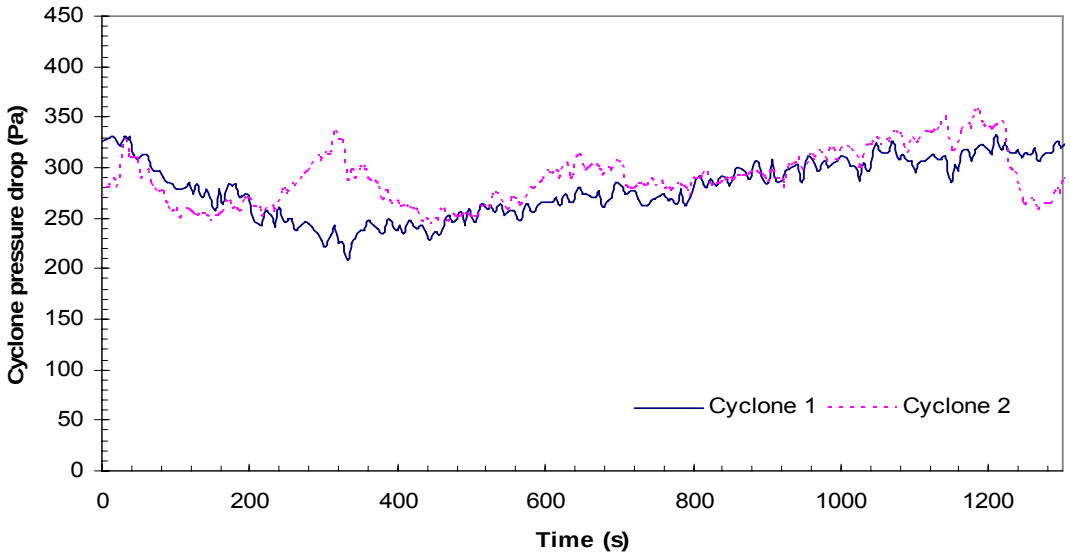

Figure 3-34. Time-varying pressure drops through cyclones 1 and 2. Cyclone geometry as in Figure 3-5; operating conditions as in Table 3-1.

3.3.3.3. Differential Fouling

As shown in Figures 3-1 and 3-2, differential fouling has occurred in a commercial unit attributable to mal-distribution of multi-phase flow through identical parallel cyclones inside a large fluidized bed. This could exacerbate the gas and solids mal-distribution through the cyclones. It is therefore of interest to investigate the effect of small differential fouling on the distribution of the flow.

In order to simulate the differential fouling, the bucket at the bottom of cyclone 1 was partially blocked by a horizontal piece of thin rubber, as demonstrated in Figure 3-35. Therefore by dropping the particles toward the bucket, some particles settled at the top of

the rubber and with the passage of time, a differential 'deposit' accumulated in cyclone 1. Figures 3-36 and 3-37 provide experimental results for the ensuing fouling simulation runs for the operating conditions in Table 3-4. It is apparent in both of these figures that for the first 800 s of operation, there was a nearly uniform distribution of solid flow to the two cyclones. However, after ~800 seconds, the growing 'deposit' inside cyclone 1 affected the solids distribution resulting in a substantial difference between the solids collected in cyclones 1 and 2. The final (after 1320 s) solids weight difference between cyclones 1 and 2 was 91 g, or 57%.

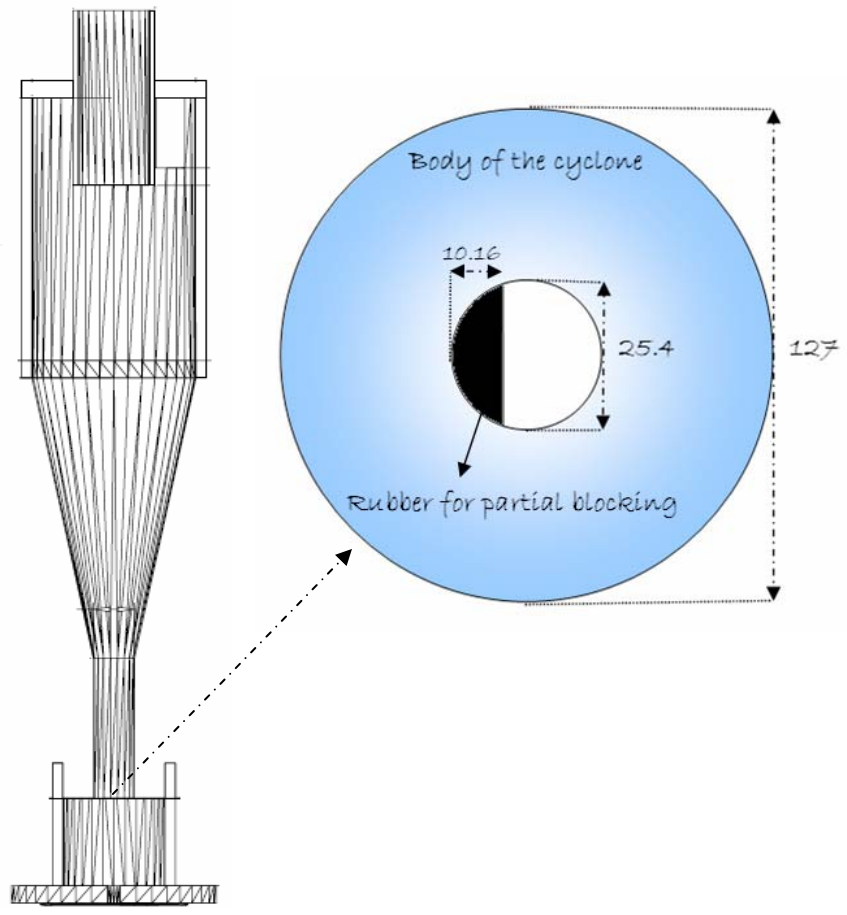

Figure 3-35. Schematic of partial blocking of cyclone 1 bottom with a piece of rubber. Cyclone geometry as in Figure 3-5 (all dimensions in mm).

Table 3-4. Empirical operating conditions for differential fouling simulation (20°C and 101.3 kPa).

Gas	
Type	Air
Density (kg/m^3)	1.225
Viscosity (kg/m.s)	1.79E-05
Flow rate (m^3/s)	0.0212
Solids	
Type	Glass Beads
Density (kg/m^3)	2500
Particle size	U.S. Mesh 80-100
Flow rate (kg/s)	0.00033

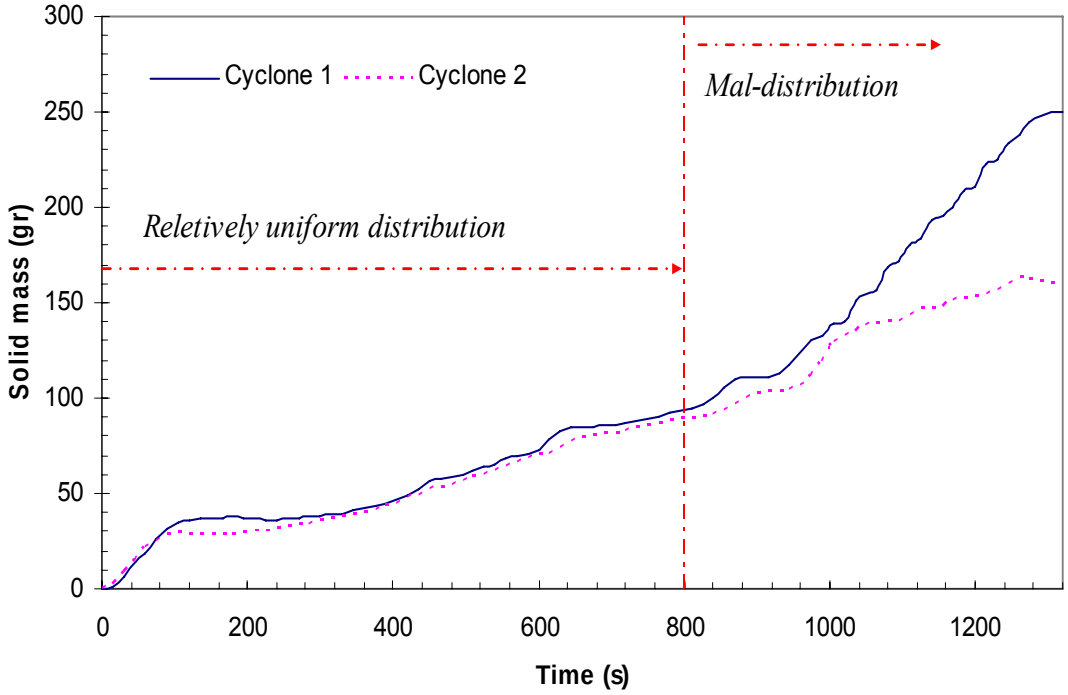

Figure 3-36. Effect of simulated differential fouling on distribution of solid flow. Cyclone geometry as in Figure 3-5; operating conditions as in Table 3-1.

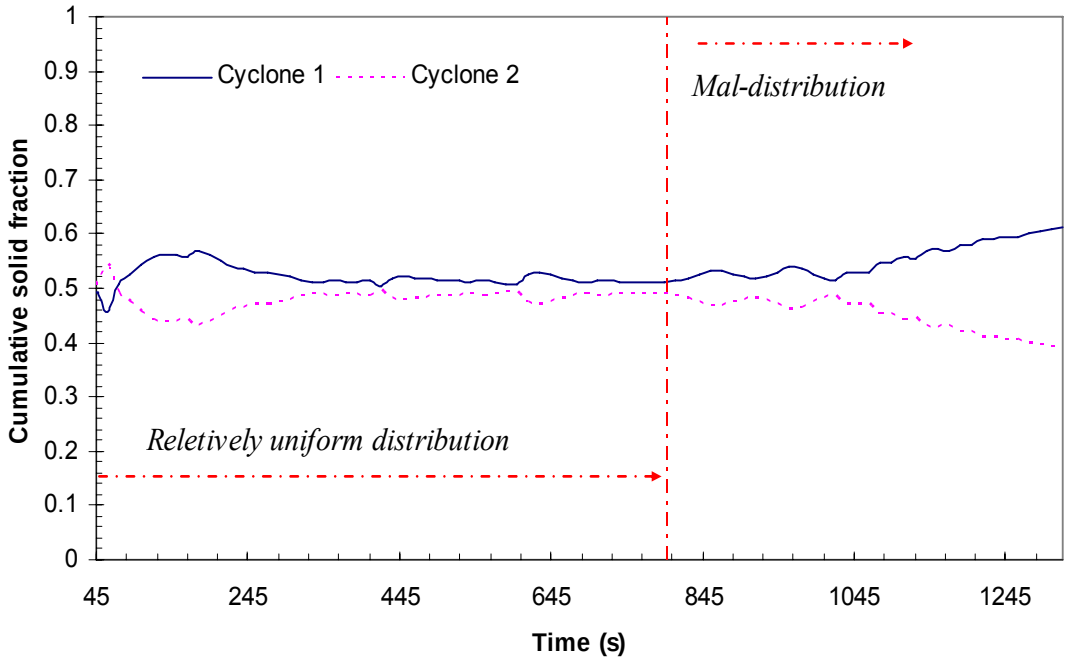

Figure 3-37. Effect of simulated differential fouling on solids mass fraction for flow through cyclones 1 and 2. Cyclone geometry as in Figure 3-5; operating conditions as in Table 3-1.

Finally Figure 3-38 shows the cyclone pressure drops in this case study. Although apparently there is only a small difference between the two pressure drops, the t-test probability was far less than 5%, 1.86E-12, indicating that the data sets for the two cyclones were not statistically equal within a 95% confidence level. Since in this dilute system, the air flow through each cyclone is the major contributor to the pressure drop across the cyclones, it can be concluded that the differential fouling affects the air distribution through the parallel cyclones as well. It should be pointed out that since entrances and exits of both cyclones are connected, the overall pressure drops across the paths should be the same. However the cyclone pressure drops (which were the measured quantities here) are only part of the overall pressure drop.

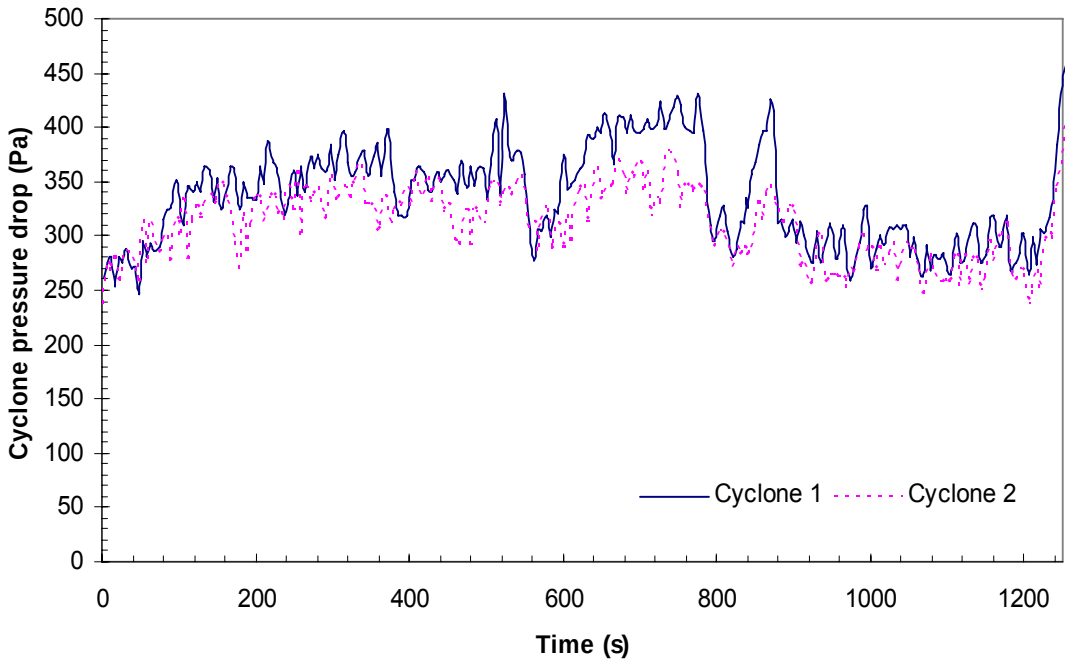

Figure 3-38. Pressure drop through cyclone 1 and 2 related to fouling study. Cyclone geometry as in Figure 3-5; operating conditions as in Table 3-1.

3.4. CONCLUSIONS

Although similar behaviour as for the corresponding 'Y branch' system of Chapter 2 was found for dilute gas-solid cyclones, in denser cyclones systems, the mechanism of gas and solids distribution to reach an equal pressure drop through identical parallel cyclone differs from that presented in Chapter 2. In dense flow, the uniform distribution solution for cyclones is predicted to have a maximum (not a minimum) pressure drop. Energy minimization then suggests that other mal-distributed solutions are more likely to occur in practice. Extensive experimental studies are needed to verify the model predictions based on the Chen and Shi [39] model for cyclone pressure drop.

Limited experimental analyses on dilute systems are consistent with the hypothesis that by utilizing the energy minimization approach in the proposed cyclone model, the

uniform gas-solid distribution solution consumes the minimum energy across cyclones in parallel and is the most likely solution for dilute cases. Also it should be pointed out that a recent CFD and experimental study[1] on two identical parallel cyclones is consistent with the presented results in this work. In addition, experimental results demonstrated that simulated differential fouling can significantly affect mal-distribution of gas-solids flow through identical parallel cyclones.

[1] Personal communication with: Li et al., Institute of Process Engineering, Chinese Academy of Sciences, Beijing, China.

Chapter 4. TECHNIQUES TO MAKE THE DISTRIBUTION UNIFORM

As mentioned in Chapter 1, there are some available techniques for making the distribution of gas-solid flow through parallel units uniform. These methods are summarized in this chapter.

4.1. PARALLEL CHANNELS INSIDE FLUIDIZED BEDS

As explained in Chapter 1, Bolthrunis et al. [36] and Boyd et al. [38] investigated mal-distribution of gas-solid flow through parallel vertical panels inside fluidized bed reactor. In practice, some slots experienced much more flow than others, with the result that the overall performance suffered and operation was difficult. Grace et al. [90] proposed a method to make the distribution uniform through the panels; as shown schematically in Figure 4-1, opening up communication between adjacent fluidization channels solved the problem of mal-distribution which plagued the earlier geometry (Figure 1-12) where parallel vertical chambers of equal dimensions where isolated from each other their entire height.

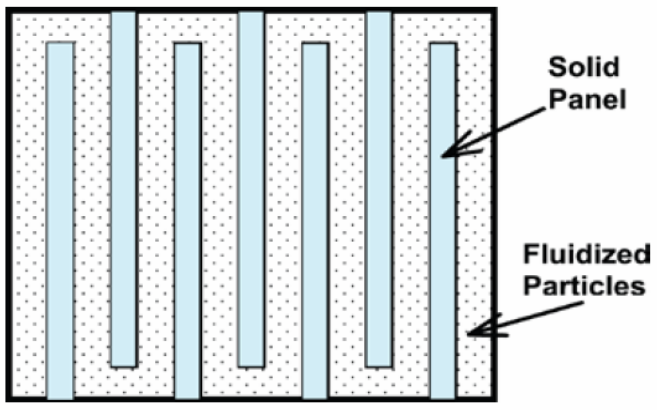

Figure 4-1. Plan view of communicating compartmentalized fluidized bed reactor developed by Membrane Reactor Technology (MRT) Ltd. to circumvent difficulties associated with parallel separate chambers [18].

4.2. BEND FLOW

As presented in Chapters 1, piping at upstream of a bifurcation can experience non-uniformity, causing mal-distribution of flow through the paths. The CFD studies in Chapter 2 demonstrated this phenomenon. In practice, this causes operating problems, for example in parallel coal-fired power plants. As a result, the problem has attracted significant attention. The following describes some of the techniques that have been explored in an effort to improve uniformity.

4.2.1. Riffle Box

The CERL riffle box, illustrated in Figure 4-2 , was developed by the UK Central Electricity Research Laboratories in the 1960s for pulverized fuel feed lines [91]. It is a series of plates that divide the flow into layers, which are diverted into parallel branches. It is most often used in bifurcations, but can be modified for trifurcations. Test results for this device showed promise. For example, for particular conveying conditions, split ratios of the order of 44:56 % could be altered to 48.4:51.6 % [91].

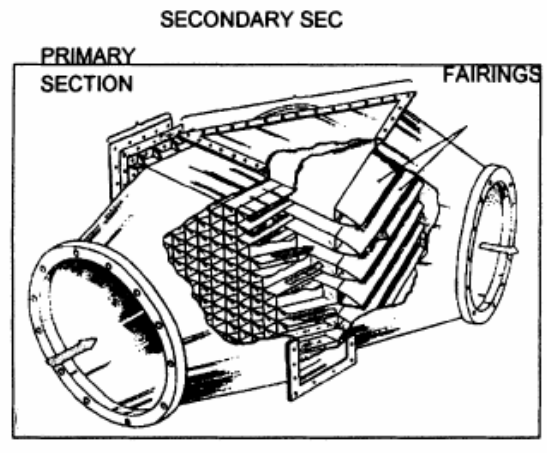

Figure 4-2. CERL riffle box [91].

Schneider et al. [32] investigated the effect of riffle box on the distribution of gas-solid flow through the vertical identical ‘Y branch’ using CFD (Lagrangian approach) and

PIV. The geometry of the riffle box considered by them is provided in Figure 4-3. As shown in Figure 4-4, introducing relatively uniform multi-phase flow upstream with a 30 m/s inlet velocity, the particles were distributed relatively uniformly through the 'Y branch'.

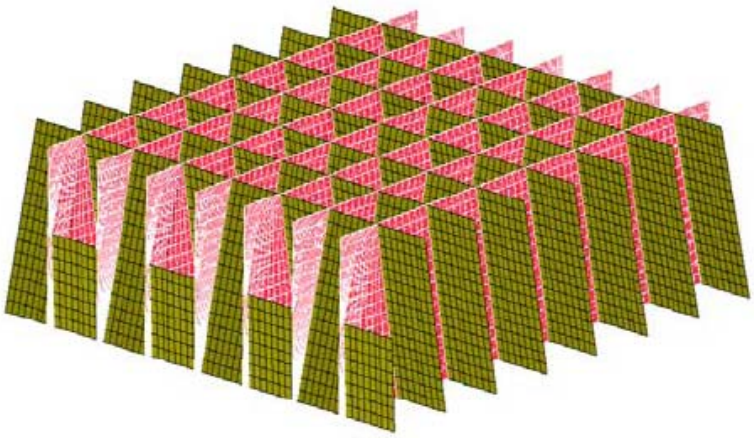

Figure 4-3. Riffle box (rope splitter) [32].

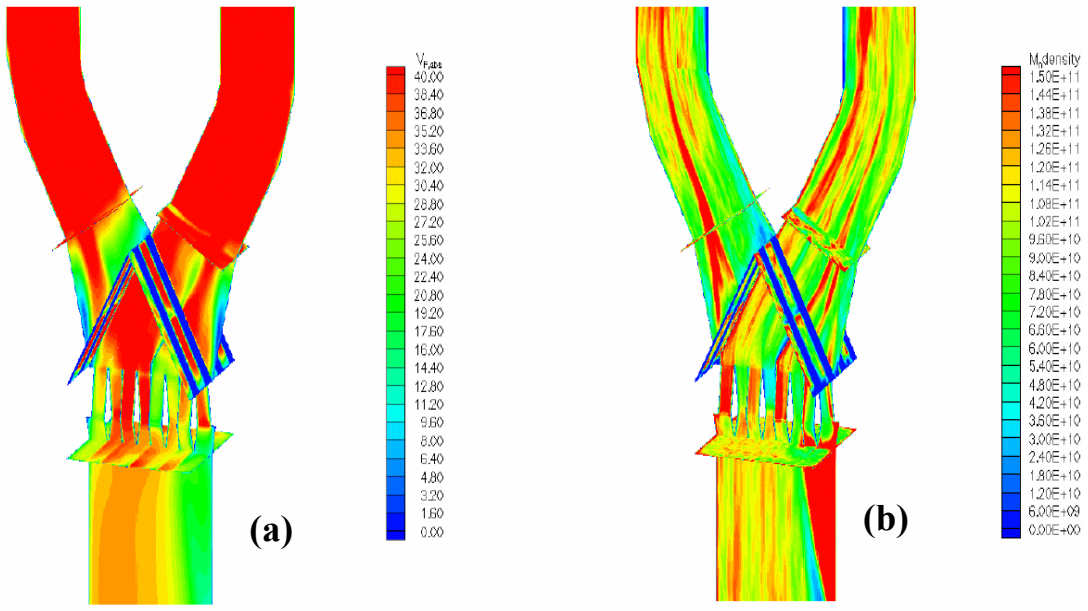

Figure 4-4. (a) Solids velocity (b) Solids number density [32].

As the next study as shown in Figure 4-5, Schneider et al. [32] studied solids distribution through a 'Y branch' with a riffle box upstream. In Figure 4-6 the operation of the riffle

box is illustrated by drawing a number of particle trajectories. The particles were injected in the stream in a cross-section that forms a distinct rope, which would leave the bifurcation completely through one leg in absence of the riffle box. But the rope is distributed relatively uniform to both legs due to two effects: First the rope is dispersed only under the influence of the turbulent motion in the flow and therefore enters more than one of the 64 channels. Secondly the rope is distributed by the riffle box to both legs, because a particle is guided through the other leg when it enters an adjacent channel even when the rope is situated very close to one wall (or even in a corner). This situation can be found e.g. when one or more bends are close to the inlet of the bifurcation. For the two outlets of the bifurcation, they obtained particle mass flow ratios of 48.14%:51.86% with 22500 particles, 48.93%:51.07% with 102400 particles and 48.74%:51.26% with 202500 particles.

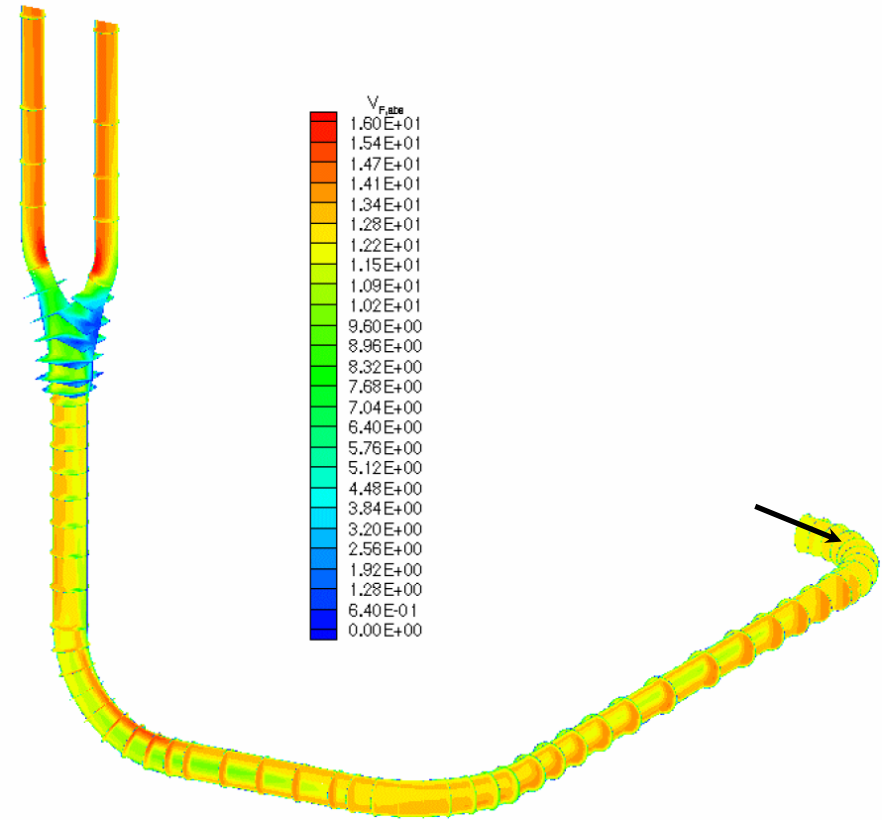

Figure 4-5. Bifurcation with pipework; solids velocity distribution [32].

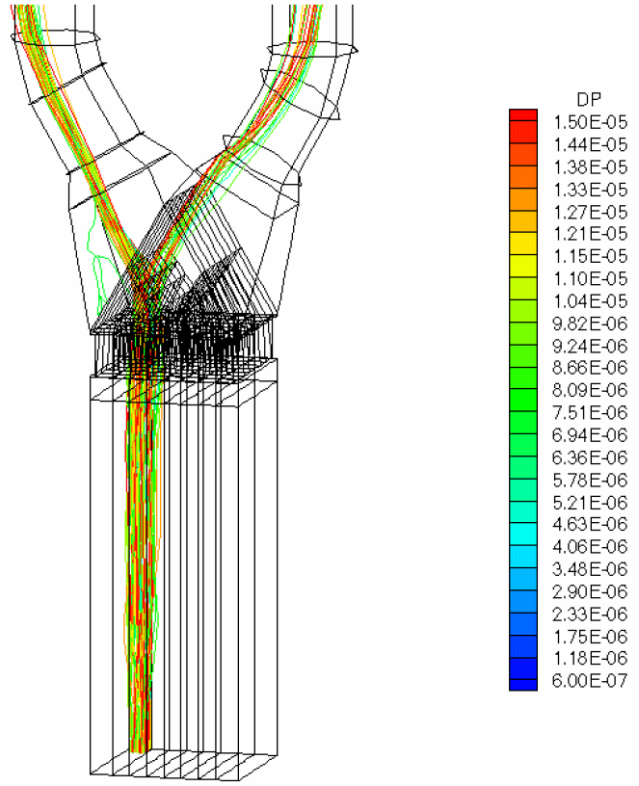

Figure 4-6. Rope splitting by bifurcation [32].

4.2.2. Fuller Splitting Cone

Fuller Company developed the splitting cone, shown in Figure 4-7 [92]. The material that enters the splitter impacts on a steel cone and is forced outwards into an annular channel, which is split into a number of outlet branches, usually three or eight. Testing on this device done by Fuller indicates that±10 per cent accuracy on split ratios can be achieved, with numbers as good as 6 or 7 percent under some conditions. There are two significant problems with using this type of device; the inherent pressure drop is extremely high and, if a mal-distribution occurs in the approaching pipe, it could be directed down only one branch. In such a case the split ratio would be severely unbalanced.

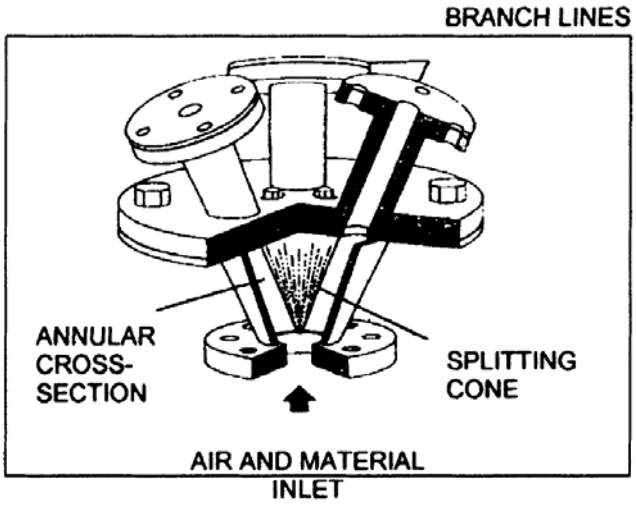

Figure 4-7. Fuller splitting cone [92].

4.2.3. Rotary Splitter

several manufacturers have developed rotary splitters. The basic design involves rotating vanes, which change the direction of the flow by 90°. The vane is in the centre of the splitter, and the branch lines project radially outward from the casing. When the vane is in line with a branch outlet, the two-phase flow (particle and air) is ejected from the splitter into the radial branch. This type of splitter can be used to divide the flow between 36 outlet branches; however, feed into the outlet branches will fluctuate with time. A rotary splitter requires additional power as the vane presents a large barrier to flow so that its pressure drop is substantial.

4.2.4. Kice Stream Splitter

Kice Metal Company developed the Kice splitter, shown in Figure 4-8 [93]. It is essentially a steel manifold designed to split flow into two, three or four branch lines. It is fitted with adjustable ‘actuators’ that are claimed to be capable of controlling split ratios, but no test results have been published to substantiate this claim. Split ratio control can probably be achieved by tuning the actuator settings on the outlet ports to bias the amount of material entering any particular branch; however, the actuators are eroded over time, and, as a result, the effectiveness and accuracy of the splitter is expected to diminish.

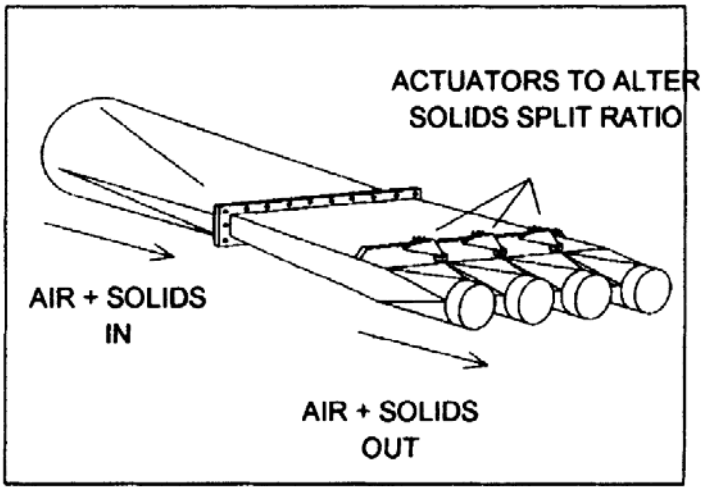

Figure 4-8. Kice stream splitter [93].

4.2.5. Orifice Plate

Humbug Mountain Research Laboratories demonstrated [94, 95] that orifice plates can be placed downstream of a bifurcation to impose a balance on the pressure drop in two lines. A computer simulation can be used to predict the required orifice size and location. This technique is often used to balance flow of pulverized fuel out of a pulverizer/classifier, but it could be adapted for use in branch lines downstream of bifurcations.

The next five methods obtained from research [96] at the Wolfson Centre for Bulk Solids Handling Technology at the University of Greenwich to control the splitting ratio of PF materials through identical parallel power stations.

4.2.6. Swirl

The swirl technique employed a modified ‘Y’-shaped bifurcation. A section of the pipe that approached the bifurcation was removed and replaced with a swirl chamber. Air injected into the casing entered the inner pipe through one series of holes, so as to impart either a clockwise or an anticlockwise rotational velocity on the two-phase flow, which, in combination with its axial velocity, resulted in a helical path, as shown in Figure 4-9.

The success of this technique depends on injecting the precise amount of air required to impart a suitable helical rotation to bias the material to the desired side of the pipe as it enters the bifurcation. The required amount of air depends on many parameters in a complex dynamic relationship. These include such items as downstream branch configurations, distance between the swirl chamber and the bifurcation, particle properties and axial velocity. The complicated nature of this technique means that it could not easily be incorporated into a feedback control loop.

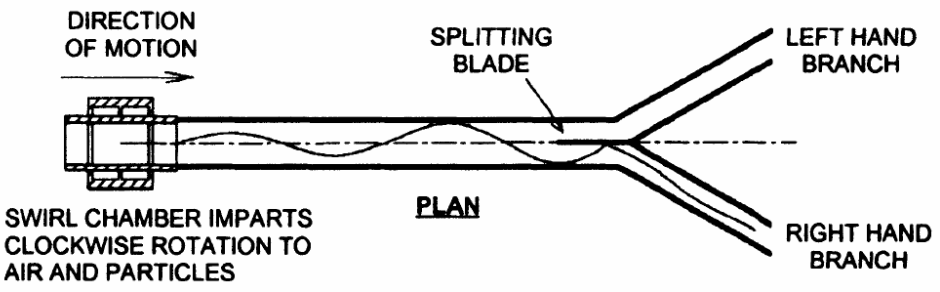

Figure 4-9. Swirl technique [96].

4.2.7. Drop Box

In this technique the 'Y'-shaped bifurcation is replaced by a drop box style bifurcation, as shown in Figure 4-10. A swirl chamber, like that used in the swirl technique, was installed in the pipe approaching the drop box. An allowance was made for the installation of a splitting blade immediately prior to the drop box. The flowing material undergoes consecutive horizontal-to-vertical and vertical-to-horizontal direction changes in a short travel distance, such that the material exits at 90° to the entry orientation. The two abrupt direction changes cause a marked reduction in particle velocity. A large pressure drop is required to reaccelerate the particles to their previous velocity. This pressure drop occurs in both branches and was much larger than the pressure drop that occurred because of air flowing alone. As a result there is a strong tendency for equal amounts of material to enter each branch.

The same problem, of predicting and achieving the amount of air injection required to ensure that the material was correctly located as it entered the bifurcation, existed with this technique as with the swirl technique. The complicated nature of the geometry combined with the inherently high pressure drop and its associated risks when handling pulverized fuel renders this technique unsuitable for power stations.

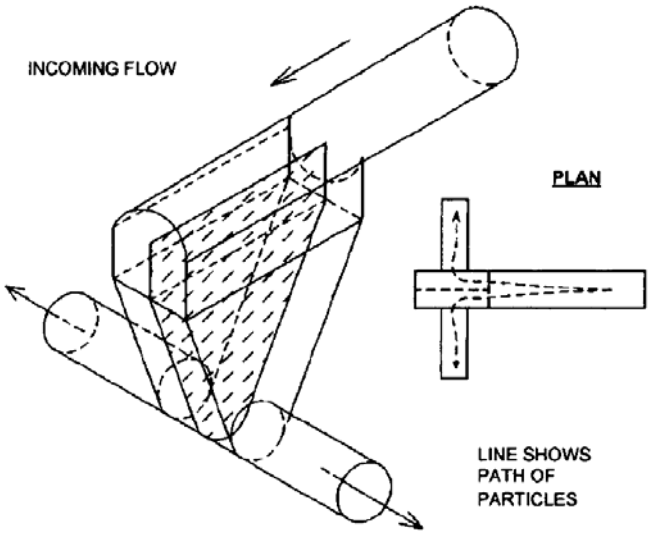

Figure 4-10. Drop box technique [96].

4.2.8. Back Pressure

In the back pressure technique, control air is injected into one of the branches downstream of a 'Y'-shaped bifurcation, as shown in Figure 4-11. The principle of operation is that the injected air increases the pressure drop through the branch into which it is injected. In order to equalize the pressure drop between the two branches, more of the two-phase flow must enter the opposing branch. The results [96] suggest that this technique would require a large quantity of injection air to balance the pressure drop in the branch lines. Retrofitting this technique into a system would only involve adding an air injection port to each branch line just downstream of the bifurcation. Erosion and pressure drops are minimized as there are no protrusions into the pipe.

Holmes et al. [96] reported discouraging result from this technique. Although small-scale testing on this technique showed promise, the scatter of data in the results from the pilot-scale rig was so great that the possibility of its application in a feedback loop was eliminated. A possible explanation for the poor performance of this technique is that the injection air does not act directly on the particles. Introducing air into a branch line creates complex flow patterns in the area just upstream of the bifurcation. Particles tend to maintain their original trajectories owing to momentum, and the indirect action of the injection air may not be sufficient and consistent enough to redirect the required number of particles into a different branch.

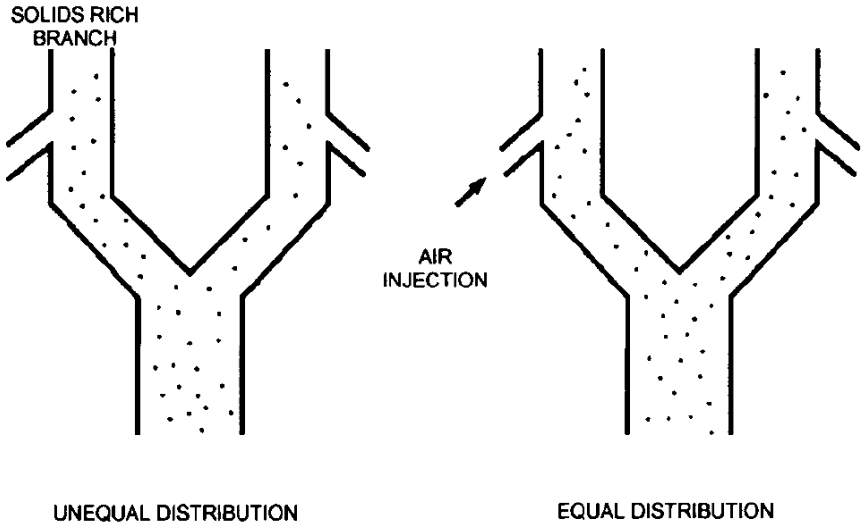

Figure 4-11. Back pressure technique [96].

4.2.9. Flow Diverter

In the flow diverter technique, control air is injected into the pipe approaching a 'Y' shaped bifurcation, as shown in Figure 4-12. The injection air was intended to divert material approaching the bifurcation into a particular branch. It was found by Holmes et al. [96] that the largest amount of solids diverted for the smallest amount of air injected occurred at an angle of 45° to the approach flow. It was possible to alter significantly the solid split ratios by injecting relatively small amounts of air upstream of the bifurcation. The results of the small-scale testing indicate that the positive action of the injected air on

the particles can accommodate fine changes in solids split ratios. Exerting a sideways force on the particles appeared to be an efficient method of diverting material [96]. Also test results on the pilot-scale rig indicated that the flow diverter technique could be used to successfully control solids split ratios. Large changes in solids split ratios were achieved for small amounts of injection air.

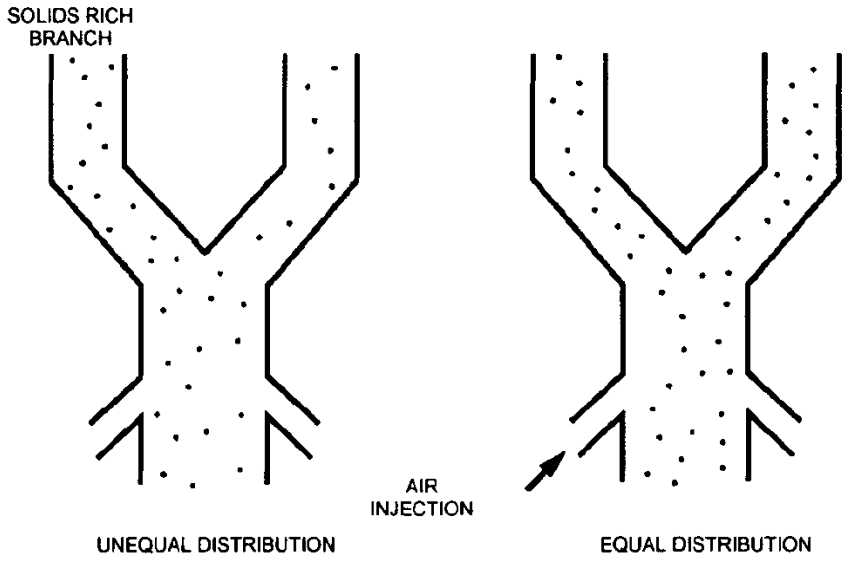

Figure 4-12. Flow diverter technique [96].

4.2.10. Active Riffle Box

The active riffle box technique makes use of a modified riffle box at the bifurcation. As presented above, the standard riffle box works reasonably well as a splitter; however, in its unmodified state, it is not active. With slots cut into the back plates, and air injected across the back of the slots, it was hoped that the solids split ratio could be controlled.

Based on an analysis by Holmes et al. [96], a model active riffle box was built with slots cut into the back plates of the two middle vanes, as shown in Figure 4-13, for use in a small-scale test rig. Without air injection, material passed through the plate instead of being diverted. When air was injected, it would act as a gate, preventing material from passing through the slot, at the same time as increasing the back pressure along the same line, thereby creating a tendency for material to enter the other branch, in order to

equalize the pressure drop. The overall pressure drop, measured across the bifurcation with the riffle plates in place, was a few millibars larger than without the riffle plates, depending on the air and solids mass flow rates and pipeline layout. This was within the acceptable limits with respect to the objectives. In summary, this extended technique showed promise with respect to the splitting ratio. (For more details see reference [96]).

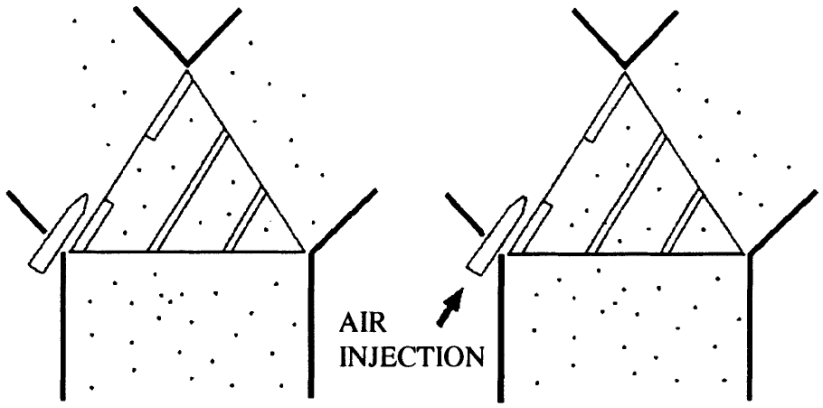

Figure 4-13. Active riffle box technique [96].

4.3. CONCLUSIONS

Of the last five methods presented, it appears that the final two techniques for control of split ratios at bifurcations are the most promising options, as these have good reproducibility and sensitivity. In order to confirm the usefulness of these, trials on a full scale installation are required, in combination with appropriate on-line flow measurement techniques.

Although some promising techniques are available to improve the uniformity of the gas-solid flows, their applicability in the multi-phase systems where fouling is occurring is questionable. For example, the draft box method is not able to make a slurry multi-phase flow uniform, since fouling occurs at the entrance of the bifurcation. Based on the method proposed by Grace et al. [90] for having the uniform distribution through parallel

channels inside a fluidized bed reactor, it is suggested that communication channels between parallel paths (e.g. parallel cyclone) be examined experimentally.

Chapter 5. CONCLUSIONS AND RECOMMENDATIONS

A fundamental study has been done on the distribution of gas-solid flow through identical parallel paths. For a 1-D Lagrangian framework, it is shown that for a simple identical parallel pipes ('Y branch'), a number of solutions satisfy pressure drop and flow balance criterion. In this case, the uniform gas and solids distribution solution had a minimum pressure drop across the paths. If energy minimization is a governing condition, the uniform distribution is the most likely solution. The linear stability analysis also predicted that the uniform distribution of gas-solid flow is the only stable solution. In addition, CFD analyses provided consistent results with the analytical conclusion. Finally the presented numerical sensitivity simulations displayed the effect of the upstream radial gas-solid distribution on the splitting pattern through the bifurcation. It is predicted that the behaviour of gas-solid flow passing across parallel pipes is not similar to gas-liquid systems presented in literature [15]. In future work, it is proposed to do some dilute and dense experimental analyses in 'Y branch' geometry to verify the model.

The distribution of gas-solid flow through identical parallel cyclones was analysed based on the Chen and Shi [39] pressure drop equation. For dilute systems behaviour was similar to that in the 'Y branch' geometry, both analytically and experimentally. On the other hand, the uniform distribution solution had a maximum pressure drop in dense gas-solid flow passing identical parallel cyclones. The possibility of mal-distributed solutions is therefore likely to be greater in dense cases. For further study, it would be of interest to examine experimentally a distribution of dense gas-solid flow through identical parallel cyclones. Also it is recommended to test alternative cyclone pressure drop equations (e.g. for conventional cyclones used in circulating fluidized beds [98]). Lastly, the behaviour of the system for >2 parallel paths should be studied as the focus in the present work was on two paths only.

Further work is also needed to explain new techniques to make the flow distribution more uniform. Desirable feature for the new methods can be summarized as follows:

- Avoiding generation of significant pressure drop relative to the original pressure drop of the system;
- Using minimum dynamic measurements and controlling instrumentation to minimize erosion;
- Capability to be applied in retrofitting.

BIBLIOGRAPHY

[1] J. Stumper, A. Roshanzamir., 210 Meeting of Electrochemical Society, Cancun, Mexico, abstr. #611, 2006.

[2] L. Zhang, H. Bi, D.P. Wilkinson, J. Stumper and H. Wang, 'Gas-liquid two-phase flow patterns in parallel channels for fuel cells', Journal of Power Sources, 94, 40-50, 2008.

[3] M. Ozawa, K. Akagawa, T. Sakaguchi, 'Flow instabilities in parallel channel flow systems of gas-liquid two-phase mixtures', Int. J. Multiphase Flow., 15, 639–657, 1989.

[4] U. Minzer, D. Barnea, Y. Taitel, 'Flow rate distribution in evaporating parallel pipes - modeling and experimental', Chem. Eng. Sci., 61, 7429-7259, 2006.

[5] K. Akagawa, T. Sakaguchi, M. Kono, M. Nishimura, 'Studies on distribution of flow rates and flow stabilities in parallel long evaporators', Bulletin of JSME., 14, 837–849, 1971.

[6] V. Jovic, N. Afgan, L. Jovic, D. Spasojevic, 'An experimental study of the pressure drop oscillations in three parallel channel two-phase flow', 4th International Heat Transfer Conference, 6, 193–198, Brighton, UK, 1994.

[7] M. Ozawa, 'Flow instability problem in steam-generating tubes', Steam power engineering, Ishigai S. ed., Cambridge University Press, 323–385, 1999.

[8] Y. Taitel, L. Pustylnik, M. Tshuva, D.Barnea, 'Flow distribution of gas and liquid in parallel pipes', Int. J. Multiphase Flow, 29, 1193-1202, 2003.

[9] R.J. Pederson, E.K. May, 'Flow instability during DSG in a line-focus solar collector system, SERI/TR- 632-1354. Golden, CO, Solar Energy Research Institute, 1982.

[10] L.M. Murphy, E.K. May, 'Steam generation in line-focus solar collectors: a comparative assessment of their mal-performance, operating stability, and cost issues', SERI/TR- 632-1311, Golden, CO, Solar Energy Research Institute, 1982.

[11] M. Ozawa, K. Akagawa, T. Sakaguchi, T. Tsukahara, T. Fujii, 'Oscillatory flow instabilities in air-water two-phase flow systems-first report', pressure drop oscillation, Bull. JSME, 22, 1763-1770, 1979.

[12] M. Ozawa, K. Akagawa, T. Sakaguchi and T. Suezawa, In: Oscillatory flow instabilities in a gas-liquid two-phase flow system, Heat transfer in nuclear reactor safety Hemisphere, Washington, DC, 379-390, 1982.

[13] N. Reinecke, P. Griffith, D. Mewes, 'Flow-reversal in vertical, two-phase, two-component flow in parallel channels', 32th Meeting of the European Two-Phase Flow Group, Siet, Piacenza, Italy, 1994.

[14] M. Tshuva, D. Barnea, Y. Taitel, 'Two phase flow in inclined parallel pipes', Int. J. Multiphase Flow 25, 1491–1503, 1999.

[15] L. Pustylnik, D. Barnea, and Y. Taitel, 'Prediction of two-phase flow distribution in parallel pipes using stability analysis', AIChE, 52, 3345-3352, 2006.

[16] K.A. Triplett, S.M. Ghiaasiaan, S.I. Abdel-Khalik, A. LeMouel, B.N. McCord, 'Gas-liquid two-phase flow in microchannels - Part II: void fraction and pressure drop', Int. J. Multi Phase Flow, 253, 395-410, 1999.

[17] A. Kawahara, P.M.Y. Chung, M. Kawaji, 'Investigation of two-phase flow pattern, void fraction and pressure drop in a microchannel', Int. J. Multi Phase Flow, 28, 1411-1435, 2002.

[18] J.R. Grace, H. Cui and S.S.E.H. Elnashaie, 'Non-Uniform distribution of two-phase flows through parallel identical paths', Canadian Journal of Chemical Engineering, 85, 662-668, 2007.

[19] A. Stern, K. Caplan and P. Bush, 'Parallel operation of cyclones in cyclone dust collectors', API Dust-Collector Subcommittee, pp. 41–43, 1955.

[20] J.L. Koffman, 'The cleaning of engine air Part 2', Gas Oil Power, 89–94, April 1953.

[21] N.J. Broodryk and T. Shingles, 'Aspects of cyclone operation in industrial chemical reactors', Preprints for Fluidization VIII Conference, p. 1083, Tours, France, May 14-19 1995.

[22] J. Smellie, 'Notes on dust suppression and collection', Iron and Coal Trades Review, 144 3860, 169 pages, p. 227, 1942.

[23] Y.Y. Lee, Chapter 11 in Circulating Fluidized Beds, Grace J.R., Avidan, A.A., Knowlton, T.M. eds., Chapman & Hall, London, pp. 417-440, 1997.

[24] E.-U. Hartge, S. Budinger, J. Werther, in Circulating Fluidized Bed Technology VIII Kefa, C., ed., International Academic Publishers, World Publishing Corp., Beijing, pp. 675-682, 2005.

[25] V.A. Shevtchenko, W. Franke, P. Gummel, M. Kotrus, G. von Wedel, Proc., 18th Int. Conf. on Fluidized Bed Combustion, ASME, New York, paper FBC2005-78034, 2005.

[26] Y. Wu, J. Lu, J. Zhang, G. Yue, and L. Yu, in Circulating Fluidized Bed Technology VIII Kefa, C., ed. International Academic Publishers, World Publishing Corp., Beijing, pp. 529-536, 2005.

[27] T. W. Kim, J. H. Choi, D. W. Shun, B. Jung, S. S. Kim, J. E. Son, S. D. Kim and J. R. Grace, "Wastage rate of waterwalls in a commercial circulating fluidized bed combustor," Can. J. Chem. Eng. 84, 680–687, 2006.

[28] T.W. Kim, J.H. Choi, D.W. Shun, S.S. Kim, S.D. Kim, J.R. Grace, 'Wear of water walls in a commercial circulating fluidized bed combustor with two gas exits', Powder Technol., 178, 143-150, 2007.

[29] J.R. Grace, 'Maldistribution of flow through parallel cyclones in circulating fluidized beds, in Circulating Fluidized Bed Technology', ed. J. Werther, W. Nowak, K-E. Wirth and E-U. Hartge, TuTech Innovation, Hamburg, Germany, pp. 969-974, 2008.

[30] I. Flour, and M. Boucker, "Numerical simulation of the gas-solid flow in the furnace of a CFB cold rig with ESTETASTRID code," in "Circulating Fluidized Bed Technology VII," J. R. Grace, J. Zhu and H. de Lasa, Eds., CSChE, Ottawa, pp. 467–474, 2002.

[31] G. X. Yue, H.R. Yang, L. Nie, Y.Z. Wang, H. Zhang, 'Hydrodynamics of 300MWE and 600 MWE CFB boilers with asymmetric cyclone layout', ed. J. Werther, W. Nowak, K-E. Wirth and E-U. Hartge, TuTech Innovation, Hamburg, Germany, pp. 153-158, 2008.

[32] H. Schneider, T. Frank, D. K. Pachler and K. Bernert, 'A Numerical study of the gas-particle flow in pipework and flow splitting devices of coal-fired power plant", 10th Workshop on Two-Phase Flow Predictions, Martin-Luther-Universitat Halle-Wittenberg, Halle Saale, Germany, pp.227-236, 2002.

[33] B.T. Kuan and W. Yang, 'Mal-distribution of coals in lignite-fired power station mill ducts: CFD simulations and experimental validation', Int. Conf. Coal Science Technol., Okinawa, Japan, 2005.

[34] T. Holmes, M.S.A. Bradley, T.P. Selves, R.J. Farnish, I. Bridle and A.R. Reed, ' Techniques for control of splitting ratios of particulate materials at bifurcations in pneumatic conveying pipelines', Proc. Instn. Mech. Engrs.,214, Part A, pp. 657-667, 2000.

[35] D. Giddings, A. Aroussi, S.J. Pickering and E. Mozaffari, 'A ¼ scale test facility for PF transport in power station pipelines', Fuel 83, 2195–2204, 2004.

[36] C.O. Bolthrunis, R. W. Silverman and D. C. Ferrari, "Rocky road to commercialization: breakthroughs and challenges in the commercialization of fluidized bed reactors," in "Fluidization XI," U. Arena, R. Chirone, M. Miccio and P. Salatino, Eds., Eng. Conf. Int., Brooklyn, NY, pp. 547–554, 2004.

[37] D.T. Boyd, J. R. Grace, C. J. Lim and A. M. Adris, "Hydrogen from an Internally circulating fluidized bed membrane reactor," Int. J. Chem. Reactor Eng. **3**, A58, p. 12, 2005.

[38] D.T. Boyd, J. R. Grace, C. J. Lim and A. M. Adris, "Cold modelling of an internally circulating fluidized bed membrane reactor," Int. J. Chem. Reactor Eng., 5, A26, 2007.

[39] J. Chen and M. Shi, 'A universal model to calculate cyclone pressure drop', Powder Technol., 171, 184–191, 2006.

[40] J. Li and M. Kwauk, 'Exploring complex systems in chemical engineering-the multi-scale methodology', Chem. Eng. Sci., 58, 521–535, 2003.

[41] S.S.E.H. Elnashaie and J. R. Grace, 'Complexity, bifurcation and chaos in natural and man-made lumped and distributed systems', Chem. Eng. Sci., 62, 3295–3325, 2007.

[42] P.W. Anderson, 'More is Different', Science 177 4047: 393–396, 1972.

[43] N. Huber, M. Sommerfeld, 'Modeling and numerical calculation of dilute-phase pneumatic conveying in pipe systems', Powder Technol, 99, 90-101, 1998.

[44] 'FLUENT User Guide', Fluent Inc., Chapter 23, 2006.

[45] B. J. Alder and T. E. Wainwright, 'Studies in molecular dynamics II: behaviour of a small number of elastic spheres', J. Chem. Phys., 33:1439-1451, 1990.

[46] S. Chapman and T. G. Cowling, 'The mathematical theory of non-uniform gases', Cambridge University Press, Cambridge, England, 3rd edition, 1990.

[47] J. Ding and D. Gidaspow, 'A bubbling fluidization model using kinetic theory of granular flow', AIChE J., 36:523-538, 1990.

[48] D. Gidaspow, R. Bezburuah, and J. Ding, 'Hydrodynamics of circulating fluidized beds, kinetic theory approach', In Fluidization VII, Proceedings 7th Engineering Foundation Conference on Fluidization, 75-82, 1992.

[49] J. L. Lebowitz, 'Exact solution of generalized Percus-Yevick equation for a mixture of hard spheres', Phy. Rev., 133: A895-A899, 1964.

[50] C. K. K. Lun, S. B. Savage, D. J. Jeffrey and N. Chepurniy, 'Kinetic theories for granular flow: inelastic particles in Couette flow and slightly inelastic particles in a general flow field', J. Fluid Mech., 140:223-256, 1984.

[51] S. Ogawa, A. Umemura and N. Oshima, 'On the equation of fully fluidized granular materials' J. Appl. Math. Phys., 31:483-493, 1980.

[52] M. Syamlal, W. Rogers and O'Brien T. J. MFIX Documentation: Volume 1, Theory Guide. National Technical Information Service, Springfield, VA, 1993, DOE/METC-9411004, NTIS/DE9400087.

[53] M. Syamlal and T. J. O'Brien, 'Computer Simulation of Bubbles in a Fluidized Bed' AIChE Symp. Series 85:22-31 (270), 1989.

[54] C.-Y. Wen and Y. H. Yu, 'Mechanics of Fluidization', Chem. Eng. Prog. Symp. Series, 62:100-111, 1966.

[55] R.G. Boothroyd, Flowing Gas Solids Suspensions, Chapman and Hall, London, 1971.

[56] S. Corrosin and J. Lumley, Appl. Sci. Res., 6A, 114, 1956.

[57] S.L. Soo, Fluid Dynamics of Multiphase Systems, Blaisdell, Waltham, Mass, 1967.

[58] C.M. Tchen, Ph.D. Thesis, Technical Univ. of Delft, Martinus Nijhoff, The Hague, 1947.

[59] Q. Wang, K.D. Squires and O. Simonin, 'Large eddy simulation of turbulent gas-solid flows in a vertical channel and evaluation of second-order models', International Journal of Heat and Fluid Flow, 19, 505-511, 1998.

[60] C.Y. Wen and H.P. Simons, 'Flow characteristics in horizontal fluidized solids transport' AIChE J., 5, 263-7, 1959.

[61] M. Weber, Stromungs-Fordertechnik, Krausskopf Verlag, 1973.

[62] S. Stemerding, 'The pneumatic transport of cracking catalyst in vertical risers', Chem. Eng. Sci., 17, 599, 1962.

[63] K.V.S. Reddy and D.C.T. Pei, 'Particle dynamics in solid gas flows in vertical pipes', I.E.C. Fund, 8, 490-497, 1969.

[64] W.P.M. Van Swaaij, C. Buurman and I.W. Breugel, 'Shear stress on the wall of the dense glass-solids riser', Chem. Eng. Sci., 25, 1818-1820, 1970.

[65] C.E. Capes and K. Nakamura, 'Vertical pneumatic conveying: An experimental study with particles in the intermediate and turbulent flow regimes', Can. J. Chem. Eng., 51, 31-38, 1973.

[66] H. Konno and S.J. Satio, 'Pneumatic conveying of solid through straight pipes', Chem. Eng. Japan, 2, 211, 1969.

[67] W.C. Yang, Int. powder & bulk solids handling and processing conference exposition, Chicago, May, 1976.

[68] W.C. Yang, 'A correlation for solid friction factor in vertical pneumatic conveying lines', AIChE J., 24, 548, 1978.

[69] W. Stegmaier, 'Zur Berechnung der horizontalen pneumatischen Förderung feinkörniger Feststoffe', Fördern Heben, 28, 363–366, 1978.

[70] M.P. Mathur and G.E. Klinzing, 'Measurements of particle and slip velocities in coal/gas system', AIChE Annual Meeting Washington, D.C., Nov., 1983.

[71] G.E. Klinzing, Gas Solid Transport, McGraw-Hill, New York, 1981.

[72] G.W. Govier and K. Aziz, 'The flow of complex mixtures in pipes', van Nostrand Reinhold, New York, 1972.

[73] B.L. Hinkle, Acceleration of particles and pressure drops in countered in horizontal pneumatic conveying: Ph.D. Thesis, Georgia Institute of Technology, Atlanta, Ga, 1953.

[74] Institute of Gas Technology, Dept. of Energy, Contract FE 2286-32, October, 1978.

[75] A. Hurwitz, 'On the conditions under which an equation has only roots with negative real parts', Selected Papers on Mathematical Trends in Control Theory, Dover Publications, 1964 .

[76] R. Clift, J. R. Grace, M.E. Weber, 'Bubbles, drops, and particles', Academic Press, New York, 1978.

[77] T.B. Drew, E.C. Koo, W.H. McAdams, 'The friction factors for clean round pipes, Trans. AIChE, 28, 56-72, 1932.

[78] C.B. Shepherd, C.E. Lapple, Flow pattern and pressure drop in cyclone dust collectors, Ind. Eng. Chem., 31:972–984, 1939.

[79] M.W. First, Fundamental factors in the design of cyclone dust collectors: Ph.D. thesis, Harvard University, Cambridge, Mass., 1950.

[80] R. McK Alexander, Fundamentals of cyclone design and operation, Proceedings Australian Institute of Mining Metals, Nos. 152–153, 203–228, 1949.

[81] C.J. Stairmand, 'Pressure drop in cyclone separators', Engineering 168, 409–412, 1949.

[82] W. Barth, L. Leineweber, Beurteilung und Auslegung von Zyklonabscheidern', Staub 24 (2), 41–55, 1964.

[83] E. Muschelknautz, Auslegung von Zyklonabscheidern in der technischen Praxis, Staub Reinhalt. Luft 30 (5), 187–195, 1970.

[84] J. Casal, J.M. Martinez-Benet, 'A better way to calculate cyclone pressure drop', Chem. Eng. 1, 99–100, 1983.

[85] L.W. Briggs, 'Effect of dust concentration on cyclone performance', Trans. Am. Inst. Chem. Eng., 42, 511–526, 1946.

[86] S. Yuu, T. Jotaki, Y. Tomita, et al., 'The reduction of pressure drop due to dust loading in a conventional cyclone', Chem. Eng. Sci., 33, 1573–1580, 1978.

[87] A.C. Hoffmann, A.V. Santen, R.W.K. Allen, et al., 'Effects of geometry and solid loading on the performance of gas cyclones', Powder Technol., 70, 83–91, 1992.

[88] X.L. Luo, J.Y. Chen, M.X. Shi, Research on the effect of the particle concentration in gas upon the performance of cyclone separators, J. Eng. Thermphys., 13, 282–285, 1992 (in Chinese).

[89] A. Ogawa, O. Seito, H. Nagabayashi, 'Distribution of the tangential velocities on the dust laden gas flow in the cylindrical cyclone dust collector', Part. Sci. Technol., 6, 17–28, 1988.

[90] J. R. Grace, C. J. Lim, A. M. Adris, H. Cui and D. A. Boyd, 'Communicating compartmentalized fluidized bed reactor', U.S. Patent Application No. 60/866247, 2006.

[91] W. L. Snowsill, 'Further developments of the C.E.R.L. pulverised fuel riffle', CERL Laboratory Report RD/L/R 1513, Job VC 058, 3 April 1968.

[92] J. D. Hilbert Jr, 'Splitting of pneumatic conveying pipelines', Bulk Solids Handling, 4, 189–192, 1984.

[93] Kice Metal Company, Wichita, Kansas. Sales literature and personal communication, 1999.

[94] A. A. Vetter and W. D. Gauntlett, 'Balance coal flows accurately to improve boiler performance', Power Mag., August 1984.

[95] A. A. Vetter and R. S. Vetter, 'Balancing pulverised coal flows in parallel piping', J. Engng for Gas Turb. Power, 679–684, July 1985.

[96] T. Holmes, M.S.A. Bradley, T.P. Selves, R.J. Farnish, I. Bridle and A.R. Reed, 'Techniques for control of splitting ratios of particulate materials at bifurcations in pneumatic conveying piplines', Proc Instn Mech Engrs, 214 A, 657-667, 2000.

[97] D. Cook, and N. R. Hurworth, 'Recent research on pulverised fuel settlements in power station pipelines, and the significance of roping', In Pneumotransport 5, Fifth International Conference on Pneumatic Transport of Solids in Pipes, 16–18, April 1980.

[98] S. Yang, H. Yang, H. Zhang, S. Li, G. Yue, 'A transient method to study the pressure drop characteristics of the cyclone in a CFB system', Powder Technology, 192, 105-109, 2009.

[99] L-S. Fan and C. Zhu, Principles of Gas-Solid Flows, Cambridge University Press, Cambridge, UK.

APPENDIX A. SIGN DETERMINATION AT THE LIMIT

As presented in Chapter 2, different gas-solid distribution solutions through two identical parallel paths with different equal pressure drops in left and right sides can be obtained (Figure 2-4). It is trivial that for the presented case study, it is assumed that the total inlet (upstream) gas and solid flows (Q_{st} and Q_{gt}) to the system, before the bifurcation, are constant. Hence as shown in Figure A-1, having constant total solids inlet, several pressure drop solutions can be predicted by the model.

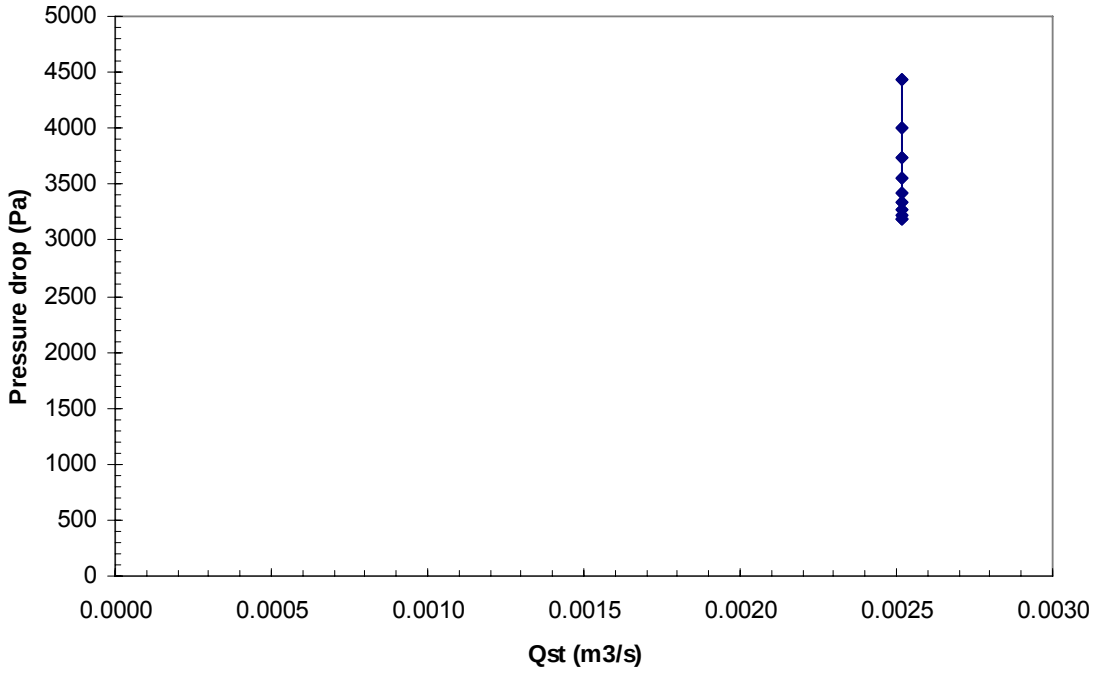

Figure A-1. Predicted different pressure drops caused by mal-distribution of gas-solid flow through the parallel paths with constant total inlet solids flow rate.

Figure A-1 presents a straight line with a slope of infinity. Based on the stability analysis presented in Chapter 2, the sign of dP_{in}/dQ_{st} is important (whether it is –infinity or +infinity). In addition, Q_{st} is constant. Therefore the sign of the dP_{in}/dQ_{st} term should be determined at the limit. Based on the basic definition of derivative:

$$f'(a) = \lim_{h \to 0} \frac{f(a+h) - f(a)}{h}$$

Given $Q_{st}=a$, by introducing a very small positive amount of solid (h):

$$P'_{in} = \frac{dP_{in}}{dQ_{st}} = \lim_{h\to 0} \frac{P_{in}(a+h) - P_{in}(a)}{h}$$

With more solids, the pressure drop through the main pipe is increased and one can obtained:

$$P_0 - P_{in}(a+h) > P_0 - P_{in}(a) \rightarrow P_{in}(a) > P_{in}(a+h)$$

where P_0 is the total inlet pressure of the upstream main pipe. Therefore:

$$P'_{in} = \frac{dP_{in}}{dQ_{st}} = \lim_{h\to 0} \frac{\overbrace{P_{in}(a+h) - P_{in}(a)}^{<0}}{\underbrace{h}_{>0}} = -\infty$$

The same approach can be followed using centric numerical differentiation method.

Physical interpretation: Since this term came at the middle of mathematical operations (stability analysis), it is difficult to interpret the tendency of the dP_{in}/dQ_{st} at the limit physically. The notable physical point that may help is that, as presented in Figure A-2, point "P_{in}" has an interface nature. In other words, point "P_{in}" is the only common point of the main entrance pipe and the bifurcation section. Thus P_{in} should not change at constant Q_{st}, but can deviate by having different gas-solid distributions.

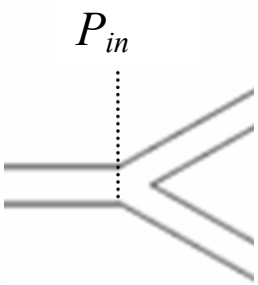

Figure A-2. Interface nature of point "P_{in}".

APPENDIX B. ROUTH-HURWITZ STABILITY CRITERION

The Routh-Hurwitz criterion is a method for determining whether a linear system is stable or not by examining the locations of the roots of the characteristic equation (polynomial) of the system [75]. The method only determines whether there are roots lying outside the left half-plane; it does not actually compute the roots. Its main application is in control engineering.

Consider the general characteristic N^{th} order polynomial with eigenvalues (λ) as its roots:

$$a_N\lambda^N + a_{N-1}\lambda^{N-1} + \ldots + a_1\lambda + a_0 = 0$$

In order to find the sign of the eigenvalues, the Routh-Hurwitz method considers the following table with N rows:

$$\begin{vmatrix} a_N & a_{N-2} & a_{N-4} & \ldots \\ a_{N-1} & a_{N-3} & a_{N-5} & \ldots \\ b_1 & b_2 & b_3 & \ldots \\ c_1 & c_2 & c_3 & \ldots \\ \ldots & \ldots & \ldots & \ldots \end{vmatrix}$$

where elements b_i and c_i can be computed by:

$$b_i = \frac{a_{N-1}a_{N-2i} - a_N a_{N-2i-1}}{a_{N-1}}$$

$$c_i = \frac{b_1 a_{N-2i-1} - b_{i+1}a_{N-1}}{b_1}$$

The necessary condition for all roots (λ) to have negative real parts (stable solutions) is that all elements of the first column of the array have the same sign. Otherwise, the number of changes of sign equals the number of roots with positive real parts (unstable solutions).

Therefore, by application of the Routh-Hurwitz criterion it is possible to find the sign of the roots without calculating their corresponding values. No change in the sign of Routh-Hurwitz's first column corresponds to a stable solution. Otherwise the system is unstable.

Some points are useful in the Routh-Hurwitz stability criterion:

1. Two necessary, but not sufficient, conditions for all roots to have negative real parts (stable solutions) are:
    - All polynomial coefficients must have the same sign.
    - All polynomial coefficients must be non-zero.
2.
    - **Special Case 1:** The first element of a row is zero, but some other elements in that row are non-zero. In this case, simply replace the zero elements by "ε", complete the table development, and then interpret the results assuming that "ε" is a small number of the same sign as the element above it. The results must be interpreted in the limit as $\varepsilon \rightarrow 0$.
    - **Special Case 2:** All the elements of a particular row are zero. In this case, some roots of the polynomial are located symmetrically about the origin of the λ-plane, e.g. as a pair of purely imaginary roots. The zero row always occurs in a row associated with an odd power of λ. The row just above the zero row holds the coefficients of the auxiliary polynomial. The roots of the auxiliary polynomial are symmetrically placed roots. One should remember that the coefficients in the array skip powers of λ from one coefficient to the next. The remedy for this case can be summarized as:

      A. Form an auxiliary polynomial from the coefficients in the row above.

B. Replace the zero coefficients from the coefficients of the differentiated auxiliary polynomial.

C. If there is no sign change, the roots of the auxiliary equation define the roots of the system on the imaginary axis.